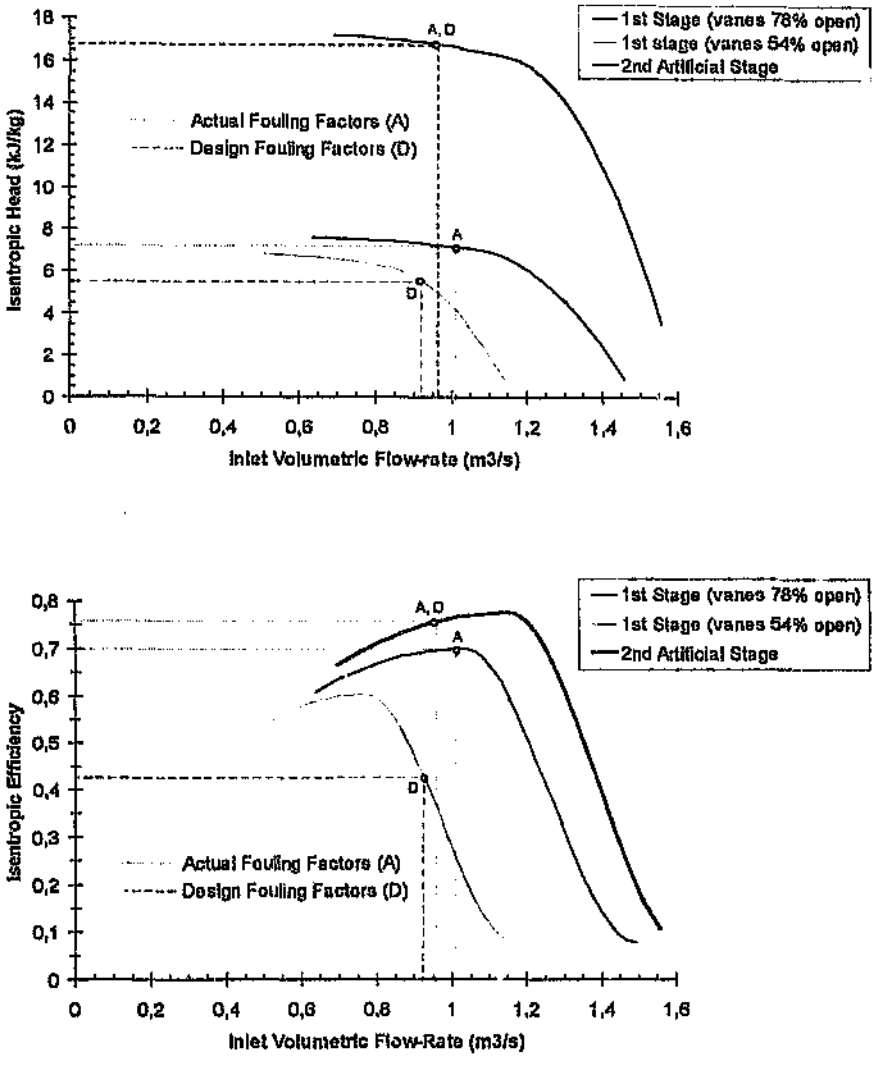

Figure 6.4 Case Study C (Lead Machine): Isentropic Heads and Efficiencies of Virtual Compressor Stages at Actual and Design Fouling Factors

In contrast to Case Study A, therefore, cleaning heat exchanger tubes was predicted to yield a power penalty instead of a power saving! This was because the modelled single-stage compressor of Case Study A

maintained its efficiency at the lower pressure ratios, and thus isentropic heads, required for cleaner tubes. The modelled multi-stage compressors of the present case study, regulated by their first stages only, did not so maintain their efficiency.[12]

Again, the accuracy of the quantitative predictions here was entirely dependent upon the degree of correspondence between the artificial compressor stage curves of CHILLER and those of the real machine. Unfortunately, the manufacturer quoted no part-duty performance data, so the degree of correspondence between predicted and actual part-duty performance was not known. Therefore, although the *qualitative* changes in behaviour predicted as operating conditions changed could reasonably be expected to be valid (because CHILLER's artificial curves have the same qualitative characteristics as typical real curves[13]), it was wise to draw no conclusions directly dependent on the accuracy of the *quantitative* predictions of compressor performance. Here, it was thus prudent to merely conclude that cleaning heat exchanger tubes was not likely to bring about any power saving.

Normal Performance of Both Machines Connected Together

The question next arose of whether there was any benefit in restoring the common condenser water flow-rate through the machines to the design

---

[12] This was because the artificial compressor stage curves of the available version of CHILLER, used to model the real three-stage compressors as virtual two-stage ones, yielded maximum efficiency at design, full machine duty, and reduced efficiency elsewhere. The real three-stage compressors were also likely to behave in this way, because their machines were manufactured before 1980, when part-load performance began to significantly influence design criteria of conventional machines (Austin, 1991). Pre-1980 conventional machines, according to Austin's field monitoring experience, are most efficient at full load, which must mean that their centrifugal compressors have this characteristic. In contrast, the machine of Case Study A was manufactured in 1985 and designed for efficient operation at several specified duties. Moreover, this machine had a single-stage compressor; such compressors, as Austin (1991) notes, have flatter efficiency curves than multi-stage compressors in any case.

[13] For example, reducing head and reducing isentropic efficiency with reducing vane opening.

value of 266 l/s - bearing in mind that the actual value (at an average of 152,9 l/s) was 57 per cent of this.

To investigate this, it was necessary to simulate both machines together, because their interconnections made their performances interdependent. CHILLER was therefore used to simulate this machine pair, connected as in Figure 5.12. Condenser water flow-rate was increased to 266 l/s. All other inputs to the machine *pair* - evaporator water flow-rate,[14] evaporator inlet water temperature of the lead machine, and condenser inlet water temperature of the lag machine[15] - remained as before. Compressor vane openings were again set so as to maintain the actual outlet water temperatures of 11,62°C and 6,03°C. Water chilling loads thus remained as before. Normal performance so predicted is given in Table 6.5, compared with that at actual condenser water flow-rate.

As seen in this table, the predicted benefit of restoring condenser water flow-rate to design value was likewise negative - there were further rises of 2,4 and 0,8 per cent in input power of the lead and lag machines respectively. This was because the increased condenser water flow-rate increased the conductances (UAs) of both condensers by 11 per cent, so the condensing pressures decreased by 8 and 4 per cent. As before, the consequent reductions in required head had to be accommodated by the first virtual compressor stages, because the second virtual stages were unregulated.

---

[14] That is, the estimated flow-rate of 118,09 l/s entering the *lead* machine. As recalled from Table 6.4, the estimated flow-rate through the *lag* machine was slightly lower at 115,44 l/s. In this simulation of the two machines connected together, therefore, the flow-rate through the lag machine was brought down to this lower value by specifying that the difference of 2,65 l/s leaked out of the connection between the evaporators of the lead and lag machines.

[15] The assumption that this temperature would remain as before, in spite of the condenser water flow-rate being substantially increased to its design value, was justified as follows. In this underground installation, there were ten machines, all connected to the same heat rejection plant. Eight machines normally operated, so the effect on condenser inlet water temperature of increasing the flow through just two machines would be small.

Table 6.5 Case Study C: Normal Performance of Both Machines Connected in Counterflow Lead-Lag Configuration

		Performance predicted by CHILLER *(with virtual 2-stage compressors)*			
		Lead Machine		Lag Machine	
	UNIT	Normal	Normal (at design condenser water flow)	Normal	Normal (at design condenser water flow)
EVAPORATOR					
Water flow-rate	l/s	118,1	118,1	115,4	115,4
Inlet water temperature	°C	17,70	17,70	11,64	11,62
Outlet water temperature	°C	11,62	11,62	6,03	6,03
Water chilling load	kW(R)	3 006	3 006	2 709	2 700
Water-side fouling factor	m²°C/W	0,000088	0,000088	0,000088	0,000088
Overall conductance (UA)	kW/°C	664,1	664,2	625,0	624,3
Refrigerant pressure	kPaa	416	416	350	350
Refrigerant temperature	°C	9,47	9,47	3,91	3,92
ECONOMISER					
Refrigerant pressure	kPaa	575	542	500	484
Refrigerant temperature	°C	20,50	18,40	15,59	14,52
CONDENSER					
Water flow-rate	l/s	149,8	266,0	156,0	266,0
Inlet water temperature	°C	48,25	46,70	43,54	43,54
Outlet water temperature	°C	54,56	50,28	48,93	46,70
Water heating load	kW(R)	3 961	3 984	3 520	3 517
Water-side fouling factor	m²°C/W	0,000176	0,000176	0,000176	0,000176
Overall conductance (UA)	kW/°C	809,2	901,4	814,2	905,2
Refrigerant pressure	kPaa	1 427	1 310	1 250	1 197
Outlet refrigerant temp.	°C	56,96	53,15	51,10	49,22
COMPRESSOR					
Vane opening	%	54,2	47,6	61,3	56,5
1st stage mass flow-rate	kg/s	22,08	21,76	19,56	19,35
1st stg. inlet vol. flow-rate	m³/s	0,92	0,90	0,96	0,95
1st stage isentropic head	kJ/kg	5,65	4,60	6,19	5,64
1st stage isentr. efficiency	%	43,5	29,1	53,0	43,4
1st stage input power	kW	286,4	344,3	228,5	251,7
2nd stage mass flow-rate	kg/s	29,97	28,87	25,98	25,44
2nd stg. inlet vol. flow-rate	m³/s	0,95	0,99	0,94	0,96
2nd stage isentropic head	kJ/kg	16,88	16,78	16,92	16,87
2nd stage isentr. efficiency	%	75,7	76,5	75,5	75,9
2nd stage input power	kW	668	633	582	566
Input power	kW	955	977	811	817
Suction temperature	°C	9,47	9,47	3,91	3,92
Discharge temperature	°C	76,08	76,26	69,31	69,36
Coefficient of perf. (COP)		3,15	3,08	3,34	3,30

The isentropic heads required of these first stages thus dropped by 19 and 9 per cent respectively. Their vane openings accordingly decreased further, thus further reducing the efficiencies of these stages (especially

that of the lead machine, which reduced from 43 to 29 per cent[16]. Input power to these first stages thus rose by 20 and 10 per cent respectively. These rises were considerably offset by the drops of 5 and 3 per cent in input power to the second, unregulated stages, owing to the combined effect of slightly lower refrigerant mass flow-rates and slightly higher isentropic efficiencies therein.

Again, due to the aforementioned limitations of compressor modelling at part-capacity, it was wise to merely conclude that for identical water chilling loads and otherwise identical inputs, there was no likely advantage in restoring either the water-side fouling factors or the condenser water flow-rate of these machines to the design values! The decreases in input power owing to the reductions in refrigerant mass flow-rate and isentropic head were likely to be mostly or completely nullified by the increase in input power due to decreasing isentropic efficiency as the inlet guide vanes of the regulated first stages closed.[16]

At first sight, this conclusion seemed paradoxical; did this then imply, for example, that the evaporator and condenser tubes should be left uncleaned, or that the condenser water flow-rate should have been left at its reduced value? Upon reflection, there was no thermodynamic advantage in remedying these conditions if each machine remained controlled to maintain a set outlet chilled water temperature.[17] (This "set water temperature" control philosophy is customary for conventional water chilling machines on South African mines.) Either cleaning heat exchanger tubes or restoring design condenser water flow-rate would

---

[16] Again, the key assumption here is that all stages of the real three-stage centrifugal compressors have their peak efficiencies at or near full (design) duty. This is because CHILLER's artificial compressor stage curves, used to model the real three-stage compressors as virtual two-stage ones, have their peak efficiencies at design machine duty, and reduced efficiency elsewhere. See footnote 12 on page 271.

[17] And thus a constant water chilling load if the inputs of evaporator water flow-rate and inlet water temperature are constant.

reduce the lift required of the machines, and hence the isentropic head required of the compressors. This would cause the vanes of the first, regulated compressor stages to close considerably, because these stages, being the only regulated ones,[18] would have to perform *all* the required reduction in isentropic head. Hence the operating points of these regulated stages would quickly enter the regions where the relative decreases in efficiency exceed those in required isentropic head - as illustrated in Figure 6.4.

Multi-stage centrifugal compressors with only their first stages regulated are hereafter termed "first-stage-regulated" compressors. With a machine with such a compressor, therefore, a preferable control philosophy is one which avoids low vane openings. If required lift is reduced, therefore - by cleaning heat exchanger tubes, for example - the only way of avoiding lower vane openings is to simultaneously increase the load (the other component of machine duty).

Optimal Performance of Both Machines Connected Together

As is now shown, therefore, there is advantage in cleaning the tubes and taking other measures to reduce lift if the "set water temperature" control philosophy is abandoned and *load on the machines is kept at the maximum,* thus keeping the compressor vanes open to the maximum.

There are three constraints on maximum loading of conventional machines: that imposed by the rated output of the compressor driving motor; that imposed by the surge lines of each compressor stage; and that imposed by the minimum allowable evaporating temperature.[19] Therefore, the machine pair was simulated again, but this time each machine was

---

[18] Of both the virtual two-stage compressors and the real three-stage compressors.
[19] To avoid freezing in tubes, this must be greater than 0°C, but it may have to be still higher to avoid surge in one or more compressor stages if the *design* evaporating temperature of a machine is well above 0°C.

controlled to accept maximum load, subject to the above three constraints. The predicted performances for this "maximum-load" control philosophy are shown in Table 6.6.

Table 6.6 Case Study C: Maximum-Load Performance of Both Machines Connected in Counterflow Lead-Lag Configuration

		"Maximum-load" performance predicted by CHILLER *(with virtual 2-stage compressors)*			
		Lead Machine		Lag Machine	
	UNIT	Actual fouling factors	Design fouling factors	Actual fouling factors	Design fouling factors
EVAPORATOR					
Water flow-rate	l/s	118,1	118,1	115,4	115,4
Inlet water temperature	°C	17,70	17,70	11,38	10,11
Outlet water temperature	°C	11,38	10,11	4,86	3,71
Water chilling load	kW(R)	3 123	3 753	3 151	3 091
Water-side fouling factor	m²°C/W	0,000439	0,000088	0,000122	0,000088
Overall conductance (UA)	kW/°C	371,7	707,6	606,6	645,5
Refrigerant pressure	kPaa	371	395	332	323
Refrigerant temperature	°C	5,75	7,72	2,26	1,43
ECONOMISER					
Refrigerant pressure	kPaa	592	621	526	512
Refrigerant temperature	°C	21,51	23,27	17,36	16,43
CONDENSER					
Water flow-rate	l/s	149,8	149,8	156,0	156,0
Inlet water temperature	°C	49,75	49,62	43,54	43,54
Outlet water temperature	°C	56,26	57,37	49,75	49,62
Water heating load	kW(R)	4 085	4 862	4 056	3 972,4
Water-side fouling factor	m²°C/W	0,000219	0,000176	0,000267	0,000176
Overall conductance (UA)	kW/°C	733,8	800,1	661,2	807,5
Refrigerant pressure	kPaa	1 499	1 538	1 314	1 279
Outlet refrigerant temp.	°C	59,20	60,38	53,30	52,11
COMPRESSOR					
Vane opening	%	100	100	100	100
1st stage mass flow-rate	kg/s	23,37	28,27	23,14	22,61
1st stg. inlet vol. flow-rate	m³/s	1,00	1,24	1,20	1,20
1st stage isentropic head	kJ/kg	8,10	7,95	8,01	8,01
1st stage isentr. efficiency	%	76,3	77,8	77,6	77,6
1st stage input power	kW	250	289	239	233
2nd stage mass flow-rate	kg/s	32,23	38,95	31,00	30,14
2nd stg. inlet vol. flow-rate	m³/s	0,98	1,12	1,05	1,05
2nd stage isentropic head	kJ/kg	16,83	16,37	16,61	16,61
2nd stage isentr. efficiency	%	76,2	77,8	77,3	77,3
2nd stage input power	kW	712	820	666	648
Input power	kW	962	1 109	905	882
Suction temperature	°C	5,75	7,72	2,26	1,43
Discharge temperature	°C	73,74	73,72	67,57	66,50
Coefficient of perf. (COP)		3,25	3,39	3,48	3,51

The third and fifth columns of this table list these performances for the estimated *actual* fouling factors. Comparing these with the third and fifth columns of Table 6.4, the compressor vane openings increased to 100 per cent. These increases made negligible difference to the performance of the lead machine. The lag machine, though, accepted 16 per cent more load, but drew only 13 per cent more power,[20] so its COP rose by 3 per cent. Under the "maximum-load" control philosophy, therefore, the machine pair, even with the actual fouling factors, was predicted to deliver water one degree colder for no deterioration in overall COP.

The fouling factors were then reduced from actual to design values. *In contrast to the "set water temperature" control philosophy,* the "maximum-load" philosophy yielded further improvements in water chilling loads and COPs, shown in the fourth and sixth columns of Table 6.6. Compared to the maximum-load performances with *actual* fouling factors in the third and fifth columns of this table, the lead machine accepted 20 per cent more load and drew 15 per cent more power, so its COP rose by 4 per cent. The lag machine accepted 2 per cent *less* load and drew 3 per cent less power, so its COP rose by 1 per cent. Combined load rose by 9 per cent and input power by 7 per cent, so overall COP rose by 2 per cent.

Finally, the condenser water flow-rate was restored to its design value. Again compared to the maximum-load performances with actual fouling factors in Table 6.6, the lead machine, now limited by rated compressor driving motor output power of 1 120 kW, accepted 24 per cent more water chilling load, but drew only 17 per cent more power. The lag machine, now limited by its evaporating refrigerant temperature reaching the allowable minimum of 1°C, accepted 1 per cent more load and drew 3 per cent less power. Outlet chilled water temperature dropped from 3,71°C to

---

[20] Mainly because the isentropic efficiency of the first virtual compressor stage improved from 60 to 78 per cent.

3,31°C. The result was that combined water chilling load rose by 12 per cent, while combined input power rose by only 7 per cent, so combined COP rose from 3,36 to 3,52 - an improvement of 5 per cent. Under the "maximum-load" control philosophy, *cleaning the tubes and restoring design condenser water flow-rate was predicted to yield 12 per cent more water chilling load at a 5 per cent improvement in COP!* In contrast, with the "set water temperature" control philosophy, the same remedial actions yielded no improvement in load and a somewhat worse predicted COP.

Again, the accuracy of these predictions is directly dependent on that of the compressor modelling.[21] (Also, for more accurate predictions, the performance of the entire underground installation under the "maximum-load" philosophy would need to be simulated.) The benefits of this alternative, "maximum-load" control philosophy are nevertheless clear. As recalled from Section 4.1.2, Chapter 4, optimal performance from the mine's viewpoint is likely to be the specified or maximum delivery of chilled water, at the specified or lowest possible temperature, without jeopardising machine effectiveness and availability. The "maximum-load" control philosophy achieves this - here, by achieving the lowest possible temperature of the actual flow-rate of chilled water - *and moreover achieves the optimum COP of which the machines are capable.*

Whereas the fouled heat exchangers and low condenser water flow-rate did not constitute faults under the "set water temperature" control philosophy, they certainly did under the "maximum-load" control philosophy, because they prevented the predicted gain of the order of 12 per cent in water chilling load.

---

[21] Particularly the locations of the surge points on the compressor characteristic curves; in reality, one or more compressor stages might reach these points before the machines reach the other constraints of compressor driving motor rating or minimum evaporating temperature.

In sum, the benefits of this alternative, "maximum-load" control philosophy for conventional machines are as follows. First, the machine *always* accepts the maximum water chilling load possible for the prevailing operating conditions. Other things being equal, this means, as in this case study, that if heat exchanger tubes are cleaned, the benefit of lower chilled water delivery temperature is immediately obtained. Alternatively, if it is desirable to increase chilled water flow-rate, the machine will chill this new flow to the maximum possible extent. Second, particularly for conventional machines with multi-stage, first-stage-regulated compressors, the optimal machine COP is likely to be attained, because the compressor inlet guide vanes are maximally open, hence maximising the efficiency of the regulated first stage. Optimal performance in two aspects - water chilling capacity and COP - results.

Assessment of Performance of Both Machines

The conclusion was clear: with the existing "set water temperature" control philosophy, no advantage in performance, even from an energy-saving point of view, was likely in either cleaning heat-exchanger tubes[22] or restoring the low condenser water flow to design value. In fact, total input power was predicted to increase! Thus the higher-than-design fouling factors were actually an advantage under this operating regime - they reduced input power! This was a consequence of the limitations of multi-stage, first-stage-regulated centrifugal compressors at part-duties. The appropriate strategy was to alter the control philosophy to that of "maximum load" for both machines; optimal performance in respect of both capacity and COP was then predicted. Only with this revised control philosophy was there any benefit in cleaning the heat exchanger tubes.

---

[22] This does not mean to imply that heat-exchanger surfaces should not be cleaned. Excessive fouling should be removed for other reasons, for example to minimise corrosion of tubes.

6.2.4 Case Study E: Overcharge of Refrigerant

How can apparent machine performance be assessed when it cannot be verified - that is, when actual performance cannot be independently and precisely ascertained through the enhanced Thorp method or machine modelling? It may nevertheless be possible, using simplified modelling, to ascertain a *range* in which actual performance must lie. The upper and lower limits of this range can then be assessed.

It is recalled from Chapter 5 that for Case Study E, one or both apparent water flow-rates were unacceptably erroneous, but the overcharge of refrigerant in this machine prevented use of the enhanced Thorp method to ascertain actual performance and so verify apparent performance. Use of the inexact Thorp method indicated, though, that the liquid fraction in the refrigerant leaving the evaporator was high enough to raise concern about possible damage to the compressor. Unfortunately, the available version of CHILLER could not be used to ascertain actual performance by machine modelling; its model of a centrifugal compressor stage did not account for the presence of liquid in the vapour being compressed. Nevertheless, it was desirable to obtain some indication of the performance *without* refrigerant overcharge, as well as the normal performance, in order to estimate the shortfall in performance due to the refrigerant overcharge and other faults possibly present, and hence to determine what corrective action was warranted.

The evaporator and condenser water flow-rates in a conventional machine are related through its overall energy balance. Therefore, as shown in Appendix 20, if inlet and outlet water temperatures and apparent input power are known with acceptable accuracy, the *implied* condenser water flow-rate corresponding to the apparent evaporator water flow-rate can be determined, and vice versa.

Hence, as deduced in Appendix 20:

A) if the apparent condenser water flow-rate of 85,5 l/s had been accurate, the implied, corresponding *evaporator* water flow-rate would have been very low at 35 l/s: 58 per cent of its design value. The corresponding COP would have been 1,61, this being the apparent rejection-load COP, $COP_{[JB]p}$, in Table 5.7;

B) on the other hand, if the apparent evaporator water flow-rate of 51,6 l/s had been accurate, the implied, corresponding *condenser* water flow-rate would have been 110,4 l/s: 87 per cent of its design value. The corresponding COP would have been 2,37, this being the apparent evaporator-load COP, $COP_{[EB]p}$, in Table 5.7. As noted in Chapter 5, this second scenario seemed more probable, because it implied a liquid fraction of only 13% - not 23% - in the refrigerant vapour entering the compressor.

It therefore seemed reasonable to assume that the probable lower limit of actual performance was this second scenario. In Chapter 5, it was concluded from the COP range plot that the actual COP had to be significantly below the full-duty design COP of 3,43. Therefore, it was assumed that the probable upper limit of actual performance was at the design evaporator water flow-rate of 60,6 l/s, which similarly implied a COP of 2,79 (81 per cent of the design value) and a condenser water flow-rate of 123,1 l/s (97 per cent of the design value).

The CHILLER program was then used to predict the following performances *without* refrigerant overcharge, with the actual evaporator and condenser inlet water temperatures, and the inlet guide vanes on the first compressor stage controlled to maintain the actual outlet chilled water temperature of 5,27°C:

1) performance at the "lower probable" conditions: that is, with the apparent evaporator water flow-rate of 51,6 l/s; the implied, corresponding condenser water flow-rate of 110,4 l/s; and the

corresponding water-side fouling factors, calculated as described in Appendix 20 by the methods of Appendix 21;

2) performance at the "higher probable" conditions: that is, with the design evaporator water flow-rate of 60,6 l/s; the implied, corresponding condenser water flow-rate of 123,1 l/s; and the corresponding water-side fouling factors, calculated as for 1);

3) normal performance - that is, with the water-side fouling factors set to design values - under the operating regime of 1);

4) normal performance under the operating regime of 2).

No compressor characteristic performance curves were available from the manufacturer. Again, therefore, those artificial curves of CHILLER which best matched the limited amount of design, full-duty performance data furnished by the manufacturer were used. The predicted performances without refrigerant overcharge at the "lower probable" and "higher probable" water flows and fouling factors are listed in Table 6.7, as well as the apparent and design performances for comparison.

Predicted Performance with No Overcharge of Refrigerant

As seen in Table 6.7, the first prediction of CHILLER, for the "lower probable" conditions, yielded an input power of 693 kW, which was 20 per cent less than the apparent value of 871 kW. The second prediction, for the "higher probable" conditions, yielded an input power of 785 kW - 11 per cent less than the apparent value of 871 kW. These predictions therefore indicated the probable range of power wastage due to the overcharge of refrigerant, assuming that apparent input power was accurate.

Table 6.7 Case Study E: Predicted Performances at "Probable" Conditions and No Refrigerant Overcharge

QUANTITY	UNIT	Apparent performance *(with refrig. overcharge)*	Predicted performance *(no refrig. overcharge)* "Lower probable" flows and foul. factors	Predicted performance *(no refrig. overcharge)* "Higher probable" flows and foul. factors	*Design full-duty values for comparison*
EVAPORATOR					
Water flow-rate	l/s	51,6	51,6	60,6	*60,6*
Inlet water temperature	°C	14,85	14,85	14,85	*18,89*
Outlet water temperature	°C	5,27	5,27	5,27	*5,00*
Water chilling load	kW(R)	2 070	2 070	2 430	*3 524*
Water-side fouling factor	m²°C/W	-	0,000368	0,000300	*0,000176*
Refrigerant pressure	kPaa	316,1	338	338	*342,4*
Refrigerant temperature	°C	no meas. point	2,80	2,79	*3,22*
ECONOMISER					
Refrigerant pressure	kPaa	no meas. point	616	640	*707,4*
Refrigerant temperature	°C	26,50	24,25	24,36	*28,07*
CONDENSER					
Water flow-rate	l/s	85,5	110,4	123,1	*126,2*
Inlet water temperature	°C	34,78	34,78	34,78	*40,56*
Outlet water temperature	°C	41,14	40,76	41,02	*49,14*
Water heating load	kW(R)	2 277	2 762	3 214	*4 533*
Water-side fouling factor	m²°C/W	-	0,00100[23]	0,00100[23]	*0,000352*
Refrigerant pressure	kPaa	1 302	1 172	1 221	*1 315,5*
Outlet refrig. temperature	°C	51,57	48,32	50,07	*53,33*
COMPRESSOR					
Vane opening	degr.	50	50	63	*100*
1st stg. inlet vol. flow-rate	m³/s	-	0,80	0,95	*1,58*
1st stage isentropic head	kJ/kg	-	10,51	11,20	*12,74*
1st stage isentr. efficiency	%	-	54,1	59,2	*72,5*
2nd stg. inlet vol. flow-rate	m³/s	-	0,59	0,67	*1,01*
2nd stage isentropic head	kJ/kg	-	12,19	12,15	*11,47*
2nd stage isentr. efficiency	%	-	61,1	65,1	*72,5*
Input power	kW	871	693	785	*1 009*
Suction temperature	°C	2,82	2,80	2,79	*2,22*
Discharge temperature	°C	56,20	73,69	72,35	*60,61*
Coefficient of perf. (COP)		2,37	2,99	3,10	*3,43*

Predicted Normal Performance

The third and fourth predictions of CHILLER, of normal performance with the "lower probable" and "higher probable" water flow-rates, and design

---

[23] From Appendix 21, these corresponding fouling factors were 0,00128 and 0,00113 m²°C/W, but the available version of the CHILLER program allowed a maximum of 0,0010 m²°C/W.

fouling factors, are listed in Table 6.8. On comparison with Table 6.7, it is seen that predicted normal performance under otherwise identical conditions yielded a *smaller* saving in input power, in spite of the evaporator and condenser water-side fouling factors being reduced twofold and threefold respectively!

Table 6.8 Case Study E: Predicted Normal Performances at "Probable" Water Flow-Rates

QUANTITY	UNIT	Apparent performance (with refrig. overcharge)	Predicted normal performance (no refrig. overcharge) "Lower probable" water flow-rates	Predicted normal performance (no refrig. overcharge) "Higher probable" water flow-rates	*Design full-duty values for comparison*
EVAPORATOR					
Water flow-rate	l/s	51,6	51,6	60,6	*60,6*
Inlet water temperature	°C	14,85	14,85	14,85	*18,89*
Outlet water temperature	°C	5,27	5,27	5,27	*5,00*
Water chilling load	kW(R)	2 070	2 070	2 430	*3 524*
Water-side fouling factor	m²°C/W	-	0,000176	0,000176	*0,000176*
Refrigerant pressure	kPaa	316,1	350	347	*342,4*
Refrigerant temperature	°C	no meas. point	3,91	3,63	*3,22*
ECONOMISER					
Refrigerant pressure	kPaa	no meas. point	505	574	*707,4*
Refrigerant temperature	°C	26,50	20,35	20,40	*28,07*
CONDENSER					
Water flow-rate	l/s	85,5	110,4	123,1	*126,2*
Inlet water temperature	°C	34,78	34,78	34,78	*40,56*
Outlet water temperature	°C	41,14	40,96	41,08	*49,14*
Water heating load	kW(R)	2 277	2 813	3 246	*4 533*
Water-side fouling factor	m²°C/W	-	0,000352	0,000352	*0,000352*
Refrigerant pressure	kPaa	1 302	1 043	1 063	*1 315,5*
Outlet refrig. temperature	°C	51,57	43,41	44,19	*53,33*
COMPRESSOR					
Vane opening	degr.	50	28	38	*100*
1st stg. inlet vol. flow-rate	m³/s	-	0,76	0,90	*1,58*
1st stage isentropic head	kJ/kg	-	8,36	8,78	*12,74*
1st stage isentr. efficiency	%	-	32,9	37,4	*72,5*
2nd stg. inlet vol. flow-rate	m³/s	-	0,64	0,73	*1,01*
2nd stage isentropic head	kJ/kg	-	12,17	12,08	*11,47*
2nd stage isentr. efficiency	%	-	63,6	67,6	*72,5*
Input power	kW	871	744	816	*1 009*
Suction temperature	°C	2,82	3,91	3,63	*2,22*
Discharge temperature	°C	56,20	77,61	73,90	*60,61*
Coefficient of perf. (COP)		2,37	2,78	2,98	*3,43*

The cause was the same as for Case Study C - the vanes of the regulated first stage closed further to accommodate the reduction in required lift. Consequently, even though the inlet volumetric flow-rate of this stage dropped relatively little, the isentropic efficiency reduced drastically to between 33 and 37 per cent (for the "lower probable" and "higher probable" water flows respectively). For the "lower probable" water flows, this reduction in isentropic efficiency is illustrated in the lower plot of Figure 6.5. As in Case Study C, therefore, reducing the fouling factors to normal (design) values was predicted to yield a power penalty rather than a power saving.

Two other points emerged from Figure 6.5. First, in contrast to the first stage, the inlet volumetric flow-rate of the second, unregulated compressor stage increased slightly.[24] The isentropic efficiency of this stage increased correspondingly, but the resulting power decrease was not sufficient to offset the power increase in the first stage. Second, at the lower vane opening, the isentropic head developed by the first stage reduced, so the unregulated second stage developed most of the total isentropic head required.

As Shone (1983) has shown, if the vane opening of the first stage of a centrifugal compressor is reduced to the point where the head required of an unregulated second or subsequent stage exceeds its capability, that unregulated stage will surge. This was the case here: the upper plot of Figure 6.5 shows that the operating point of the second stage was at almost maximum head, and hence almost at its surge point. Fortunately, the operating point of this stage for corresponding normal performance, with design fouling factors, was slightly further away from its surge point,

[24] The specific volume of the vapour entering this stage increased, because of both the lower pressure (due to the lower first stage head) and the higher temperature (due to the lower first stage efficiency) of the vapour leaving the first stage.

but the reverse would have occurred if the reduction in head developed by the first stage had exceeded the *total* required reduction in isentropic head.

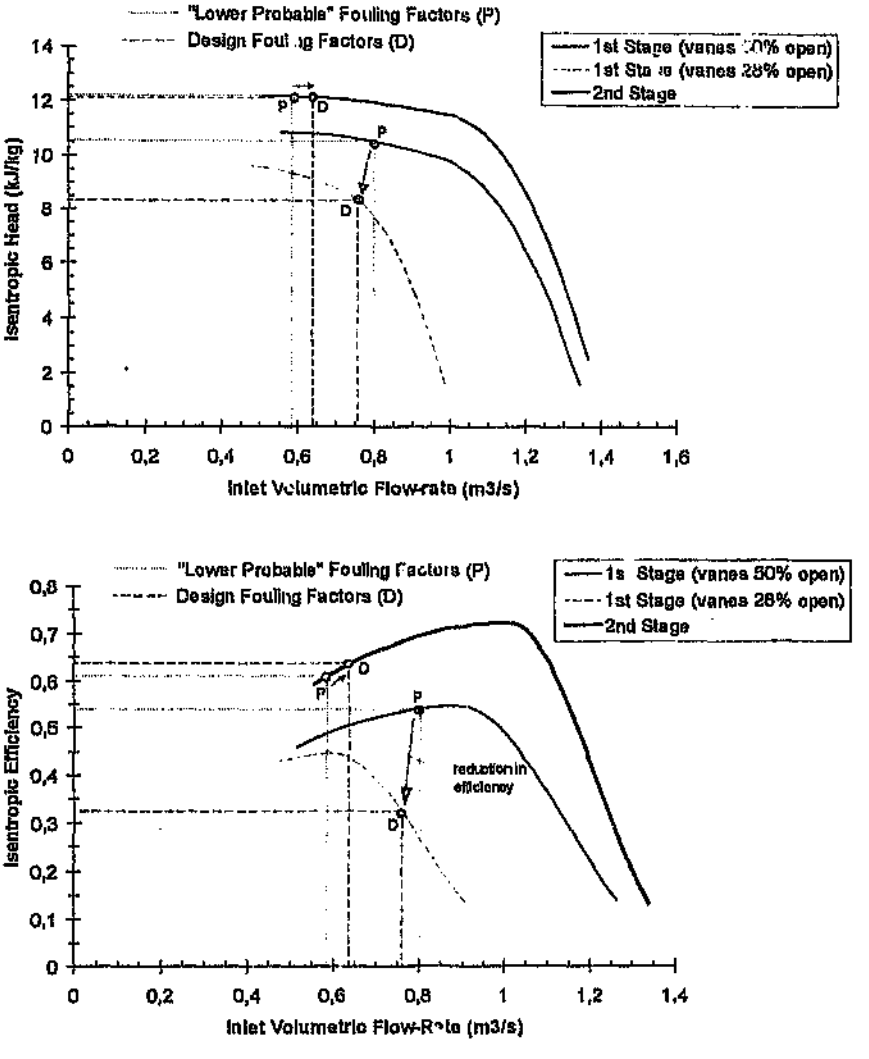

Figure 6.5 Case Study E: No Refrigerant Overcharge: Operating Points on CHILLER's Compressor Characteristic Curves at "Lower Probable" Water Flow-Rates

In reality, under these conditions, the controller of the machine will open its hot gas bypass valve (shown in Figure 3.18) sufficiently to keep the operating point of the second stage safely away from its surge point. Here, therefore, this would have occurred for *all* predicted performances in Tables 6.3 and 6.4. As explained in Chapter 3, hot gas bypass increases input power without any increase in refrigerating load, and so if the effect of this hot gas bypass had been modelled,[25] predicted COPs would have been lower than in Tables 6.3 and 6.4. Thus, ironically, simply restoring the refrigerant charge to normal would probably have necessitated bypassing hot gas, thereby partially or wholly nullifying the anticipated power saving!

As for the other case studies, the accuracy of the quantitative predictions here was directly dependent upon the degree of correspondence between the artificial compressor stage curves of CHILLER and those of the real machine. Again, the manufacturer had quoted no part-duty performance data, so the degree of correspondence between the artificial and actual curves of the first compressor stage at part-capacities was not known. As for Case Study C, therefore, it was wise to draw no conclusions directly dependent on the accuracy of the quantitative predictions of compressor performance. It was prudent to merely conclude that to protect the compressor, the refrigerant charge should be restored to normal; the resulting power saving, though, was uncertain because of the probability of the machine having to bypass hot gas to keep the compressor stable.

Predicted Optimal Performance

As for Case Study C, it was thus seen that if this machine were required to maintain a specified outlet chilled water temperature - that is, to operate under a "set water temperature" control philosophy - the compressor vane

---

[25] The available version of CHILLER had no facility to model the effect of hot gas bypass.

opening would be considerably below 100 per cent. The operating point of its first, regulated stage would thus be in the region where the relative decrease in isentropic efficiency exceeded that in required isentropic head. As for Case Study C, therefore, it was preferable to adopt a "maximum-load" control philosophy for this machine - which had also been manufactured before 1980, and was therefore likely to have been designed for optimum efficiency at full load (Austin, 1991).

Accordingly, CHILLER was used to predict normal performance under this alternative control philosophy, for the same inputs as before. Here, for the "higher probable" water flows (that through the evaporator being the design value of 60,6 l/s), the compressor vane opening could increase to 70 per cent before the evaporating temperature decreased to the minimum allowable value of 1°C. The resulting benefits of this "maximum-load" control philosophy were significant. Outlet chilled water temperature decreased to 2,83°C, water chilling load increased to 3 049 kW(R), and COP increased to 3,42. Compared to the predicted normal performance with "higher probable" water flows in Table 6.8, improvements in water chilling load and COP were 25 and 15 per cent respectively! Moreover, at this increased vane opening, the greater proportion of total head developed by the first stage moved the operating point of the second stage safely away from its surge point. For the "lower probable" water flows, CHILLER's predictions were similar.

Compressor vane opening was still considerably below 100 per cent, though, so a further idea was considered to improve machine utilisation. This machine was one of four in its water chilling plant, with the water circuits connected in parallel as in Figure 3.19. Normal performance was next predicted, therefore, with the evaporator water flow-rate increased from 60,6 l/s to 80 l/s. The total design chilled water flow-rate of 240 l/s could then be delivered by *three* machines, freeing one machine for maintenance during normal working hours. For the other inputs remaining

as before,[26] compressor vane opening could now increase to 97 per cent, being limited there by the refrigerant evaporating temperature again reaching 1°C.[27] Predicted outlet chilled water temperature, water chilling load and COP were 3,47°C, 3 812 kW(R) and 3,49 respectively. Compared to predicted normal, maximum-load performance at the "higher probable" (design) evaporator water flow-rate of 60,6 l/s (see previous paragraph), the further improvements in water chilling load and COP were 25 and 2 per cent respectively.

Here, the maximum-load control philosophy thus offered improved availability (by reducing the likelihood of surge), as well as greatly improved effectiveness and significantly improved quality of performance.

Assessment of Performance

The "lower probable" and "higher probable" limits of the performance of this machine were therefore assessed as follows. The excess refrigerant had to be removed at the earliest opportunity, both to avoid possible damage to the compressor and to eliminate the consequent, quite unnecessary input power penalty of the order of at least 10 per cent. As for the previous case study, cleaning heat exchanger tubes was predicted to yield no thermodynamic benefit unless the "maximum-load" control philosophy was adopted. Here, very significant improvements in water chilling capacity and COP were predicted. In particular, the possibility existed of letting three machines perform the task of four, freeing one machine for maintenance during normal working hours.

---

[26] Except that the condenser water flow-rate was increased from 110,4 l/s to the design value of 126,2 l/s.

[27] At which point the compressor driving motor had reached 98 per cent of its rated output power.

6.3 Review

In the case studies of this chapter, it has been seen how performance of conventional machines is assessed. It is vital to bear in mind that accuracies of quantitative predictions of normal or optimal performance, and quantitative comparisons with actual performance, critically depend on accuracy of compressor characteristic performance curves.

The first two case studies involved machines operating at full compressor capacity. The first, Case Study A, concerned a machine operating at close to design duty. This machine had been designed for efficient operation at specified part-duties as well as full duty, and employed a single-stage centrifugal compressor. Here, an expanded, fundamental machine model showed that slight flooding of the condenser with liquid refrigerant did not amount to a fault. Also, keeping heat exchanger tubes as clean as possible, so minimising water-side fouling factors, was predicted to minimise input power and hence optimise performance. The second such case study, G, concerned a machine with a two-stage, first-stage-regulated centrifugal compressor. The evaporator and condenser water flow-rates turned out to be 23 and 71 per cent above their design values. This amounted to a badly off-design operating regime, which afforded no benefit and was wholly responsible for the machine being unable to attain its specified outlet chilled water temperature.

The other case studies, C and E, involved machines with three- or two-stage, first-stage-regulated centrifugal compressors operating at *part*-capacity (i.e. with the inlet guide vanes on the first stages partially open). Moreover, these machines were manufactured before 1980, so their compressors were thus likely to have been designed for optimal efficiency at full capacities. First, comparisons of actual with predicted normal performance have shown that if a machine with such a compressor operates at part-duty with partially open inlet guide vanes under the customary "set water temperature" control philosophy, no improvement in

quality of performance is likely if heat exchanger tubes are cleaned or other measures are taken to reduce lift. This is due to the rapid deterioration in efficiency of the regulated first stage, which has to perform all the regulation by closing its vanes further and rapidly. (Hence this phenomenon is most likely to occur with multi-stage, first-stage-regulated centrifugal compressors.) Second, comparisons of actual and predicted normal performance with predicted performance under an alternative "maximum-load" control philosophy have shown that operating such machines at maximum load (either lowest outlet chilled water temperature, or higher chilled water flow-rate) offers optimal performance in both effectiveness (load) and quality (COP). Cleaning heat exchanger tubes or undertaking other measures to reduce lift yields immediate benefits in such effectiveness and quality of performance. *The "maximum-load" control philosophy is only of benefit when, under a "set water temperature" control philosophy, the vanes of the regulated first compressor stage are not fully open, as happened with Case Studies C and E.* This is because these vanes must have opportunity to open further.

Finally, where it is not possible to precisely verify apparent performance of conventional machines by either the enhanced Thorp method or the available computer-based machine models, it has been shown that simplified machine modelling based on the overall energy balance may yield a probable range of actual performance. Machine modelling can then predict normal or optimal performance at the upper and lower limits of this range, enabling assessment of these limits.

In the case studies of this chapter, faults have been detected by manual reasoning on the basis of discrepancies between actual and predicted normal or optimal performance. The next chapter reviews established methods of fault diagnosis, shows where the work of the thesis is valuable here, and examines the extent to which fault diagnosis has been automated.

7. DIAGNOSING FAULTS IN WATER CHILLING MACHINES

The case studies in the previous two chapters have illustrated how performance assessed as unsatisfactory may be due to an off-design operating regime, machine faults, or both. Actual machine performance is ascertained as accurately as possible by the methods of Chapter 5. Off-design inputs are detected here. Actual performance is then assessed by comparing it with normal or optimal performance, predicted by the methods of Chapter 6, under identical or alternative operating regimes. Abnormalities in process parameters or state variables are detected here, and those constituting faults diagnosed if performance is unsatisfactory. This final step of fault diagnosis, which constitutes the ultimate benefit of performance assessment and should ideally be automated, is the subject of this chapter. Methods of fault diagnosis, and the automation thereof, in vapour-compression water chilling machines are reviewed, and it is shown where the work of the thesis is of value here.

7.1 Definitions and Classes of Fault Detection and Diagnosis

In the South African mining industry, two computer-based, off-line procedures for assessing performance and diagnosing faults in conventional water chilling machines have been reported. The earlier one is by Hall and Unst [1] (1976) and the later and more comprehensive one is by Hemp et al. (1986). Other applicable methods will be examined as well, but the basic definitions and classes of fault detection and diagnosis will first be outlined.

Following Isermann (1982), fault *detection* is defined as identification of the presence of a fault, its type and the time of its occurrence. Fault *diagnosis*, the succeeding step, is defined as identification of the location, size and cause of a fault. Fault diagnosis therefore includes fault detection as a prior step. Isermann identifies four classes of fault diagnosis, utilising the following variables:

1) measurable quantities (inputs and outputs);

2) non-measurable state variables;

3) non-measurable process parameters;

4) non-measurable characteristic quantities (termed *measures of quality of performance* in this thesis).

Methods of fault diagnosis in water chilling machines, where the static performance is of chief interest, belong mainly to classes 1), 3) and 4). Both established and some recently-proposed methods are now reviewed, and the quantities of actual performance utilised, the manner of obtaining the corresponding quantities of normal (fault-free) performance, and the fault symptoms and other knowledge of the process used will be examined.

Accuracy of measured quantities is, of course, an absolute prerequisite for valid fault diagnosis. Where calibration of instruments is not assured, the methods offered in Chapter 5 for independently ascertaining actual performance are of material aid in identifying any unacceptably erroneous such quantities.[1] In this chapter, it is assumed that all measurements, and quantities derived or estimated therefrom, are sufficiently accurate for performance assessment and fault diagnosis. Furthermore, the term "fault" has the meaning assigned to it in Chapter 4: an abnormal, undesirable value of a state variable or process parameter, contributing to unsatisfactory performance.

[1] The procedures of Hall and Unsted (1976) and Hemp et al. (1986) first check the measurements for obvious absurdities, and then use Thorp's original method (Thorp, 1974) to check for errors in water-circuit measurements. As shown in Chapter 4, this original method is deficient and can lead to erroneous conclusions.

7.2 Fault Diagnosis Directly from Measurements

Many common faults in refrigerating machines reveal themselves through well-known symptoms. Gluckman (1986) gives a list, summarised in Table 7.1, of some common faults and their primary symptoms.

Table 7.1 Primary Symptoms of Common Faults in Refrigerating Machines (Gluckman, 1986)

Fault	Primary Symptoms
Condenser air blanketing (non-condensable gas in condenser)	high condensing pressure, apparent liquid subcooling
Liquid flooding in condenser	high condensing pressure, apparent liquid subcooling
Condenser water-side fouling	high condensing pressure, no liquid subcooling, high water pressure drop
Low condenser water flow[2]	high condensing pressure, no liquid subcooling, low water pressure drop
Oil in refrigerant in evaporator	low evaporating temperature[3]
Insufficient refrigerant charge	low evaporating pressure

Common faults such as in Table 7.1 can be inferentially diagnosed directly from measured quantities or elementary derivations therefrom, such as saturated refrigerant temperature corresponding to a measured pressure. Gluckman (1986) notes that the main drawback is that little can be learned about "compressor problems" (faults in compressors), apart from inferences on the cause of high superheat.[4]

A cautionary observation must immediately be made here. The words "high" and "low" in Table 7.1 imply qualitative comparisons with *normal* values. Comparisons are commonly and intuitively made with design values, *but normal values are not synonymous with design values unless the operating regime* (the inputs and control philosophy) *is at design*

---

[2] This is an off-design input, *not* a machine fault.

[3] For ammonia as refrigerant, because oil tends to foul the heat-transferring surfaces. Oil dissolves in halocarbon refrigerants, so the symptom is different for them.

[4] For example, abnormally high superheat at the outlet of a multi-stage centrifugal compressor is symptomatic of leakage of vapour from higher to lower stages through worn labyrinth shaft seals.

specification. Furthermore, if some inputs or the control philosophy do deviate from design specification, such deviations - and not machine faults - may be the whole or a partial cause of output quantities deviating from design values, and of unsatisfactory performance.

7.2.1 Deviations from Design Values

The deviations in Table 7.2 below, reported by the programs of Hall and Unsted (1976) and Hemp et al. (1986) to aid the user in inferential fault diagnosis, provide an illustration of this. Deviations 1 and 2 in this table are the most useful ones, being of *input* quantities from their design values. Such reported deviations at least draw the user's attention to off-design inputs, which may be the primary or at least a contributory cause of unsatisfactory performance.

Table 7.2 Deviations Reported by Programs of Hall and Unsted (1976) and Hemp et al. (1986)

	DEVIATION IN MEASURED QUANTITY	Hall and Unsted (1976)	Hemp et al. (1986)
	EVAPORATOR AND CONDENSER		
1.	Water flow-rate < 50% of design value	√	
2.	Inlet water temperature > 3°C above or below design value	√	
3.	Refrigerant pressure > 5% above or below design value	√	
4.	Water pressure drop too low or too high		√
5.	Difference between temperature of condensing/evaporating refrigerant, and saturation temperature at refrigerant pressure, too high		√
	CONDENSER		
7.	Outlet refrigerant temperature > saturation temperature at condensing pressure, or more than 1°C below this	√	
	COMPRESSOR		
	Excessive superheat at compressor inlet		√
8.	Outlet superheat > 2°C above or below design value	√	

Deviations 3 through 8 in Table 7.2 are of output quantities. As just mentioned, they may not be due to faults unless the operating regime conforms to design specification. This is because these deviations are from *design* values, not from the normal values yielded by the machine

performing normally (without faults) under the identical operating regime. *The more the actual operating regime deviates from its design specification, the less informative and more misleading Deviations 3 through 8 are as indicators of possible faults.*

For example, all state variables and process parameters may be at their design values, meaning that the machine is performing normally with no faults. The operating regime may furthermore be at design specification except for two inputs: a condenser water flow-rate of less than 80 per cent of design value (Deviation 1 in Table 7.2) *and* an evaporator inlet water temperature more than 3°C above design value (Deviation 2). If the control philosophy attempts to maintain a specified outlet chilled water temperature, Deviation 2 causes the water chilling load to rise above design value. The load in the condenser rises correspondingly, and this effect combined with that of Deviation 1 may well cause refrigerant pressure in the condenser to rise more than 5 per cent above its design value (Deviation 3) and compressor outlet superheat to exceed its design value by more than 2°C (Deviation 8). Deviations 3 and 8 are then not due to faults, but due to an off-design operating regime - two off-design inputs!

As recalled from Table 2.1, diurnal and seasonal duties imposed on many mine water chilling plants, particularly those on surface, are variable. The operating regimes of at least some water chilling machines within such plants will hence vary substantially from design specification for considerable portions of their daily or yearly operating periods. For such machines, fault diagnosis on the basis of comparing measured quantities with their design values is misleading and invalid; comparisons must be made with corresponding *normal* values.

7.2.2 Deviations from Normal Values

Grimmelius et al. (1995) have made a comprehensive and researched attempt at fault diagnosis from qualitative comparisons of measured with

corresponding normal quantities. The water chilling machine involved was custom-built, with two reciprocating compressors. Twenty *diagnostic variables*, consisting of measured inputs and outputs and elementary derivations therefrom,[5] were monitored for measurable deviations from normal values. These normal values were obtained from a linear regression model, developed from 8 000 sets of measured data under fault-free conditions. This model predicts the normal values of 19 measurable outputs[6] as functions of inlet water temperatures at the evaporator and condenser.[7] No less than 37 possible "failure modes" (manifestations of faults) for static performance were identified. The effects of each such mode on the 20 diagnostic variables were analysed and these analyses checked by interviews with experts. A qualitative *failure mode symptom matrix* was hence constructed, an extract of which is in Table 7.3.

This symptom matrix was validated by deliberately maladjusting machine controls to simulate failure modes.[8] A computerised "fuzzy-pattern" recognition routine determines the probability of a failure mode from similarities between the symptom pattern arising from the measurements and those of the 37 pre-defined failure modes. Grimmelius et al. note that this recognition routine tends to prematurely conclude that faults with few symptoms are present, but that it is being developed further to improve diagnostic capacity.

---

[5] Compressor pressure ratio; superheat at compressor outlet; subcooling of refrigerant at condenser outlet; difference between refrigerant and heat-removing water temperatures at condenser outlet; temperature ranges of heat-removing water and water being chilled.

[6] Oil temperatures and pressure; refrigerant pressures and temperatures; amount of acting cylinders in compressors; and electrical current of compressor driving motors.

[7] The flows of water being chilled and of heat-removing (condenser) water always remained constant, and so were not included as inputs in the regression model.

[8] Where the actual symptoms did not match those in the initial matrix, closer analyses were made to determine the reasons, and the matrix was then changed appropriately.

Table 7.3 Extract from Failure Mode Symptom Matrix for Water Chilling Machine (Grimmelius et al., 1995)

Failure Mode	Compressor				Evaporator			Condenser	
	Inlet pressure	*Electrical power*	*Superheat*	*(other measurements)*	*Outlet Pressure*	*Chilled water temp. change*	*(other measurements)*	*Subcooling at outlet*	*(other measurements)*
1a	<	<	>		>	<			
1b	>		>		>	<			
2		>						<	
3		<	>			<			
4	>	>	<		>	>			
5	<	<	>		<	>			

<: decreased value due to fault >: increased value due to fault

a: Compressor, suction side, increase in flow resistance
1b: Compressor, discharge side, increase in flow resistance
2: Condenser, water side, increase in flow resistance
3: Refrigerant liquid line from condenser, increase in flow resistance
4: Thermostatic expansion valve, control unit: power element loose from pipe
5: Evaporator, chilled water side, increase in flow resistance

Even if the correct, corresponding normal quantities are available, though, fault detection and diagnosis from qualitative symptoms in measurable quantities has its limitations. First, unanticipated faults may produce unfamiliar symptoms which are difficult to interpret. Second, different faults can sometimes produce the same obvious, primary symptoms. For example, as seen in Table 7.1, both non-condensable gas in the condenser and liquid flooding therein produce the same primary symptom of high condensing pressure and apparent liquid subcooling. Even with the comprehensive symptom matrix of Table 7.3, some failure modes[9] proved indistinguishable because of identical or empty symptom patterns. Additional analysis on the basis of more information is then necessary to distinguish between such faults.[10] Finally, when multiple faults exist, they are liable to interfere with each other's symptoms unless their symptoms

[9] Which Grimmelius et al. (1995) unfortunately do not specify.

[10] For example, in Case Study A in Chapter 5 (see footnotes on page 242), the symptom of high condensing pressure and apparent liquid subcooling occurred. However, actual condenser flooding was confirmed because outlet refrigerant temperature was lower than outlet water temperature.

involve no common quantities. An example of this is given later, in the discussion on Table 7.4 on page 314.

These limitations may be partially overcome if the quantitative information in measured quantities is used to impart *quantitative* content to fault symptoms. Here, Yu and Lee (1991) propose an approach for chemical processes in general. Their approach uses a simple qualitative model, the *signed directed graph* (SDG) in tree form for each fault deemed possible, in order to systematise fault diagnosis from measurements. The quantitative information in measurements is utilised in the form of *ratios* of steady-state deviations (from normal[11]) of adjacent measured variables in each such tree. Membership functions of fuzzy-set theory are assigned to these deviation ratios (termed *gains* by Yu and Lee) to account for the degree of certainty of the quantitative information. These membership functions are then integrated into the branches of the trees for each possible fault; one such tree from Yu and Lee's own example of a continuous stirred-tank reactor is reproduced in Figure 7.1.

Actual faults are diagnosed by computing the actual deviation ratios of the on-line measurements, and then identifying that fault tree whose membership functions are most consistent with these actual deviation ratios. As Yu and Lee show, this technique can distinguish between faults producing the same *qualitative* symptoms wherever one or more such membership functions in the fault trees differ significantly. Moreover, the technique can, in principle, diagnose anticipated multiple faults if the corresponding SDG-type trees with multiple faulty variables are available.

However, the SDGs and membership functions for each possible fault - and each possible combination of multiple faults - have to be derived from

---

[11] Actually *deviation indices*, defined as (measured z – nominal z)/(threshold for z). Unfortunately, Yu and Lee (1991) do not define the meanings of "nominal" and "threshold". It is thus presumed that "nominal" means "normal".

either a quantitative, mathematical process model by simulating such faults, or from the real process by deliberately inducing such faults. A mathematical process model suitable for such simulations must incorporate the relevant state variables and process parameters which, if abnormal, possibly constitute faults. Wherever such a model is available, therefore, it seems simpler to use it directly to estimate actual state variables and process parameters, and hence directly ascertain which ones are abnormal and so possibly constitute faults. Such estimation, using fundamental, detailed models of water chilling machines, has been done as part of the performance assessments in Chapter 6, and is reviewed in Sections 7.3.2 and 7.3.3 below. Also, in common with all techniques of fault diagnosis directly from measurements, Yu and Lee's technique makes no use of quantities readily derived from measurements. Such quantities, such as water chilling load and COP for water chilling machines, are most helpful in detecting and diagnosing faults, as discussed in Section 7.3.1 below.

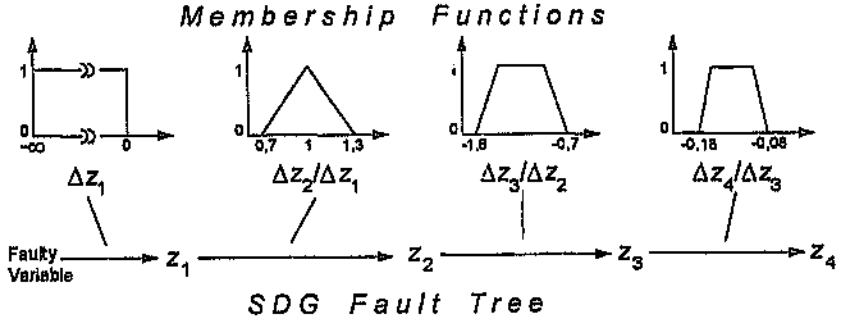

z: measured quantity Δz: deviation of measured quantity from normal value

$\Delta z_n/\Delta z_m$: deviation ratios (gains)

Figure 7.1 Example of Signed Directed Graph Fault Tree and Membership Functions (Yu and Lee, 1991)

Yet another approach is fault diagnosis from statistical analysis of measured quantities. Pape et al. (1991) present a methodology, tested by simulation only, of detecting faults from statistical analyses of measured power demands of each component - including a conventional water chilling machine with a single-stage compressor - of a building HVAC system. A strategy for optimal control of this system was formulated, based on quadratic formulas - in terms of controlled variables, loads, ambient conditions, and coefficient vectors and matrices - for input power to the system and to each system component. (The formula for predicting input power to the water chilling machine is a quadratic function of its load and the difference between condenser and evaporator outlet water temperatures.) Linear regression was used to derive these coefficient vectors and matrices from data yielded by simulations[12] over a wide range of near-optimal, fault-free operating conditions.

The methodology monitors the actual power demands of the complete HVAC system and its components over time, and uses the regression model to predict the corresponding optimal values. Non-optimal performance of the system, and thus the presence of one or more faults, is detected by a statistically significant deviation between actual system power and the predicted optimal value.[13] Faults causing relatively large departures from optimal power demand are detected more quickly. Next, the actual and predicted optimal power demands of each system *component* are examined for similar statistically significant deviations. Using such individual power deviations[14] as qualitative symptoms,[15] the fault(s) can then be diagnosed by manual reasoning.

---

[12] The complete HVAC system was simulated by a fundamentally-based computer program.

[13] Which will also be the normal value if all state variables and process parameters are at design values (see definitions of normal and optimal performance, page 123, Chapter 4). There is nothing indicating the contrary in Pape et al. (1991).

[14] If more than one component exhibits such deviations, cause-and-effect analysis has to be performed, because a fault in one component may of course affect the performance of other components.

In the example given by Pape et al., a fault in the chilled water temperature sensor of the HVAC system was deliberately induced in a simulation. This caused the water chilling machine to deliver water at below optimal temperature. Its COP was thus reduced, so its power demand increased above the optimal value. Because of the lower chilled water temperature, however, the system controller reduced the flow through the chilled water circulating pump in order to maintain the specified air temperature. The power demand of this pump thus decreased below its optimal value. Using cause-and-effect analysis on the basis of these two qualitative symptoms, the faulty temperature sensor was manually diagnosed.

The focus of this chapter of the thesis is diagnosing faults *within* water chilling machines, so two observations must be made here. First, the symptoms produced by this methodology enable positive, unambiguous fault diagnosis only if they are unique for every possible single and multiple fault. This is *not* the case for water chilling machines, because their compressors are the only components absorbing major amounts of power. There are many faults in water chilling machines which could cause higher-than-normal compressor input power: for example, an overcharge of refrigerant, a high water-side fouling factor in the evaporator or condenser, or excessive oil in the evaporating refrigerant. Therefore, statistically significant deviations of *other* measured quantities from their normal values must be examined as well for additional symptoms to aid in positively diagnosing faults. Nothing seems to prevent the methodology of Pape et al. being readily extended to do this.

Second, the symptoms yielded by this methodology, even if so extended, are qualitative. Apart from the extra reliability of these symptoms because

---

[15] The algorithm of Pape et al. (1991) qualitatively indicates statistically significant negative and positive deviations by flags of -1 and +1 respectively. A flag of zero indicates individual power deviations which are not statistically significant.

of their statistical foundation, this methodology thus suffers from the limitations mentioned on page 298 for all techniques of fault diagnosis from qualitative symptoms in measured quantities. Therefore, the *quantitative* information content of the statistical analyses should also be used in diagnosing faults, and this merits investigation.

The most useful benefit from examination of measurements alone is the detection of off-design *inputs*, which may be the whole or a partial cause of unsatisfactory performance.[16] In order to confirm or deny fault symptoms in measurements, though, it is most desirable to perform analyses based on derived measures of performance and, where possible, estimated non-measurable state variables and process parameters. Such analyses are also the procedures most likely to reveal faults not detectable by measurements alone, or unanticipated faults.

7.3 Fault Diagnosis by Process Modelling

Higher classes of fault diagnosis make use of derived or estimated quantities and other information, not just the measurements themselves. Modelling of the process on one or more levels is inevitably required. Isermann (1982) elegantly outlines the key concepts here in his proposed general methodology of fault diagnosis by process modelling. This is illustrated in Figure 7.2 and employs three models:

(i) a model of the *observed* (actual) process;

(ii) a model of the *normal* process;

(iii) a model of the *faulty* process.

---

[16] An example is Case Study G in Chapters 5 and 6, where evaporator and condenser water flow-rates could not be measured; thus had to be derived from other measurements; and exceeded design values by 23 and 71 per cent respectively. The excessive former flow-rate prevented the machine from attaining its specified chilled water delivery temperature.

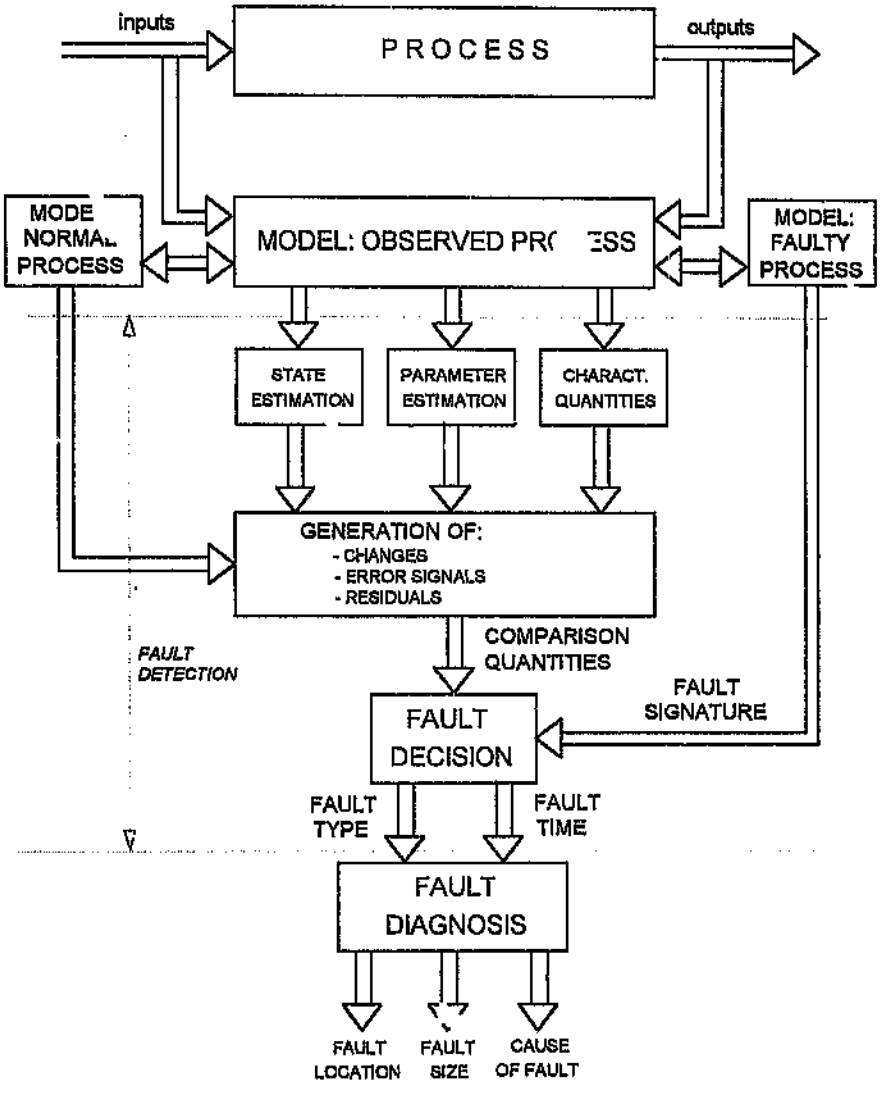

Figure 7.2 Generalised Methodology of Fault Diagnosis by Process Modelling (Isermann, 1982)

Isermann rightly observes that the goal is not only to detect but to diagnose process faults, so the process models should express, as closely as possible, the physical laws which govern the process behaviour.

The first model, of the observed (actual) process, is used to estimate non-measurable state variables and process parameters from the measured inputs and outputs. Characteristic quantities and other measures of performance such as COP and water chilling load for water chilling machines, are also derived from these inputs and outputs.

The second model is of the normal process, and "normal" must first be defined. Isermann (1982) suggests, as an example, that the normal model is that for "normal" values of the process parameters. In this thesis, to accord with the definition of normal performance in Chapter 4, the normal process is defined as that in which all state variables and process parameters are at their *design* values. For the same operating regime as for the observed (actual) process, the model of the normal process yields the normal values of the outputs, characteristic quantities, state variables and process parameters. Fault detection then commences with comparing the measured outputs, derived characteristic quantities, and estimated state variables and process parameters of the *observed* (actual) process against these corresponding normal values. This yields the *comparison quantities* in Figure 7.2 - for example, deviations from such normal values, or error signals or residuals.

The third model in Figure 7.2, that of the faulty process, is a knowledge base of the effects of known types of faults on these comparison quantities. These effects are termed *fault signatures*. These, together with the aforementioned comparison quantities, are the basis for the last step in fault detection: the *fault decision* in Figure 7.2, which yields the fault type and the time of its occurrence. Fault diagnosis then follows, which determines the location, size and cause of each fault, again with the aid of the models of the observed (actual) and normal processes.

7.3.1 Fault Diagnosis from Characteristic Quantities

This class of fault diagnosis uses, in addition to the measurements themselves, characteristic quantities such as COP derived therefrom.

Gluckman (1986) recommends that if derived evaporator or condenser loads signal unsatisfactory performance, analysis through evaporator, condenser or compressor energy balances be undertaken to identify faults that are not apparent from measurements alone.[17] He gives an example of one such fault: worn rotor tip seals in an oil-injected screw compressor, which decrease its volumetric efficiency and hence the refrigerant mass flow-rate that it draws. Evaporator load thus decreases, but power demand does not, because worn tip seals also increase internal leakage, decreasing the isentropic efficiency of the compressor. As Gluckman points out, this fault would be expected to reveal itself through high discharge temperature. However, this temperature may not significantly increase beyond its normal value, because the injected oil in such screw compressors is cooled to prevent excessively high discharge temperature. The controller of the oil cooling system, therefore, is liable to maintain the specified discharge temperature by increasing the cooling rate, so masking this fault.

Gluckman states that "the only way to identify such a fault is recognising the shortfall in duty with a thermal balance". A compressor energy balance is meant here. However, this thesis offers a more convenient way of detecting faults such as these: *the corrected refrigerant-circuit COP, determined by the methods of Chapter 5, will be lower than its normal value.* This is elaborated upon later.

For conventional machines, the program of Hall and Unsted (1976) calculates evaporator and condenser refrigerant mass flows from evaporator and condenser energy balances. It merely reports if these are more than 5 per cent above or below design values. It also calculates overall isentropic efficiency of the single- or multi-stage centrifugal

---

[17] Gluckman draws attention to the required accuracy of temperature measurement for accurate computations in such energy balances, but makes no mention of the equally important need for accurately measured water flow-rates in this regard.

compressor, and reports if this is more than 5 per cent below the design value. Again, the comparisons are with design values, so they are less informative and valid the further the operating regime deviates from design specification.

Correctly, of course, actual quantities of performance should be compared with their corresponding normal values. As Chapter 4 points out, corresponding normal performance generally has to be predicted on the basis of regression modelling, fundamental mathematical modelling, or combinations thereof. If *all* quantities of normal performance are to be predicted, detailed models are required: for example, regression models like that of Grimmelius et al. (1995), reviewed above,[18] or fundamental ones such as those used in this thesis for conventional machines. On the other hand, if it is judged too laborious and impracticable to develop such detailed models, simpler ones predicting just key normal quantities such as input power or COP may be developed.

One approach using such a simpler model is now reviewed. As will be seen, it can detect the presence of faults, but its key disadvantage is that other important quantities of normal performance *not* predicted, and thus not available, cannot be compared with actual values and thus yield symptoms or signatures to aid in diagnosing faults. As will also be seen, the corrected refrigerant-circuit COP of this thesis is thus a most useful supplementation to such simpler models in diagnosing faults at refrigerant-circuit level.

Predicting Normal COP from Fundamental, Empirically Attuned Model

Normal COP for a given *load* can be predicted using the relatively simple thermodynamic model of Gordon and Ng (1994, 1995), attuned to a particular machine by regression as described in Chapter 4. This

---

[18] This model only predicts measurable quantities, and would have to be extended to predict derived quantities like loads and COP.

approach is inherently sound because this simplified model is fundamentally based, and promisingly practicable because it requires minimum normal operating data for attuning. The temperature-independent and -dependent versions of this model, described in Chapter 4, predict COP from load and (for the temperature-dependent model) outlet chilled water and inlet condenser water temperatures. The temperature-independent model, as recalled from (4-9a), predicts a linear relation between the reciprocals of COP and water chilling load Q_E:

$$\frac{1}{COP} \cong C_0 + \frac{C_1}{Q_E} \tag{7-1}$$

Both constants C characterise the internal irreversibilities of a machine, but C_0, as explained in Appendix 5, also characterises the external irreversibilities of heat transfer through the evaporator and condenser. Statistically significant discrepancies between actual and predicted normal COP signal the presence of faults through their effect on the internal or external irreversibilities of the process. However, diagnosing the faults must be done by manual reasoning, with the following exception.

Gordon, Ng and Chua (1995) show that faults affecting only the *external* irreversibilities of heat transfer through the evaporator and condenser can be identified as such. They used the temperature-independent model to detect water-side fouling in the evaporator and condenser of a conventional water chilling machine. Briefly, this model was attuned to the full- and part-load performance of this machine both before and after its heat-exchanger tubes were cleaned. The constant C_1 in (7-1) obtained before and after this cleaning changed negligibly; this, as the authors point out, suggested that the internal irreversibilities of the machine were negligibly affected thereby. However, the constant C_0 decreased by 36 per cent. Changes in just the external irreversibilities of

heat transfer - due to high heat exchanger fouling in this case - thus manifest themselves as a vertical shift in the straight line of (7-1). However, this does not identify the precise location of such fouling; that is, whether it is in the evaporator, the condenser, or both.

Two further remarks must be made here. First, the machine studied employed a *single-stage* centrifugal compressor, manufactured in 1971 (Gordon, Ng and Chua, 1995 : 257). For a machine with a multi-stage, first-stage-regulated compressor manufactured before 1980, however, removing heat-exchanger fouling may *not* leave internal irreversibilities unaffected at part loads. As explained in Chapter 6, for such machines operating with partially open inlet guide vanes under a "set water temperature" control philosophy, cleaning heat-exchanger tubes causes the efficiency of the regulated first stage to deteriorate rapidly (and thus the degree of irreversibility of its compression process to rise rapidly) as its vanes close further. Hence, at part loads, the relationship of the reciprocals of load and COP may well deviate from a straight line, and the curves of actual and normal reciprocals of COP may approach or even cross each other.[19] This possibility will have to be borne in mind in applying this technique to machines with multi-stage, first-stage-regulated centrifugal compressors.

Second, the temperature-independent model is only valid where the outlet chilled water and inlet condenser water temperatures are relatively constant with load. For cases where this is not so, as for water chilling machines in surface installations on mines, Gordon and Ng's temperature-dependent model must be used instead. The use of this latter model to detect such changes in external irreversibilities, caused by water-side fouling or other faults, has not yet been reported.

---

[19] This will occur if, for the same load at part-duty, negligible power saving or even a power penalty arises from cleaning heat-exchanger tubes, as explained in Chapter 6.

This thermodynamic model of Gordon and Ng (1994, 1995), then, has the potential to identify faults affecting just external irreversibilities, but otherwise does not diagnose faults - that is, identify their locations, sizes and causes. Nevertheless, because of its simplicity and practicability, it appears to have considerable promise in *detecting* faults, especially in custom-built machines which are more complicated than conventional machines to fundamentally model in detail.[20] However, as noted in Chapter 4, it must be modified in order to apply to custom-built machines.

Diagnosing Faults through Refrigerant-Circuit COP

For diagnosing faults detected by such relatively simple models, the corrected refrigerant-circuit COP, obtained as in Chapter 5, may aid considerably. Because it is the thermodynamic efficiency of the refrigeration cycle, it is useful in diagnosing faults at refrigerant-circuit level. For this purpose, though, this COP should be precisely determined, so all the measured quantities required to compute it should be obtainable. Moreover, the corresponding normal values of these quantities (or at least approximate indications thereof, as discussed below) must also be available, for comparing with the actual values. It is the information yielded by these comparisons which aids in fault diagnosis.

The aforementioned example on page 306 of worn rotor tip seals of a screw compressor - this fault being masked because the controller of the oil cooling system increases the oil cooling rate to maintain the specified discharge temperature - is returned to. With such a fault, the corrected refrigerant-circuit COP will be less than the normal COP predicted by, for example, the temperature-independent or -dependent model of Gordon

---

[20] Of course, custom-built machines can be fundamentally modelled using already-developed, flexible software, such as that of Cleland and Cleland (1989) briefly reviewed in Chapter 4. This option will become more practicable as such software inevitably develops further.

and Ng (1994, 1995), discussed above. If at least approximate indications of the *normal* values of the quantities upon which the corrected refrigerant-circuit COP depends are available, the actual value of this COP will then reveal the greater-than-normal oil cooling load through:

- either the greater-than-normal correction ratio $R_{[VCB]}$ in (5-10b) or (5-10c) if the oil is cooled in an oil-to-water or oil-to-refrigerant heat exchanger (as, for instance, in the machine of Figure 3.24);
- or the greater-than-normal liquid injection ratio if the oil is cooled by liquid injection (see, for instance, the liquid injection ratio in (3-24) for the machine of Figure 3.22).

The set of possible known faults is then restricted to those known to cause a signature of greater-than-normal oil cooling load; one such fault is worn rotor tip seals (an abnormal, undesirable change in a process parameter, namely a dimension of the rotors).

Such use of the corrected refrigerant-circuit COP and the quantities upon which it depends - in conjunction with a simplified model predicting corresponding normal COP - to aid in fault diagnosis may find particular application with custom-built water chilling machines. From the viewpoint of a mine with such machines, this option is likely to be more practicable than developing detailed fundamental or regression models predicting *all* normal quantities of performance and estimating all relevant process parameters and state variables to enable direct fault diagnosis. Not only are custom-built machines more complicated than conventional ones to so model, but custom-built machines are mostly unique and thus require unique effort in developing such models.

As noted above, if corrected refrigerant-circuit COP is to be so used to aid fault diagnosis, it should be precisely determined. Therefore, if measurements of main and auxiliary refrigerant mass flows are required to

precisely compute the corrected refrigerant-circuit COP of custom-built machines - such as for the machines of Figures 3.22 and 3.23 - it will be worthwhile to install the necessary refrigerant flow meters.[21] As also noted above, at least approximate indications of the *normal* values of all quantities upon which corrected refrigerant-circuit COP depends must be available. Such indications can be obtained by referring to values of such quantities recorded under fault-free operating conditions spanning the entire operating range of the machine. Such values can be conveniently recorded at the same time as those measurements necessary for attuning the simplified model predicting *normal* COP to the machine, as described in Chapter 4 for the thermodynamic model of Gordon and Ng (1994, 1995).

An issue remaining to be fully explored here is identification of the *minimal* set of measurements required to obtain all quantities needed to compute the corrected refrigerant-circuit COP. If the refrigerant circuit is not in good order, and two-phase refrigerant flows instead of single-phase flows thus occur - or the refrigerant is contaminated - an otherwise sufficient set of measurements becomes insufficient. An example is Case Study E in Chapter 5, where an overcharge of refrigerant in the evaporator caused liquid to be entrained in the vapour entering the compressor. An extra quantity - the non-measurable liquid fraction in this vapour - was thus needed to calculate corrected refrigerant-circuit COP.

Where it is thus impracticable to precisely determine the refrigerant-circuit COP, the COP range plot may be of use. In Case Study E, the COP range plot of Figure 5.21 could confirm the symptom of refrigerant overcharge. From this figure, if the liquid fraction in the refrigerant leaving the evaporator had been zero, the actual COP would have been 5,2. This

---

[21] Installing such flow meters also enables actual performance to be independently and precisely ascertained by the refrigerant flow/quantity confirming method described in Chapter 4. Thus apparent performance can be positively verified - an additional, most practical benefit.

was 50 per cent above the design full-duty COP of 3,43 and thus impossible!

7.3.2 Fault Diagnosis from Estimation of Process Parameters

This class of fault diagnosis uses, in addition to the measurements and characteristic quantities, theoretical models of machine components in order to estimate non-measurable process parameters therefrom.

In the South African mining industry, the important, non-measurable water-side fouling factors of the evaporator and condenser of conventional machines are estimated as described in Appendix 21. This method derives the fouling factor from the estimated fouling resistance, which is the remaining portion of the total resistance to heat transfer after subtracting the thermal resistance of the heat-exchanger tube material and the *modelled* thermal resistances of the boundary layers of water and refrigerant on either side of the tubes.

The accuracy of the fouling factor so estimated is at least moderately sensitive to the accuracy of the measured water flow-rate through the evaporator or condenser in question, for the reasons given in Appendix 21. Before estimating fouling factors, therefore, it is essential to verify apparent water flow-rates, and accurately ascertain their actual values. Hence where the enhanced Thorp method of Chapter 5 is sufficient to verify apparent performance and hence ascertain actual water flow-rates - as in Case Studies A and B in Chapter 5 - actual water-side fouling factors can be estimated per Appendix 21 without difficulty. Where apparent performance must be verified by machine modelling, actual fouling factors are estimated along with the other unknown quantities, as in Case Studies C, C and A in Chapter 5 (Tables 5.11, 5.12 and 5.14 respectively).

The computer programs of Hall and Unsted (1976) and Hemp et al. (1986) estimate these water-side fouling factors by the same method. Hall and

Unsted's program then attempts elementary fault diagnosis. If the estimated fouling factor exceeds 1½ times the design value, a message to investigate possible cleaning of the tubes is printed. If it exceeds twice the design value, a message that the tubes require cleaning is printed.

The program of Hemp et al. (1986) attempts more realistic fault diagnosis, recognising that fouling is not the only cause of inadequate heat exchanger performance. It supplements modelling with a knowledge base. The fouling factor estimated per Appendix 21 is termed the "app ent" water-side fouling factor. The program calculates maximum, mos. likely, and minimum values of apparent fouling factor, based on the lower and upper limits of the estimated accuracy of the measurements. If the *minimum* apparent fouling factor so calculated exceeds the design value, the apparent fouling factor is definitely too high, and is reported as such. However, this really just indicates that the thermal performance of the heat exchanger has deteriorated unacceptably, because the heat-exchanger modelling of Appendix 21 has simplifying assumptions[22] and assumes fault-free operation. There are many faults apart from high water-side fouling which could cause such inadequate performance. The program therefore attempts diagnosis of the fault(s) responsible on the basis of the known fault symptoms in Table 7.4. This is a case of fault diagnosis by fairly deep, automated reasoning.

As seen, Table 7.4 assumes that fouled tubes will be confirmed by the symptom of higher-than-normal water pressure drop through the heat exchanger (as also assumed in Table 7.1 above). Otherwise, one or more of the other possible faults are more likely. Hemp et al. (1986) acknowledge that this procedure is not guaranteed to yield an accurate diagnosis. For example, it is certainly possible for both leaking division plates and fouled tubes to occur simultaneously; the first would decrease

---

[22] See Appendix 15, Sections A15.2.1 and A15.3.1 for the key simplifying assumptions.

water pressure drop, while the second would increase it, so a diagnosis could result which includes neither of these causes! This is a good example of multiple faults interfering with each other's symptoms.

Table 7.4 Possible Faults Causing Inadequate Heat Exchanger Performance in Conventional Machines (Hemp et al., 1986)

		Water Pressure Drop in Evaporator or Condenser		
		Too low	*Normal*	*Too high*
Difference between refrigerant temperature and saturation temperature at refrigerant pressure	*Normal*	Leaking water-box division plates[23]	Oil in refrigerant (evaporator)[24]	Fouled tube surfaces Blocked tubes
	Too high	Leaking water-box division plates Low refrigerant level (evaporator) Non-condensable gas in refrigerant (condenser)	Low refrigerant level (evaporator) Non-condensable gas in refrigerant (condenser)	Fouled tube surfaces Blocked tubes Low refrigerant level (evaporator) Non-condensable gas in refrigerant (condenser)

The models of the shell-and-tube heat exchangers of conventional machines could be expanded to include parameters enabling positive diagnosis of these other faults, but such diagnosis would require commensurately more measurements as well. For example, measuring water pressure drop across every pass of tubes would be required to diagnose leaking division plates or blocked tubes. Measuring concentrations of oil or non-condensable gases in refrigerant liquid and vapour respectively, and quantitatively modelling their effects, is very difficult.[25] A far more complex evaporator model would be needed to model low refrigerant liquid level.[26] However, well-known qualitative

---

[23] Division plates are illustrated in Figures 3.13 and 3.14, Chapter 3.

[24] This is not necessarily true. With high concentrations of dissolved oil, the boiling points of halocarbon refrigerants rise (see page 87, Chapter 3), so evaporating refrigerant temperature will be significantly above the saturation temperature at the prevailing refrigerant pressure.

[25] See pages 86 and 88, Chapter 3, for qualitative descriptions of these effects.

[26] Webb, Choi and Apparao (1989) present a model of a shell-and-tube evaporator taking this into account.

symptoms, listed in Table 7.1 as well as Table 7.4, indicate oil or non-condensable gas in refrigerant, and low evaporator level. On a large machine, therefore, the most cost-effective measure would probably be to monitor water pressure drop across each pass of tubes and diagnose other faults in Table 7.4 through their well-known symptoms.

As described earlier above, heat-exchanger fouling can also be detected through the relatively simple, thermodynamic model of Gordon and Ng (1994, 1995). However, because high fouling factors significantly affect the performance of large water chilling machines, it is obviously desirable to pinpoint the heat exchangers with such fouling factors, and to estimate these factors wherever possible. For conventional machines, the method of Appendix 21 is thus obviously preferable.

Finally, it is recalled from Chapter 6 that for conventional machines with multi-stage, first-stage-regulated centrifugal compressors, and designed for maximum COP at full, design duty but operating at part-duty under a "set water temperature" control philosophy, cleaning heat-exchanger tubes may not improve, or may even worsen, the COP.[27] This illustrates that customary remedial actions or maintenance undertaken to restore or maintain normal values of process parameters, and hence satisfactory performance, may not always do so, and should be justified by a soundly based prediction of improved performance to be gained thereby. The work of this thesis encourages such an holistic approach through proper performance assessment, with normal or even optimal performance predicted by fundamental modelling. This, in contrast to regression modelling, reveals the precise roles of process parameters in effectiveness and quality of performance. As noted previously, however, fundamental modelling can become impracticably complex.

---

[27] This does not mean to imply that heat-exchanger surfaces should not be cleaned. Excessive fouling should be removed for other reasons, for example to minimise corrosion of tubes.

7.3.3 Fault Diagnosis from Estimation of State Variables

This class of fault diagnosis uses, in addition to the measurements and characteristic quantities, theoretical models of machine components in order to estimate non-measurable state variables as well as process parameters therefrom.

An example, mentioned in the discussion on Table 7.4 above, is the use of a more complex model of a shell-and-tube evaporator to estimate liquid refrigerant level therein, and thus diagnose low refrigerant level. A second example is that of Case Study A, Chapter 5, where a partially flooded condenser was diagnosed through estimating the amount of tubes submerged in liquid refrigerant. As noted in Chapter 5, though, this latter example illustrates that expanding a fundamentally-based machine model to account for all possible abnormalities may increase its complexity to the point of impracticality and unwieldiness. This approach is thus not necessarily the most effective way of detecting abnormal state variables constituting faults. Amounts of liquid refrigerant in heat exchangers and other components, for example, are easily ascertainable through measurement of liquid levels, and even retrofitting machines with such level sensors is a far more cost-effective option.

7.3.4 Fault Diagnosis through Supplementing Models with Knowledge Bases

Detailed, fundamental machine models estimating values of *all* relevant process parameters and state variables, therefore, are unlikely to be available for two reasons. First, such models can easily approach impracticable levels of complexity, and second quantitatively modelling the effects of some such parameters (for example, excessive concentrations of oil or non-condensable gases in the refrigerant) is difficult. In the example of Hemp et al. (1986) already quoted (Table 7.4), the limited models of the heat exchangers yield apparent water-side fouling factors. If these are reported as definitely too high, further

modelling is not carried out: this information is supplemented with a knowledge base of symptoms of all possible faults.

As has been seen, all classes of fault detection and diagnosis inevitably use knowledge bases of machine characteristics, and fault symptoms and signatures, to some extent. Such knowledge bases assume greater importance for faults whose effects are difficult to model quantitatively, such as the aforementioned excessive concentrations of oil or non-condensable gases in the refrigerant. This is because the *qualitative* symptoms of such faults are generally well known (see, for example, Table 7.1).

Fathi, Ramirez and Korbicz (1993) advocate an integrated, top-down, systematic approach to fault diagnosis by supplementing fundamental, detailed process models with a knowledge base. In this approach, compiled qualitative knowledge is at high level, and analytical process estimation knowledge (in the fundamental, detailed models) is at low level. The high-level, compiled, qualitative knowledge consists of relatively general malfunction hypotheses. These are used first to narrow down the search space (the range of possible faults). Then, within this narrowed search space, the lower-level, fundamental models estimating the parameters or states possibly constituting faults are triggered to resolve and refine more specific malfunction hypotheses. This integrated approach increases the completeness and reliability of the diagnostic procedure.

Gluckman and Hart (1992) have implemented a comprehensive approach similar to this,[28] and very similar to the manual one used in this thesis. Their model-based expert system (recommended to be used off-line) is termed a "Refrigeration Fault Diagnostic System". The knowledge base

---

[28] Except that they make no mention of actual state variables and process parameters being estimated.

of this expert system is programmed with rules that are able to diagnose particular machine faults based on a relevant combination of measured input data. It also contains a detailed model of the refrigerating machine (in terms of design data such as compressor characteristics, heat-exchanger surface areas, etc.) that can be used to carry out the necessary calculations that will identify the optimum or design performance of the machine under any particular combination of "load conditions" (operating conditions). This detailed model thus performs the same function as the machine modelling of Chapter 6, namely prediction of corresponding normal or possibly optimal performance under identical or alternative operating regimes.[29]

After the initial data has been entered into the computer, Gluckman and Hart's system carries out a set of calculations to compare the observed conditions with those expected by the machine model contained within the expert system. If a fault is suspected it is possible at this stage to indicate the general area in which the fault is occurring (e.g. that there is a "condenser problem"). It is also possible to estimate the difference between the observed COP and the optimal COP and hence to predict an annual cost of the fault that has been diagnosed. This is very useful, as it gives a priority ranking to any faults that have been identified.

Gluckman and Hart's expert system then issues a follow-up log sheet with more detailed questions relating to the suspected fault. Once the user has supplied this requested information, the diagnostic rules (which essentially recognise fault symptoms and signatures) are applied to identify the exact cause of the particular "problem". For example, if a preliminary analysis reveals excessive condensing temperature leading to

---

[29] It is noted here that the program of Hemp et al. (1986) also allows the user to manually predict performance of conventional machines for any specified inputs and water-side fouling factors. However, such performance is predicted by the technique of Hemp (1981), briefly reviewed in Section 4.3.3, Chapter 4. As noted there, the most significant limitation of this technique is that a two-stage centrifugal compressor is modelled as an equivalent single-stage compressor.

a drop in COP, the more detailed analysis may show that the outlet refrigerant is excessively subcooled, but the level in the liquid receiver is normal. These collective symptoms can be explained by the presence of non-condensable gas in the condenser. The expert system reports this to the user, together with the inferences that led to the diagnosis, and then proposes remedial action, which in this case is the purging of non-condensable gas from the condenser. This system enables relatively unqualified machine operators to do fault diagnosis regularly with minimal effort. It can also predict how a machine will operate under unusual off-design conditions. It also affords the facility of trend analysis, which can be used to predict faults before they become too serious, and even to recommend which compressors should be in use under prevailing load conditions.

This high- and low-level automated procedure of fault diagnosis accords with established, good practice when manually diagnosing faults, and corresponds with what has been done manually in Chapters 5 and 6. For example, in Case Study E, the preliminary analysis revealed unusually low superheat in the compressor discharge temperature. This was a symptom of an overcharge of refrigerant; the COP range plot of the inexact Thorp method confirmed this. The input power and COP with no overcharge were then predicted for apparent and design evaporator water flow-rates; these at least indicated the probable range of power wastage due to the overcharge, and the annual cost thereof. Optimum COP with the alternative maximum-load control philosophy was also predicted. Finally, the remedial action was obvious - the excess refrigerant had to be removed from the evaporator.

7.3.5 Unanticipated Faults

A remaining issue concerns detection and diagnosis of unanticipated faults. Neither operator training nor expert systems help with these. Such faults can be design faults, their presence becoming apparent at the

commissioning stage, or unanticipated operational ones. Here, as mentioned earlier, an expanded, fundamentally-based model, estimating *all* state variables and process parameters, is one option, but this is likely to be impracticable for most situations. Any fault, though, manifests itself through symptoms or signatures constituting deviations from normal behaviour. The work of Ng (1990) reverts to this basic fact in offering a promising way of detecting and pinpointing unanticipated faults, including multiple ones. Ng's approach computes *conflict sets*, defined to be sets of machine components where assuming that all components in such sets are normal (i.e. fault-free) is inconsistent with observed behaviour and the rules characterising normal behaviour. At its reported state of development, this approach assumes that each constraint defining normal operation can be localised to one and only one component of the machine; thus, each violated constraint points conclusively to a corresponding faulty component.

An example where this approach was useful in principle concerned an unanticipated fault in the machine of Figure 3.24. There was a gradual, unexplained decrease in the water temperature drop through Evaporator 1 of this machine, even though the water flow-rate remained at design value. This evaporator was a closed-plate heat exchanger as in Figure 3.30. Intriguingly, the refrigerant at *one* of its two refrigerant outlets was markedly superheated; this was certainly inconsistent with normal behaviour. The fault was thus pinpointed as within this evaporator, and was found to be settled solids blocking the water passages at one end. The water was channelling through the unblocked passages, so only these passages were transferring heat.

7.4 Assessment

The work of this thesis is of value in fault detection and diagnosis through its encouraging a holistic approach thereto, albeit manual at present. In principle, this approach is to:

- use the enhanced Thorp method or machine modelling to independently ascertain actual performance and so detect erroneously measured quantities. Any off-design quantities in the operating regime are detected here as well;

- next, compare actual with normal or optimal performance, predicted by detailed, fundamental machine models. Hence assess actual performance for satisfactoriness;

- if actual performance is unsatisfactory, estimate non-measurable process parameters and state variables to find any abnormal ones constituting faults (whilst taking into account that an off-design operating regime may also contribute to unsatisfactory performance).

This approach follows the general methodology of Isermann (1982), except that it first checks for erroneous measurements and an off-design operating regime. The advantage of so doing is alerting operating staff, at the start, to such measurements and such a regime, and hence to the possible contributions of such a regime to unsatisfactory performance. All quantities in the operating regime are measurable and verifiable, and relatively easily restored to design values if off-design.

In the realms of practicability, though, there are two obstacles to this approach. First, detailed, fundamental machine models either may not be available, especially for custom-built machines; or are unlikely to be comprehensive enough to estimate *all* relevant process parameters and state variables. Second, some measurements required to estimate some such parameters and states may not be obtainable. Therefore, if performance is unsatisfactory, the best that can be done in the absence of complete, fundamental models, and all measurements required to estimate all relevant parameters and states therefrom, is as follows. As many characteristic quantities - and estimates of states and parameters - as possible must be derived from the available measurements and

models. All symptoms and signatures appearing therefrom must be examined in the light of the available knowledge bases of fault symptoms and signatures. Undesirable values of states and parameters which cannot be practicably estimated quantitatively - such as levels of contaminants in the refrigerant - must also be diagnosed through these available knowledge bases.

Such bases, which must take account of the characteristics of both the particular machine and its particular vapour-compression refrigerating cycle, must therefore be sufficiently comprehensive to enable diagnosis of as many single and multiple faults as possible. Here, the corrected refrigerant-circuit COP of the thesis can assist materially in diagnosing faults at the refrigerant-circuit level. If this COP is lower than the normal COP yielded by a simplified machine model, then, as shown in this chapter, the quantities upon which the corrected refrigerant-circuit COP depends can be examined for symptoms and signatures of possible faults - provided that at least approximate indications of the corresponding normal values of these quantities are available. Where the corrected refrigerant-circuit COP cannot be precisely determined, the next best option, the COP range plot of the thesis, may be of assistance. Unanticipated faults, as suggested by Ng (1990), can be detected from inconsistency of observed component behaviour with normal behaviour.

Concerning automation of fault diagnosis, the approach of Gluckman and Hart (1992) - using an expert system to suggest possible faults on the basis of comparison of actual performance with predicted normal or optimal performance - is considered to be the most promising way forward. It is highly desirable to supplement the methods of Chapters 5 and 6 with such automated fault diagnosis, enhanced where appropriate by the other methods described in this chapter. Performance assessment is not an end in itself. The objective of burdened mine staff, who are mostly not refrigeration experts, is the correct and speedy identification of the faults present, so that these may be remedied.

8. CONCLUSIONS

The objectives of this study, stated in Chapter 1, were improved techniques of quickly, accurately and convincingly (a) ascertaining actual performance of water chilling machines, and (b) predicting normal or optimal performance under identical or even alternative operating regimes, thus having valid yardsticks to compare actual performance with. Qualified mine personnel would thus be timeously provided with the two sets of information necessary to properly assess actual performance, diagnose faults and take remedial action.

Chapter 4 accordingly identified three desirable improvements to current practice. The first two, directly addressing the above objectives, were:

1) enhanced, more conclusive methods of independently ascertaining actual performance, so verifying apparent performance and detecting unacceptable errors in the principal measurements; and

2) a practicable method of accurately predicting corresponding normal or optimal performance under identical or alternative operating regimes.

The contributions of the thesis have effectively achieved both of these desirable improvements for conventional water chilling machines, and partially achieved the first for custom-built machines. These contributions are now reviewed.

8.1 Review of Contributions

8.1.1 Verifying Apparent Performance by Enhanced and Inexact Thorp Methods

The first contribution in this work is that Thorp's original method (Thorp, 1974) of verifying the apparent performance of machines determined from water-circuit measurements has been enhanced and placed on a firm theoretical and implementational basis. The improvements to the original

method and its reported implementations (Hall and Unsted, 1976; Hemp, 1981; Hemp et al., 1986), and the resulting findings, are as follows.

A. On the basis of the limits of accuracy of ISO R916 (ISO, 1968) for the apparent constituents of the heat balance, realistic unacceptability confirmation limits of -15% and +13% have been laid down for the heat imbalance in routine performance surveys.

B. For routine performance surveys where calibration of site-fitted measuring instruments is not assured, an "acceptable" heat imbalance *does not* guarantee acceptably accurate measurements and hence accuracy of apparent performance. A small heat imbalance may be concealing similar and *large, unacceptable* relative errors in the apparent constituents of the heat balance.

C. Therefore, whatever the heat imbalance, the enhanced Thorp method should *always* be used to verify apparent performance. This method can be used wherever the corrected refrigerant-circuit COP can be precisely determined *and* at least one apparent constituent of the heat balance is independently known to be acceptably accurate.

D. The acceptability plot of the enhanced Thorp method clearly indicates whether one or more apparent constituents of the heat balance must be unacceptably erroneous, together with the reasons.

E. In each case study involving the enhanced Thorp method - provided that refrigerant temperature and pressure measurements were accurate to within ±0,2°C and ±2 per cent of full scale respectively - the uncertainty in the corrected refrigerant-circuit COP did not affect the indications of the acceptability plot. Obviously, though, this uncertainty has to be evaluated in each case to check whether these indications are affected or not. As will be appreciated from Appendix 12 and footnotes 8, 10 and 11 in Chapter 5, this uncertainty is a function of the sensitivity of refrigerant-circuit COP to

each refrigerant temperature and pressure upon which it depends, and the measurement uncertainty in each such quantity.

F. For machines with evaporators or condensers connected in series in their water circuits, the enhanced Thorp method provides an additional check on the accuracy of either the apparent input powers or measured water temperatures, whichever is more uncertain. An example is Case Study C, Chapter 5.

G. However, the enhanced Thorp method cannot precisely ascertain actual performance, and hence verify apparent performance, if *either* the corrected refrigerant-circuit COP cannot be precisely determined, *or* no apparent constituent of the heat balance is independently known to be acceptably accurate.

H. Where the first event in G. above occurs - that is, the corrected refrigerant-circuit COP cannot be precisely determined due to *insufficient obtainable measurements* - an alternative form of the enhanced Thorp method, the *inexact Thorp method,* can be applied. The acceptability band plot of this method clearly indicates the relative likelihood of the apparent constituents of the heat balance being acceptably accurate, together with the reasons. Where the heat imbalance is significant, this method may be able to identify unacceptable measurement errors if a COP range plot can be constructed. Where the heat imbalance is small, however, it cannot prove that unacceptable errors are absent from apparent performance, because it is not able to precisely ascertain actual performance. Examples are Case Studies D, E and F in Chapter 5. Apparent performance can be verified by a sufficiently comprehensive computer-based machine model, if available.

The enhanced and inexact Thorp methods apply to all classes of water chilling machines, both conventional and custom-built. They thus constitute partial fulfilment of desirable improvement 1) above.

8.1.2 Verifying Apparent Performance by Machine Modelling

The second contribution is that where the enhanced Thorp method, due to either event in G. above, cannot precisely ascertain actual performance and so verify apparent performance, the fundamental models of conventional machines in the CHiLLER program (Bailey-McEwan and Penman, 1987) - and an extension to one such model - have been used for this purpose. Examples are Case Studies G, C and A in Section 5.4 of Chapter 5. The specific requirements and implications are as follows.

I. A fundamental, computer-based model, sufficiently comprehensive to account for possible abnormalities in internal process parameters or state variables, must be available.

J. If sufficient inputs and outputs, such as water and refrigerant temperatures, are accurately known, such a model can be solved for the unknown or uncertain inputs and outputs needing to be ascertained or verified. Valuable initial estimates of such inputs can be provided through the enhanced Thorp method (if the refrigerant-circuit COP can be precisely determined) or the inexact Thorp method (if this COP cannot be so determined, but a COP range plot can be constructed).

K. The values of relevant process parameters, such as water-side fouling factors, and state variables are also yielded thereby.

L. Where the available model does not account for significant abnormalities present in process parameters or state variables, and so cannot precisely ascertain actual performance and hence verify apparent performance, it may be possible, using simplified modelling, to ascertain a range where actual performance must lie. An example is Case Study E in Section 6.2.4, Chapter 6.

In this thesis, fundamental machine modelling has been used to verify the performance of only conventional machines. The available version of the

CHILLER program did not model custom-built machines, which are mostly unique and thus require unique models. Desirable improvement 1) above - enhanced, more conclusive methods of independently ascertaining actual performance, so verifying apparent performance - has thus been effectively achieved for conventional machines, but only partially for custom-built machines. An obvious area for further work is utilisation and extension of available models of custom-built machines to verify their apparent performance where the enhanced Thorp method, for either reason in G. above, does not suffice.

8.1.3 Assessing Actual Performance through Machine Modelling

The third contribution is that the same fundamental machine models in the CHILLER program, and the aforementioned extension thereto, have been used to predict normal and optimal performance under identical and alternative operating regimes, for the purpose of assessing actual performance. The use of machine modelling for this purpose is not original; however, this is the first such use within the South African mining industry of fundamental, detailed models of conventional machines, modelling each stage of a multi-stage compressor separately and thus accounting for the interacting effects between the stages. Such modelling enables off-design performance to be predicted accurately, highlights the reasons for poor or inadequate off-design performance, and enables options for optimal performance to be realistically explored. Interesting outcomes of such modelling are as follows.

M. An abnormality within a machine may not always amount to a fault, and may be quite tolerable or even beneficial. An example is liquid refrigerant flooding the first few bottom rows of tubes in the condenser in Case Study A, Section 6.2.1, Chapter 6.

N. An abnormality may be quite tolerable under one operating regime and be a fault under an alternative one. For example, higher-than-normal water-side fouling factors in Case Study C, Section 6.2.3,

Chapter 6, were advantageous under the prevailing "set water temperature" control philosophy, but were faults under the alternative "maximum-load" control philosophy!

O. Pre-1980 conventional machines are likely to be designed for maximum efficiency at full duty. If they have a multi-stage centrifugal compressor with capacity-regulating inlet guide vanes on the first stage only, and are operating at moderate to low part-duties, quality of performance (COP) under a "set water temperature" control philosophy is not likely to improve, and may worsen, if water-side fouling factors are reduced by cleaning heat exchanger tubes. The reason is that the vanes of the regulated first compressor stages will close further and reduce the efficiency of these stages. If the control philosophy is altered to one of maximising load, both COP as well as load are likely to be maximised. Cleaning heat exchanger tubes or taking other measures to reduce lift then has a direct and immediate benefit: it allows load to be further increased and so improves effectiveness and quality of performance further. An example is Case Study C, Section 6.2.3, Chapter 6.

P. Where actual performance cannot be precisely determined, but only a range within which actual performance lies, it is still possible to assess the upper and lower limits of this possible range for satisfactoriness, and so to evaluate whether abnormalities constitute faults, as well as the merits of the alternative "maximum-load" control philosophy. An example is Case Study E, Section 6.2.4, Chapter 6.

The most serious present handicap in fundamental machine modelling is the lack of accurate compressor characteristic performance curves, which are only available from manufacturers, but are proprietary information. Especially at part-duties, the lack of these curves can make quantitative predictions of performance, and comparisons between these, very

dubious. It is fair to expect that such information will only be released if manufacturers perceive sufficient advantage therein.

Again, in this thesis, performance of just conventional machines has been predicted by such machine modelling, so desirable improvement 2) above has only been achieved for such machines. Predicting normal and optimal performance of custom-built machines by utilising and extending available, flexible computer-based models is again an obvious area for further work. Alternatively, as discussed in Chapter 7, simplified modelling predicting just key quantities of performance like normal COP may be more practicable than detailed fundamental modelling. However, as noted in Chapter 4, such simplified modelling has limitations, particularly in predicting normal and optimal performance under alternative operating conditions and regimes.

8.1.4 Fault Diagnosis

A fault is an undesirable value of a process parameter or state variable within a machine. The third desirable improvement to current practice identified in Chapter 4 was automated diagnosis of faults causing unacceptable shortfalls in performance. The thesis does not contribute here, but critically analyses pertinent literature in fault diagnosis and the automation thereof.

A rigorous approach to fault diagnosis is parameter estimation (Isermann, 1982). Here, fundamental, detailed machine models are used to estimate non-measurable process parameters and state variables, in order to find any abnormal ones constituting faults (whilst taking into account that an off-design operating regime may also contribute to unsatisfactory performance). In the realms of practicability, however, detailed, fundamental machine models either may not be available, especially for custom-built machines; or are unlikely to be comprehensive enough to estimate *all* relevant process parameters and state variables. Also, some

measurements required to estimate some such parameters and states may not be obtainable.

In these events, the best that can be done is to derive as many characteristic quantities - and estimates of states and parameters - as possible from the available measurements and models. All fault symptoms and signatures appearing therefrom must be compared with the available knowledge bases of known symptoms and signatures. Undesirable values of states and parameters which cannot be practicably estimated quantitatively - such as levels of contaminants in the refrigerant - must also be diagnosed through these available knowledge bases.

Here, the corrected refrigerant-circuit COP of the thesis can assist materially in diagnosing faults at the refrigerant-circuit level. If this COP is lower than the normal COP, then the quantities upon which the corrected refrigerant-circuit COP depends can be examined for symptoms and signatures of possible faults. Where the corrected refrigerant-circuit COP cannot be precisely determined, the next best option, the COP range plot yielded by the inexact Thorp method, may be of assistance. Case Study E provides an example of this, discussed in Chapter 7.

To aid burdened mine staff who are not refrigeration experts, fault diagnosis should be automated, and fundamental modelling supplemented by a knowledge base seems the most promising way forward here.

8.2 Limitations of Contributions and Envisaged Further Work

In principle, ascertaining and assessing performance of machines by the enhanced or inexact Thorp methods and machine modelling should be feasible for any continuous, steady refrigeration process. As noted in Chapter 7, though, an issue remaining to be fully explored here is identification of the minimal set of measurements required to obtain all quantities needed to compute the corrected refrigerant-circuit COP. An

abnormality in the refrigerant circuit can render an otherwise sufficient set of measurements insufficient for this purpose.

The contributions of this thesis are not adequate for unsteady processes which may also be discontinuous. An example is batch-type ice-making by building ice up on cold surfaces and then releasing it by warming those same surfaces. Such processes are dynamic, involving cyclic, distributed heating and cooling of masses of refrigerant; the medium being cooled; the heat-rejection fluid; and the material of the components and piping of the machine itself. For such processes, both actual and normal or optimal performance must be expressed in terms of integrated quantities over the period of a complete cycle, as illustrated by the overall energy balance (2-1) of a fluid cooling installation in Section 2.3.2, Chapter 2. In addition, both to measure and to model such time-dependent, cyclic heating and cooling of complex machine configurations and refrigerant liquid and vapour moving therein are uncommonly difficult.

As noted earlier, the machine models used to independently ascertain actual performance, so verifying apparent performance, and to predict normal or optimal performance must model the real process accurately and be sufficiently comprehensive to account for suspected, known abnormalities. In this regard, the available version of the CHILLER program only models conventional packaged machines, and does not model condensed liquid subcoolers, pressure drops in refrigerant pipelines,[1] and auxiliary components such as flash gas control valves and hot gas bypass valves. It also does not model the effects of known abnormalities in a machine. Examples of these are refrigerant overcharge or undercharge; liquid flooding in the condenser; and contaminants such as oil or non-condensable gas in the refrigerant. For more accurate performance modelling and assessment, it is envisaged that a future,

---

[1] The extended model used for Case Study A models these two phenomena.

upgraded version of CHILLER may allow for such effects and include such auxiliary components.

Such a future version of CHILLER may also model custom-built machines, if possible utilising and extending available software in this regard. For such machines employing single or multiple screw compressors, the effect of oil injection and liquid injection (for oil cooling) on the compression process must be modelled accurately, particularly at part-duties, if performance is to be properly assessed and faults reliably diagnosed. Models of open- and closed-plate heat exchangers and their auxiliary components will also have to be incorporated.

It would also be a natural further step to include the facility of automated fault diagnosis along the lines suggested above. This will be an incentive to burdened, non-expert mine staff to use such an upgraded version of CHILLER. As suggested in Chapter 7, it may be possible to detect unanticipated faults through inconsistency of observed component behaviour with normal behaviour.

Finally, it is necessary to recall the *raison d'être* of the whole work: to ensure acceptable conditions for the underground workforce in deep South African mines. It is hoped that the continued development and automation of the contributions of this thesis will contribute materially to maximum availability and optimal performance of the large water chilling machines upon which the underground workforce on South African mines is so dependent.

APPENDIX 1

COP OF CONVENTIONAL WATER CHILLING MACHINE WITH SINGLE-STAGE CENTRIFUGAL COMPRESSOR

A1.1 Oil-to-Water Compressor Oil Cooler

Referring to Figure 3.6, let $m_{(r)Eo}$, $m_{(r)EX}$ and $m_{(r)HG}$ denote the refrigerant mass flows through the evaporator outlet, expansion valve and hot gas bypass valve respectively. Let h_{Eo}, h_{EXi}, h_{HGi} and h_{Po} denote the refrigerant enthalpies at the evaporator outlet, expansion valve inlet, hot gas bypass valve inlet and compressor outlet respectively.

From (3-11b) for the generalised machine,

$$COP = \frac{-\sum m_{(r)EB}h_{(r)EB} - \sum Q_{(w)EB(VCB)} - \sum Q_{(s)EB}}{\left(\begin{array}{c} -\sum m_{(r)VCB}h_{(r)VCB} + \sum Q_{(w)EB(VCB)} + \sum Q_{(w)CB(VCB)} \\ -\sum Q_{(w)VCB(Ms)} - \sum Q_{(s)VCB} \end{array}\right)} \qquad \text{(A1-1)}$$

For the single-stage machine of Figure 3.6,

$$-\sum m_{(r)EB}h_{(r)EB} = -m_{(r)EX}h_{EXo} - m_{(r)HG}h_{HGo} + m_{(r)Eo}h_{Eo} \qquad \text{(A1-2a)}$$

However, as no change of enthalpy occurs while the refrigerant is passing through the expansion and hot gas bypass valves, $h_{EXo} = h_{EXi}$ and $h_{HGo} = h_{HGi}$. Also, it is obvious that $m_{(r)Eo} = m_{(r)EX} + m_{(r)HG}$. Hence (A1-2a) becomes

$$-\sum m_{(r)EB}h_{(r)EB} = m_{(r)EX}(h_{Eo} - h_{EXi}) - m_{(r)HG}(h_{HGi} - h_{Eo}) \qquad \text{(A1-2b)}$$

Similarly, it can be shown that

$$-\sum m_{(r)VCB}h_{(r)VCB} = (m_{(r)EX} + m_{(r)HG})(h_{Po} - h_{Eo}) \qquad \text{(A1-3)}$$

Substituting (A1-2b) and (A1-3) into (A1-1), and noting that for the machine of Figure 3.6, $Q_{(w)EB(VCB)} = Q_{(w)E(OC)}$, $Q_{(w)CB(VCB)} = Q_{(w)C(OC)}$ and $Q_{(w)VCB(Ms)} = Q_{(w)OC(Ms)}$,

$$COP = \frac{m_{(r)EX}(h_{Eo} - h_{EXi}) - m_{(r)HG}(h_{HGi} - h_{Eo}) - Q_{(w)E(OC)} - \sum Q_{(s)E}}{\left[\begin{array}{l}(m_{(r)EX} + m_{(r)HG})(h_{Po} - h_{Eo}) \\ +Q_{(w)E(OC)} + Q_{(w)C(OC)} - Q_{(w)OC(Ms)} - \sum Q_{(s)VCB}\end{array}\right]} \qquad \text{(A1-4)}$$

A1.2 Oil-to-Refrigerant Compressor Oil Cooler

Figure 3.6a applies here. Let $m_{(r)OC}$ denote the refrigerant mass flow-rate through the oil cooler, and h_{OCi} and h_{OCo} the enthalpies at its refrigerant inlet and outlet.

Relation (A1-1) for the generalised machine still holds. If the oil cooler circulates its refrigerant between itself and the condenser (alternative (a) in Figure 3.6a), (A1-2b) applies. It is also readily shown that

$$-\sum m_{(r)VCB} h_{(r)VCB} = (m_{(r)EX} + m_{(r)HG})(h_{Po} - h_{Eo}) + m_{(r)OC}(h_{OCo} - h_{OCi}) \qquad \text{(A1-5a)}$$

or, noting that $m_{(r)OC}(h_{OCo} - h_{OCi}) = Q_{(r)C(OC)}$,

$$-\sum m_{(r)VCB} h_{(r)VCB} = (m_{(r)EX} + m_{(r)HG})(h_{Po} - h_{Eo}) + Q_{(r)C(OC)} \qquad \text{(A1-5b)}$$

Substituting (A1-2b) and (A1-5b) into (A1-1), and noting that for Figure 3.6a, $\sum Q_{(w)EB(VCB)} = \sum Q_{(w)CB(VCB)} = \sum Q_{(w)VCB(Ms)} = 0$,

$$COP = \frac{m_{(r)EX}(h_{Eo} - h_{EXi}) - m_{(r)HG}(h_{HGi} - h_{Eo}) - \sum Q_{(s)E}}{(m_{(r)EX} + m_{(r)HG})(h_{Po} - h_{Eo}) + Q_{(r)C(OC)} - \sum Q_{(s)VCB}} \qquad \text{(A1-6a)}$$

It can similarly be shown that if the oil cooler circulates its refrigerant as in alternative (b) in Figure 3.6a, *or* in thermosyphon fashion between itself

and the evaporator, with the oil cooling load then being

$m_{(r)OC}\left(h_{OCo} - h_{OCi}\right) = Q_{(r)E(OC)}$,

$$COP = \frac{m_{(r)EX}\left(h_{Eo} - h_{EXi}\right) - m_{(r)HG}\left(h_{HGi} - h_{Eo}\right) - Q_{(r)E(OC)} - \sum Q_{(s)E}}{\left(m_{(r)EX} + m_{(r)HG}\right)\left(h_{Po} - h_{Eo}\right) + Q_{(r)E(OC)} - \sum Q_{(s)VCB}} \qquad \text{(A1-6b)}$$

The similarity of (A1-6a) and (A1-6b) to (A1-4) suggests the following general relation for COP:

$$COP = \frac{m_{(r)EX}\left(h_{Eo} - h_{EXi}\right) - m_{(r)HG}\left(h_{HGi} - h_{Eo}\right) - Q_{(fl)E(OC)} - \sum Q_{(s)E}}{\left[\begin{array}{l}\left(m_{(\ )EX} + m_{(r)HG}\right)\left(h_{Po} - h_{Eo}\right) \\ +Q_{(fl)E(OC)} + Q_{(fl)C(OC)} - Q_{(fl)OC(Mo)} - \sum Q_{(s)VCB}\end{array}\right]} \qquad \text{(A1-7)}$$

where the subscript *(fl)* denotes either refrigerant or water. If $\sum Q_{(s)E}$ and $\sum Q_{(s)VCB}$ are negligible compared to the sums of the other terms in the numerator and denominator respectively, (A1-7) reduces to (3-13b).

APPENDIX 2

RUNNING COSTS OF FLUID COOLING INSTALLATIONS ON SOUTH AFRICAN GOLD MINES

In 1990 - the last year for which the Chamber of Mines of South Africa published costs of stores and electrical energy consumption - the cost of stores consumed by "ventilation, cooling and air-conditioning plants" (these being fluid cooling installations) on gold mines which were members of the Chamber was 19,4-million South African Rands (SAR), a mere 0,11 per cent of these mines' total working cost of SAR18 109-million (Chamber of Mines of South Africa, 1991a).

The cost of the electrical energy consumed by these installations during that year is estimated at approximately SAR118-million.[1] This is only 7,4 per cent of the total cost of SAR1 596-million of electrical energy purchased by these mines during 1990 (Chamber of Mines of South Africa, 1991a), and only 0,65 per cent of the aforementioned total working cost.

Of course, running costs of such installations will be a higher proportion of total working costs for those mines, or sections of mines, more dependent on refrigeration.

---

[1] In 1990, approximately 750 MW(R) and 550 MW(R) of water chilling capacity was installed at these mines on surface and underground respectively; and 70 per cent of these capacities were in use (Chamber of Mines of South Africa, 1991b). For these surface and underground capacities in use, respective seasonal load factors of 0,67 and 1, and average *installation* COPs (see Section 2.3.3, Chapter 2) of 5,5 and 3,0, were assumed in estimating the resulting average electric power requirements during 1990 of 64 and 128 MW respectively. Finally, the average cost to mines in 1990 of approximately SAR0,07 for 1 kilowatt-hour of electrical energy (Chamber of Mines of South Africa, 1991b) was used in estimating the cost of the electrical energy so consumed.

APPENDIX 3

CONFIRMING TESTS BY ENERGY BALANCE METHODS IN STANDARDS FOR TESTING WATER CHILLING MACHINES

A3.1 Condenser Energy Balance Method

This uses the heat-removing water load and the refrigerant-circuit measurements. The energy balances for the condenser and evaporator blocks of the generalised water chilling machine are, from (3-8b) and (3-9),

$$\begin{aligned} \sum Q_{(w)CB} + \sum m_{(r)CB} h_{(r)CB} + \sum Q_{(w)CB(VCB)} + \sum Q_{(s)CB} = 0 \\ \sum Q_{(w)EB} + \sum m_{(r)EB} h_{(r)EB} + \sum Q_{(w)EB(VCB)} + \sum Q_{(s)EB} = 0 \end{aligned} \qquad \text{(A3-1a)}$$

If these blocks have only one refrigerant inlet and outlet,[1] these reduce to

$$\begin{aligned} \sum Q_{(w)CB} + m_{(r)CB}(h_{CBi} - h_{CBo}) + \sum Q_{(w)CB(VCB)} + \sum Q_{(s)CB} = 0 \\ \sum Q_{(w)EB} + m_{(r)EB}(h_{EBi} - h_{EBo}) + \sum Q_{(w)EB(VCB)} + \sum Q_{(s)EB} = 0 \end{aligned} \qquad \text{(A3-1b)}$$

where $m_{(r)CB}$ is the single refrigerant mass flow-rate through the condenser block; h_{CBi} and h_{CBo} are the refrigerant enthalpies at its inlet and outlet; and $m_{(r)EB}$, h_{EBi} and h_{EBo} have corresponding meanings.

A3.1.1 Refrigerant Mass Flow-Rate through Condenser Block

From the first relation in (A3-1b), $m_{(r)CB}$ can be estimated as

$$m_{(r)CB} = \frac{\sum Q_{(w)CBp} + \sum Q_{(w)CB(VCB)} + \sum Q_{(s)CB}}{h_{CBo} - h_{CBi}} \qquad \text{(A3-2)}$$

---

[1] These blocks may have one *main* refrigerant inlet and outlet, but small, auxiliary refrigerant inlets and outlets, serving, for example, oil-to-refrigerant oil coolers of compressors. Account may be taken of such auxiliary refrigerant flows in a manner analogous to that in Section A1.2, Appendix 1.

This is (4-1a) in Chapter 4. $\sum Q_{(w)CBp}$ is the apparent value of $\sum Q_{(w)Cb}$ derived from the principal test, and $\sum Q_{(s)CB}$ is estimated by the approximate methods described in the standards (e.g. ASHRAE, 1978 : 7).

A3.1.2 Refrigerant Mass Flow-Rate through Evaporator Block

Next, $m_{(r)EB}$ must be determined. Recalling the definition of refrigerant-circuit COP $COP_{(r)}$ in (3-11c),

$$COP_{(r)} \equiv \frac{-\sum m_{(r)EB} h_{(r)EB}}{-\sum m_{(r)VCB} h_{(r)VCB}} \qquad \text{(A3-3a)}$$

In the generalised water chilling machine (Figure 3.5), all refrigerant streams pass into or out of the vapour-compression block, and out of or into *either* the evaporator *or* the condenser blocks. Hence

$$\sum m_{(r)VCB} h_{(r)VCB} = -\sum m_{(r)EB} h_{(r)EB} - \sum m_{(r)CB} h_{(r)CB} \qquad \text{(A3-3b)}$$

From (A3-3a) and (A3-3b),

$$1 + COP_{(r)} = \frac{-\sum m_{(r)VCB} h_{(r)VCB} - \sum m_{(r)EB} h_{(r)EB}}{-\sum m_{(r)VCB} h_{(r)VCB}} = \frac{\sum m_{(r)CB} h_{(r)CB}}{-\sum m_{(r)VCB} h_{(r)VCB}} \qquad \text{(A3-3c)}$$

and it follows that

$$\frac{-\sum m_{(r)EB} h_{(r)EB}}{\sum m_{(r)CB} h_{(r)CB}} = \frac{COP_{(r)}}{1 + COP_{(r)}} \qquad \text{(A3-3d)}$$

For machines with single refrigerant mass flows entering and leaving their evaporator and condenser blocks, this becomes, after manipulation

$$m_{(r)EB} = m_{(r)CB} \cdot \frac{h_{CBi} - h_{CBo}}{h_{EBo} - h_{EBi}} \cdot \frac{COP_{(r)}}{1 + COP_{(r)}} \qquad \text{(A3-3e)}$$

For a conventional packaged machine, the evaporator and condenser blocks *EB* and *CB* reduce to a single evaporator *E* and condenser *C* respectively. For such a machine with a single-stage centrifugal compressor, as in Figure 3.6, *bypassing no hot gas,*[2] with $COP_{(r)}$ given by (3-14b), (A3-3e) reduces to

$$m_{(r)E} = m_{(r)C} \qquad \text{(A3-4a)}$$

and for such a machine with a two-stage centrifugal compressor and economiser, as in Figure 3.18, *bypassing no hot gas,* with $COP_{(r)}$ given by (3-22c), (A3-3e) reduces to

$$m_{(r)E} = m_{(r)C} \Big/ \left(1 + \frac{h_{ECi} - h_{ECto}}{h_{ECvo} - h_{ECi}}\right) \qquad \text{(A3-4b)}$$

as also given by ISO/DIS 916-3 (ISO, 1994 : 15[3]), where h_{ECi}, h_{ECto} and h_{ECvo} are the refrigerant enthalpies at the inlet, liquid outlet, and vapour outlet, respectively, of the economiser.

A3.1.3 Confirming Value of Water Chilling Load

Finally, the confirming value of net water chilling load, $\sum Q_{(w)EBo}$, is determined by rearranging the second relation of (A3-1b) to give (4-1c).

---

[2] If hot gas is being bypassed, there are *two* refrigerant flows, differing in properties, leaving the condenser and entering the evaporator - violating the assumption of single mass flows through these components.

[3] ISO/DIS 916-3 actually gives this formula as $m_{(r)E} = m_{(r)C} \cdot \left(1 + \frac{h_{ECi} - h_{ECto}}{h_{ECvo} - h_{ECi}}\right)$. This is an obvious misprint: $m_{(r)E}$ cannot be greater than $m_{(r)C}$.

A3.2 Compressor Energy Balance Method

This uses the input power and the refrigerant-circuit measurements. The energy balance for the vapour-compression block of the generalised water chilling machine is, from (3-10),

$$\sum W_{VCB} + \sum m_{(r)VCB} h_{(r)VCB} - \sum Q_{(w)EB(VCB)} - \sum Q_{(w)CB(VCB)} + \sum Q_{(w)VCB(Ms)} + \sum Q_{(s)VCB} = 0 \qquad \text{(A3-5a)}$$

If the evaporator and condenser blocks have only one refrigerant inlet and outlet, it follows from (A3-3b) that

$$\sum m_{(r)} h_{(r)VCB} = m_{(r)CB}(h_{CBo} - h_{CBi}) + m_{(r)EB}(h_{EBo} - h_{EBi}) \qquad \text{(A3-5b)}$$

(A3-5a) thus becomes

$$\sum W_{VCB} + m_{(r)CB}(h_{CBo} - h_{CBi}) + m_{(r)EB}(h_{EBo} - h_{EBi}) - \sum Q_{(w)EB(VCB)} - \sum Q_{(w)CB(VCB)} + \sum Q_{(w)VCB(Ms)} + \sum Q_{(s)VCB} = 0 \qquad \text{(A3-5c)}$$

A3.2.1 Refrigerant Mass Flow-Rate through Evaporator Block

From (A3-3e),

$$m_{(r)CB} = m_{(r)EB} \cdot \frac{h_{EBo} - h_{EBi}}{h_{CBi} - h_{CBo}} \cdot \frac{1 + COP_{(r)}}{COP_{(r)}} \qquad \text{(A3-6)}$$

Substituting (A3-6) into (A3-5c) and then solving the latter for $m_{(r)EB}$ yields

$$m_{(r)EB} = COP_{(r)} \cdot \frac{\left[\begin{array}{l} \sum W_{VCBp} + \sum Q_{(w)VCB(Ms)} \\ -\sum Q_{(w)EB(VCB)} - \sum Q_{(w)CB(VCB)} + \sum Q_{(s)VCB} \end{array}\right]}{h_{EBo} - h_{EBi}} \qquad \text{(A3-7)}$$

where $\sum W_{VCBp}$ is the apparent value of $\sum W_{VCB}$ derived from the principal test. This is (4-4) in Chapter 4.

As noted previously, for a conventional packaged machine, the evaporator and condenser blocks reduce to a single evaporator *E* and condenser *C* respectively. For such a machine with a single-stage centrifugal compressor, as in Figure 3.6, *bypassing no hot gas*, $COP_{(r)}$ is given by (3-14b):

$$COP_{(r)} = \frac{h_{Eo} - h_{EXI}}{h_{Po} - h_{Eo}} = \frac{h_{Eo} - h_{EI}}{h_{CI} - h_{Eo}} \qquad \text{(A3-8a)}$$

since $h_{EXI} = h_{EI}$ and $h_{Po} = h_{CI}$. (A3-7) thus reduces to

$$m_{(r)E} = \frac{\left[\begin{array}{l}\sum W_{VCB} + \sum Q_{(w)VCB(Ms)} \\ -\sum Q_{(w)E(VCB)} - \sum Q_{(w)C(VCB)} + \sum Q_{(s)VCB}\end{array}\right]}{h_{CI} - h_{Eo}} \qquad \text{(A3-8b)}$$

A3.2.2 Confirming Value of Water Chilling Load

Once $m_{(r)EB}$ is determined, $\sum Q_{(w)EBc}$ is again determined per (4-1c).

For a conventional packaged machine with a single-stage centrifugal compressor, bypassing no hot gas, (A3-8b) may be substituted into (4-1c) to yield

$$Q_{(w)Ec} = \frac{h_{Eo} - h_{EI}}{h_{CI} - h_{Eo}} \cdot \left[\begin{array}{l}\sum W_{VCB} + \sum Q_{(w)VCB(Ms)} \\ -\sum Q_{(w)E(VCB)} - \sum Q_{(w)C(VCB)} + \sum Q_{(s)VCB}\end{array}\right] \qquad \text{(A3-9a)}$$
$$-\sum Q_{(w)E(VCB)} - Q_{(s)E}$$

As noted in the description of the generalised water chilling machine (Figure 3.5) in Chapter 3, the net heat flow $Q_{(s)E}$ entering the external surfaces of the evaporator comprises the net heat flow $Q_{(Ms)E}$ from the machine surroundings, and the additional net heat flow $\left(Q_{(s)E} - Q_{(Ms)E}\right)$

originating from *within* the machine boundary. (A3-9a) can accordingly be rewritten as

$$Q_{(w)Ec} + Q_{(Ms)E} = \frac{h_{Eo} - h_{Ei}}{h_{Ci} - h_{Eo}} \cdot \left[\begin{array}{l} \sum W_{VCB} + \sum Q_{(w)VCB(Ms)} \\ -\sum Q_{(w)E(VCB)} - \sum Q_{(w)C(VCB)} + \sum Q_{(s)VCB} \end{array} \right] \quad \text{(A3-9b)}$$
$$-\sum Q_{(w)E(VCB)} - \left(Q_{(s)E} - Q_{(Ms)E}\right)$$

The left-hand side of (A3-9b) comprises the rate of heat removal from *external* media by the refrigerant, this rate being the "overall refrigerating capacity" as defined by ISO R916 (ISO, 1968). ISO R916 defines this to exclude all heat removal resulting from internal heat exchanges within the "refrigerating circuit"; here, these are $\sum Q_{(w)E(VCB)}$ and $\left(Q_{(s)E} - Q_{(Ms)E}\right)$. If these terms are neglected, (A3-9b) is equivalent to equation (9) on page 16 of ISO R916. This equation determines overall refrigerating capacity of a machine with a single stage of compression by the compressor energy balance method. ISO R916 does not explicitly state, though, that it is this method which is the basis of its equation (9).

APPENDIX 4

IMPLICATIONS OF ACCURACIES IN PRINCIPAL MEASUREMENTS REQUIRED BY STANDARDS FOR TESTING WATER CHILLING MACHINES

If a function Θ of multiple variables $z_1, z_2, \ldots z_n$ is continuous, has derivatives and varies slowly enough to be adequately represented by its first derivatives in a Taylor-series expansion, then (see, for example, Meyer, 1975 : 40) the uncertainty $\delta\Theta$ of the function can be expressed in terms of the uncertainties $\delta z_1, \delta z_2, \ldots \delta z_n$ in the individual variables, provided that they are all independent, as follows:

$$\delta\Theta = \sqrt{\sum_{k=1}^{n}\left(\frac{\partial\Theta}{\partial z_k}\cdot\delta z_k\right)^2} \qquad \text{(A4-1)}$$

A4.1 Uncertainty in Water Chilling Load

In an evaporator with a single water flow $m_{(w)E}$ and inlet and outlet water temperatures $t_{(w)EI}$ and $t_{(w)Eo}$, the water chilling load $Q_{(w)E}$ is given by

$$Q_{(w)E} = m_{(w)E}c_{(w)}\left(t_{(w)Eo} - t_{(w)EI}\right) \qquad \text{(A4-2)}$$

where $c_{(w)}$ is the specific heat of the water, assumed constant. By (A4-1), the uncertainty $\delta Q_{(w)E}$ in $Q_{(w)E}$ is thus

$$\delta Q_{(w)E} = c_{(w)}\sqrt{\left(t_{(w)Eo} - t_{(w)EI}\right)^2\left(\delta m_{(w)E}\right)^2 + m_{(w)E}^2\left[\left(\delta t_{(w)Eo}\right)^2 + \left(\delta t_{(w)EI}\right)^2\right]} \qquad \text{(A4-3a)}$$

where $\delta m_{(w)E}$, $\delta t_{(w)Eo}$ and $\delta t_{(w)EI}$ are the uncertainties in the measured values of $m_{(w)E}$, $t_{(w)Eo}$ and $t_{(w)EI}$ respectively. Dividing both sides of

(A4-3a) by the corresponding sides of (A4-2), the *relative* uncertainty $\delta Q_{(w)E}/Q_{(w)E}$, after algebraic manipulation, is

$$\frac{\delta Q_{(w)E}}{Q_{(w)E}} = \sqrt{\left(\frac{\delta m_{(w)E}}{m_{(w)E}}\right)^2 + \frac{\left(\delta t_{(w)Eo}\right)^2 + \left(\delta t_{(w)Ei}\right)^2}{\left(t_{(w)Eo} - t_{(w)Ei}\right)^2}} \qquad \text{(A4-3b)}$$

This yields the relative uncertainty in calculated water chilling load $Q_{(w)E}$ for known or assumed relative uncertainty $\delta m_{(w)E}/m_{(w)E}$ in measured water flow-rate, and uncertainties $\delta t_{(w)Eo}$ and $\delta t_{(w)Ei}$ in measured water temperatures. Figure 4.3 is plotted on this basis, with $\delta m_{(w)E}/m_{(w)E}$ set to the values in Table 4.3 required by ISO/DIS 916 and BS 7520, and ASHRAE 30-78 and ARI 550-92.

A4.2 Required Accuracy in Measured Water Temperatures for Specified Uncertainty in Water Chilling Load

If the uncertainties $\delta t_{(w)Eo}$ and $\delta t_{(w)Ei}$ in the temperature measurements are identical at $\delta t_{(w)}$, then solving (A4-3b) for $\delta t_{(w)}$ yields

$$\delta t_{(w)} = \left(t_{(w)Eo} - t_{(w)Ei}\right)\sqrt{\frac{\left(\delta Q_{(w)E}/Q_{(w)E}\right)^2 - \left(\delta m_{(w)E}/m_{(w)E}\right)^2}{2}} \qquad \text{(A4-4)}$$

This yields the required accuracy $\pm\delta t_{(w)}$ in the water temperature measurements to achieve a specified relative uncertainty $\delta Q_{(w)E}/Q_{(w)E}$ in calculated water chilling load, for a known or assumed relative uncertainty $\delta m_{(w)E}/m_{(w)E}$ in measured water flow-rate. Figure 4.6 is plotted on this basis, with $\delta Q_{(w)E}/Q_{(w)E} = \pm 0{,}07$, the limit specified by ISO R916 (ISO, 1968), and assumed uncertainties $\delta m_{(w)E}/m_{(w)E}$ of ±0,02, ±0,05 and ±0,06.

APPENDIX 5

SIMPLIFIED THERMODYNAMIC MODEL OF GORDON AND NG (1994, 1995) FOR VAPOUR-COMPRESSION REFRIGERATING MACHINES

Gordon and Ng (1995) report the development of a universal thermodynamic model for vapour-compression, absorption, thermoelectric and thermoacoustic refrigerating devices. They also describe its application to vapour-compression refrigerating machines. The application to such machines with reciprocating and centrifugal compressors is elaborated upon in Gordon and Ng (1994) and Gordon, Ng and Chua (1995) respectively. The harmony between these three papers is difficult to grasp at first sight. This appendix therefore summarises the basis and development of the model as reported in these papers, and then remarks on its validity, limitations and advantages.

The basic vapour-compression refrigerating machine of Figure 3.4 is considered. The First Law of Thermodynamics yields the energy balance (3-4). The Second Law yields the following *entropy* balance:

$$\Delta S = 0 = \frac{Q_C + q_{l\text{-}p.side}}{T_{(r)C}} + \frac{Q_E + q_{l\text{-}p.side}}{T_{(r)E}} \qquad \text{(A5-1)}$$

where Q_E and Q_C are evaporator and condenser load,[1] and $T_{(r)C}$ and $T_{(r)E}$ are the absolute evaporating and condensing temperatures of the refrigerant. $q_{l\text{-}p.side}$ and $q_{h\text{-}p.side}$ are the rates of "losses" (i.e. work expended non-usefully) due to the internal thermodynamic irreversibilities in the low-pressure (evaporator) side and high-pressure (condenser) side of the machine's refrigerant circuit.[2] These internal irreversibilities of

---

[1] It will be recalled that Q_C, being an energy flow out of the machine, is negative.

[2] Gordon and Ng (1994) correctly assign a positive sign to $q_{h\text{-}p.side}$ in (A5-1), but Gordon and Ng (1995) and Gordon, Ng and Chua (1995) assign a negative sign thereto. This is

throttling through the expansion valve, non-isentropic compression, fluid friction and heat leaks cause increases in refrigerant entropy.[3]

Combining (3-4), (3-5a) and (A5-1), the COP of the basic vapour-compression machine is obtained as:

$$\frac{1}{COP} = -1 + \frac{T_{(r)C}}{T_{(r)E}} + \frac{1}{Q_E} \cdot \left[q_{\text{l-p.side}} \cdot \frac{T_{(r)C}}{T_{(r)E}} + q_{\text{h-p.side}} \right] \tag{A5-2}$$

Gordon and Ng (1994) show that (A5-2) can be expressed in terms of absolute condenser inlet fluid temperature $T_{(fl)Ci}$ and evaporator outlet fluid temperature $T_{(fl)Eo}$ instead of $T_{(r)C}$ and $T_{(r)E}$:

$$\frac{1}{COP} = -1 + \frac{T_{(fl)Ci} + Q_E\left(1 + 1/COP\right)/F_C}{T_{(fl)Eo} - Q_E/F_E} + \frac{1}{Q_E} \cdot \left[q_{\text{l-p.side}} \cdot \frac{T_{(fl)Ci} + Q_E\left(1 + 1/COP\right)/F_C}{T_{(fl)Eo} - Q_E/F_E} + q_{\text{h-p.side}} \right] \tag{A5-3a}$$

where F_C and F_E are factors for the condenser and evaporator respectively, depending on heat-exchanger thermal conductance UA, and flow-rate $m_{(fl)}$ and specific heat $c_{(fl)}$ of the heat-carrying fluids:

Incorrect; both $q_{\text{l-p.side}}$ and $q_{\text{h-p.side}}$ must be positive, because both are rates of work "loss" due to irreversibilities, and hence cause *increases* of entropy in (A5-1).

[3] $q_{\text{l-p.side}}$ and $q_{\text{h-p.side}}$ are defined as if these entropy increases occur at the constant evaporating and condensing temperatures $T_{(r)E}$ and $T_{(r)C}$ respectively. That is, $q_{\text{l-p.side}}/T_{(r)E} \equiv \sum \Delta S'_{(\text{internal})\text{l-p.side}}$ and $q_{\text{h-p.side}}/T_{(r)C} \equiv \sum \Delta S'_{(\text{internal})\text{h-p.side}}$. In parenthesis, it must not be assumed that $q_{\text{l-p.side}}$ and $q_{\text{h-p.side}}$ are independent. The thermodynamic irreversibilities in a vapour-compression refrigerating machine are not independent of each other, as pointed out for example by Alefeld (1987). As shown by that author, the work "loss" rate due to internal irreversibilities can be expressed as $T_{(r)C} \cdot \sum \Delta S'_{(\text{internal})}$. This is more physically meaningful, because all such work is transformed into additional heat, rejected at the constant condensing temperature $T_{(r)C}$.

$$F_C \equiv m_{(fl)C} c_{(fl)} \left[1 - \exp\left(-UA_C / m_{(fl)C} c_{(fl)}\right)\right]$$
$$F_E \equiv m_{(fl)E} c_{(fl)} \left[\exp\left(UA_E / m_{(fl)E} c_{(fl)}\right) - 1\right] \qquad \text{(A5-3b)}$$

Solving (A5-3a) for $1/COP$,

$$\frac{1}{COP} = -1 + \frac{\left\{\begin{array}{l} T_{(fl)Cl} / \left(T_{(fl)Eo} - Q_E / F_E\right) \\ +(1/Q_E) \cdot \left[q_{h\text{-}p.side} + q_{l\text{-}p.side}\, T_{(fl)Cl} / \left(T_{(fl)Eo} - Q_E / F_E\right)\right] \end{array}\right\}}{1 - \left(Q_E + q_{l\text{-}p.side}\right) / \left[F_C \left(T_{(fl)Eo} - Q_E / F_E\right)\right]} \qquad \text{(A5-4)}$$

Gordon, Ng and Chua (1995) show that if the internal irreversibilities are dominant, and if (A5-4) is thus expanded about the limit in which "F_C and F_E are effectively infinite",[4] it approximates to

$$\frac{1}{COP} \cong -1 + \frac{T_{(fl)Cl}}{T_{(fl)Eo}} + \frac{1}{Q_E} \cdot \left(q_{l\text{-}p.side} \frac{T_{(fl)Cl}}{T_{(fl)Eo}} + q_{h\text{-}p.side}\right) + \Theta(1/Q_E) + \Theta(Q_E) + \Theta_{[E],[C]} \qquad \text{(A5-5a)}$$

where

$$\Theta(1/Q_E) \equiv \frac{1}{Q_E} \cdot \frac{q_{l\text{-}p.side}}{T_{(fl)Eo} F_C} \cdot \left(q_{l\text{-}p.side} \frac{T_{(fl)Cl}}{T_{(fl)E}} + q_{h\text{-}p.side}\right)$$
$$\Theta(Q_E) \equiv \frac{Q_E}{T_{(fl)Eo}} \cdot \frac{T_{(fl)Cl}}{T_{(fl)Eo}} \cdot \left(\frac{1}{F_C} + \frac{1}{F_E}\right) \qquad \text{(A5-5b)}[5]$$
$$\Theta_{[E],[C]} \equiv \frac{q_{l\text{-}p.side}\left[T_{(fl)Cl} / \left(T_{(fl)Eo} F_C\right) + \left(T_{(fl)Cl} / T_{(fl)Eo}\right)\left(1/F_C + 1/F_E\right)\right] + q_{h\text{-}p.side}/F_C}{T_{(fl)Eo}}$$

---

[4] Note from (A5-3b) that while $F_E \to \infty$ as $UA_E \to \infty$, $F_C \to m_{(fl)} c_{(fl)}$ as $UA_C \to \infty$. Thus F_C cannot become "effectively infinite". The approximation of (A5-5a) is valid, though, because terms of higher order all have F_E in their denominators, and thus tend to zero as $F_E \to \infty$.

Gordon, Ng and Chua (1995) state that:

- $\Theta(1/Q_E)$ is a negligible correction to (A5-5a);
- $\Theta(Q_E)$ can play an important role in machines where the *external* irreversibilities of heat transfer through the condenser and evaporator cause work "loss" rates comparable to those of the internal irreversibilities. However, this turns out *not* to be the case for the commercial machines using reciprocating and centrifugal compressors for which data have been reported;[6]
- $\Theta_{[E][C]}$, which is independent of Q_E, is normally negligible, but can grow to be non-negligible if noticeable heat-exchanger fouling occurs.

Therefore, provided that the external irreversibilities of heat transfer through the condenser and evaporator cause small work "loss" rates compared to those due to the internal irreversibilities, (A5-5a) can be approximated further to

$$\frac{1}{COP} \cong -1 + \frac{T_{(fl)Cl}}{T_{(fl)Eo}} + \frac{1}{Q_E}\cdot\left(q_{l\text{-p.side}}\frac{T_{(fl)Cl}}{T_{(fl)Eo}} + q_{h\text{-p.side}}\right) \qquad \text{(A5-6a)}$$

or if it is desired to take possible heat-exchanger fouling into account,

$$\frac{1}{COP} \cong -1 + \frac{T_{(fl)Cl}}{T_{(fl)Eo}} + \frac{1}{Q_E}\cdot\left(q_{l\text{-p.side}}\frac{T_{(fl)Cl}}{T_{(fl)Eo}} + q_{h\text{-p.side}}\right) + \Theta_{[E][C]} \qquad \text{(A5-6b)}$$

---

[5] Gordon and Ng (1995) express $\Theta_{[E][C]}$ differently as $q_E F_{[E][C]} T_{(w)Cl}/T_{(w)Eo}$, where $F_{[E][C]}$ "is a factor depending only on the heat exchanger properties...". This is not equivalent to $\Theta_{[E][C]}$ in (A5-6b) unless $q_C/F_C << q_E\left[T_{(w)Cl}/\left(T_{(w)Eo}F_C\right) + \left(T_{(w)Cl}/T_{(w)Eo}\right)\left(1/F_C + 1/F_E\right)\right]$.

[6] Austin (1991), Beyene et al. (1994) and one other reference are cited in support of this.

Depending on whether $T_{(fl)Cl}$ and $T_{(fl)Eo}$ are relatively constant or not, there are two forms of this approximate thermodynamic model.

A5.1 Heat-Carrying Fluid Temperatures Relatively Constant

If $T_{(fl)Cl}$ and $T_{(fl)Eo}$ are relatively constant, (A5-6a) or (A5-6b) is a *temperature-independent* model, predicting a straight-line relationship between $1/COP$ and $1/Q_E$:

$$\frac{1}{COP} \cong C_0 + \frac{C_1}{Q_E}$$

where $C_0 \cong -1 + \frac{T_{(fl)Cl}}{T_{(fl)Eo}}$ {$+\Theta_{[E][C]}$ if accounting for heat-exch. fouling} (A5-7)

and $C_1 \equiv q_{l\text{-p.side}} \frac{T_{(fl)Cl}}{T_{(fl)Eo}} + q_{h\text{-p.side}}$

The slope C_1 of this line depends on the "loss" rates $q_{l\text{-p.side}}$ and $q_{h\text{-p.side}}$, that is, on the internal irreversibilities. If $\Theta_{[E][C]}$ is included to account for heat-exchanger fouling, the constant C_0 depends thereon and thus on the heat-exchanger factors F_C and F_E as well as $q_{l\text{-p.side}}$ and $q_{h\text{-p.side}}$.

A5.2 Heat-Carrying Fluid Temperatures Varying

If $T_{(fl)Cl}$ and $T_{(fl)Eo}$ vary appreciably, Gordon and Ng (1994, 1995) derive a *temperature-dependent* model, assuming that the internal irreversibilities of throttling through the expansion valve, non-isentropic compression and fluid friction are not excessive, and that heat leaks are dominated by a linear heat transfer law.[7] This temperature-dependent model is

---

[7] As Phelan, Brandemuehl and Krarti (1997) point out, this is equivalent to assuming that the "losses" due to internal irreversibilities can be expressed as linear functions of either $T_{(r)E}$ or $T_{(r)C}$.

$$\frac{1}{COP} \cong -1 + \frac{T_{(ll)Ci}}{T_{(ll)Eo}} + \frac{-C_0 + C_1 T_{(ll)Ci} - C_2\left(T_{(ll)Ci} - T_{(ll)Eo}\right)}{Q_E} \qquad \text{(A5-8)}$$

where the constants C_0, C_1 and C_2 characterise the internal irreversibilities of a particular machine.

The appropriate model, (A5-7) or (A5-8), is attuned to a particular machine by determining the constants C through regression analyses of sets of accurately recorded values of $T_{(w)Ci}$, $T_{(w)Eo}$, Q_E and COP over the machine's entire operating range (Gordon and Ng, 1994, 1995). The attuned model can then be used to predict COP.

A5.3 Validity, Limitations and Advantages of Model

(A5-7) and (A5-8) are two forms of Gordon and Ng's relatively simple, fundamentally-based, empirically attuned thermodynamic model of a simple vapour-compression water chilling machine. Put another way, their model is a relatively simple regression one with a fundamental basis. The output is COP and the inputs are Q_E (and hence, to obtain this, $T_{(ll)Eo}$, $m_{(ll)E}$, and $T_{(ll)Ei}$) and, for the temperature-dependent model, $T_{(ll)Eo}$ and $T_{(ll)Ci}$.[8] The model makes no use of process parameters or state variables in the refrigerant circuit, and yields no refrigerant quantities as outputs.

This model, being a combination of the First and Second Laws of Thermodynamics and heat-exchanger theory at the outermost or global level, is limited to incorporating the capabilities and limitations of a machine *at that level*. All that appears at this outermost, global level are

---

[8] In addition, for both the temperature-independent and -dependent models, it is wise to record the condenser fluid flow-rate $m_{(ll)C}$ as an input; although it does not explicitly appear as such, it is a term in the condenser factor F_C. Hence, if it varies significantly, one or more of the constants C in (A5-7) and (A5-8) may change significantly, hence invalidating the attuned model. (The same obviously applies for $m_{(ll)E}$.)

the *effects* of the machine's capabilities and limitations (here, rates $q_{l\text{-}p,side}$ and $q_{h\text{-}p,side}$ of work "loss" in internal irreversibilities, and heat-exchanger factors F_C and F_E). The underlying process parameters and state variables *causing* these effects only appear at inner, more detailed levels of fundamental modelling. Modelling at global level thus cannot predict how these process parameters and state variables will change as the operating regime changes. Hence this model, as for regression models, may not be valid outside the range of the operating data for which it has been attuned.[9]

Two other corollaries also follow from this absence of inner modelling. First, if (A5-7) or (A5-8) is to be used to predict *normal* performance, the operating data used to attune the model *must be verified as representing normal performance*. That is, all process parameters and state variables must be ascertained by other means and verified as being sufficiently close to their design values. Second, in general, the model cannot be directly used to predict *optimal* performance, because the operating regime may alter and no longer specify the load,[10] allowing this or some process parameters to vary to satisfy the specified criteria of optimality.

Finally, it is recalled that the model has been derived for the basic refrigerating machine of Figure 3.4. The model requires modification, although this does not appear difficult in principle, to make it applicable to the generalised machine of Figure 3.5, and hence to the more complex, large-capacity water chilling machines considered in this thesis.

Nevertheless, the advantage of the model is simplicity and ability to predict the performance quantities of immediate practical and economic

---

[9] For example, if hot gas bypass commences in a conventional machine, one or both work "loss" rates $q_{l\text{-}p,side}$ and $q_{h\text{-}p,side}$ will change in step fashion. At least some constants in the model will therefore change similarly.

[10] In (A5-7) and (A5-8), the load appears as an input, so it must be known beforehand.

relevance - *COP* and hence power and energy demand. Once the model has been modified to apply to the generalised machine of Figure 3.5 and the required operating data base has been built up, it should thus be especially useful and convenient for predicting *normal* COP and power demand of custom-built water chilling machines employing multiple evaporators, condensers and screw compressors. Predicting these normal quantities of performance by detailed fundamental modelling is less preferable, because such custom-built machines are more complicated than conventional ones to so model. In principle, there seems to be no reason why the model cannot be extended to such machines.

APPENDIX 6

RELATIVE HEAT IMBALANCE IN TERMS OF COP AND RELATIVE ERRORS IN APPARENT CONSTITUENTS OF HEAT BALANCE

From (5-5) and (5-2), the relative heat imbalance is

$$\varepsilon \cong \frac{\delta Q_{EBp} + \delta W_{VCBp} + \delta Q_{JBp}}{\sum Q_{JBp}} = \frac{\delta Q_{EBp} + \delta W_{VCBp} + \delta Q_{JBp}}{\sum Q_{(w)JB} + \delta Q_{JBp}} \tag{A6-1}$$

Using the definitions of the relative errors in (5-3), this can be expressed as

$$\begin{aligned} \varepsilon &\cong \frac{\sum Q_{(w)EB} \cdot n_{EBp} + \sum W_{VCB} \cdot n_{VCBp} + \sum Q_{(w)JB} \cdot n_{JBp}}{\sum Q_{(w)JB} \cdot (1 + n_{JBp})} \\ &= \frac{1}{1+n_{JBp}} \cdot \left[\frac{\sum Q_{(w)EB} \cdot n_{EBp}}{\sum Q_{(w)JB}} + \frac{\sum W_{VCB} \cdot n_{VCBp}}{\sum Q_{(w)JB}} + n_{JBp} \right] \end{aligned} \tag{A6-2}$$

By appropriate substitution from (5-1c) into (5-6), it is easily shown that

$$\frac{\sum Q_{(w)EB}}{\sum Q_{(w)JB}} \cong \frac{-COP}{1+COP} \qquad \text{and} \qquad \frac{\sum W_{VCB}}{\sum Q_{(w)JB}} \cong \frac{-1}{1+COP} \tag{A6-3}$$

Substituting these into (A6-2),

$$\varepsilon \cong \frac{1}{1+n_{JBp}} \cdot \left[-\frac{COP \cdot n_{EBp}}{1+COP} - \frac{n_{VCBp}}{1+COP} + n_{JBp} \right] \tag{A6-4}$$

which is (5-7).

APPENDIX 7

REFRIGERANT-CIRCUIT COP OF CONVENTIONAL MACHINES

Formulae for refrigerant-circuit COP are given here for the key types of conventional water chilling machines in use on mines. To save space, derivations of these formulae, which are done in like manner to Appendix 1, are omitted.

A7.1 Machines with a Single-Stage Centrifugal Compressor

The refrigerant circuit of these machines is as in Figure 3.6.

A7.1.1 Machine Operating Normally

Normally, the machine does not bypass hot gas. The well-known formula for refrigerant-circuit COP in this case is (3-15b):

$$COP_{(r)} = \frac{h_{Eo} - h_{EXI}}{h_{Po} - h_{Eo}} \qquad \text{(A7-1a)}$$

where h_{Eo} is enthalpy of vapour at evaporator outlet, h_{EXI} is enthalpy of liquid entering the expansion valve,[1] and h_{Po} is enthalpy of vapour at compressor discharge.

A7.1.2 Machine Bypassing Hot Gas

If hot gas is being bypassed directly from condenser to evaporator, as in Figure 3.6 when the hot gas bypass valve is open, the refrigerant-circuit COP is (3-15a):

---

[1] This liquid, of course, comes from the condenser, but it may be subcooled if it passes through a subcooler following the condenser. Sometimes a subcooler is even built into the condenser. If a subcooler is present, its effect must be accounted for in calculating the enthalpy of this liquid.

$$COP_{(r)} = \frac{(h_{Eo} - h_{EXI}) - \frac{m_{(r)HG}}{m_{(r)EX}} \cdot (h_{HGI} - h_{Eo})}{\left(1 + \frac{m_{(r)HG}}{m_{(r)EX}}\right) \cdot (h_{Po} - h_{Eo})} \qquad \text{(A7-1b)}$$

Here, $m_{(r)HG}/m_{(r)EX}$ denotes the ratio of mass flow of bypassing hot gas to mass flow through the expansion valve. h_{HGI} denotes the enthalpy of the vapour entering the hot gas bypass valve; because this vapour comes from the condenser, its enthalpy is normally assumed to be that of saturated vapour at the condensing temperature.

In some older machines, hot gas is bypassed to the compressor suction, not to the evaporator. The machine is then fitted with an accompanying *liquid injection valve.* This injects a small amount of liquid from the condenser into the bypassing hot gas, to de-superheat it and thus prevent excessively high compressor discharge temperature. In such cases, the refrigerant-circuit COP is given by

$$COP_{(r)} = \frac{h_{Eo} - h_{EXI}}{(h_{Po} - h_{Eo}) + \frac{m_{(r)HG}}{m_{(r)EX}} \cdot (h_{Po} - h_{HGI}) + \frac{m_{(r)LI}}{m_{(r)EX}} \cdot (h_{Po} - h_{LII})} \qquad \text{(A7-1c)}$$

where $m_{(r)LI}$ is the mass flow through the liquid injection valve, and h_{LII} is the enthalpy of the liquid entering this valve (normally assumed equal to that of saturated liquid at the condensing temperature).

A7.2 Machines with a Two-Stage Centrifugal Compressor and Economiser

The refrigerant circuit of such machines is as in Figure 3.18.

A7.2.1 Machine Operating Normally

If no hot gas is being bypassed, then as in (3-23c):

$$COP_{(r)} = \frac{h_{Eo} - h_{ECro}}{(h_{Po} - h_{Eo}) + A(h_{Po} - h_{ECvo})} \qquad \text{(A7-2a)}$$

where $$A = \frac{h_{EX1i} - h_{ECro}}{h_{ECvo} - h_{EX1i}}$$

h_{ECIo} and h_{ECvo} are the enthalpies of the liquid and vapour, respectively, leaving the economiser; and h_{EX1i} is the enthalpy of the liquid entering the first expansion valve[2] (expansion valve 1 in Figure 3.18).

A7.2.2 Machine Bypassing Hot Gas

When the hot gas bypass valve in Figure 3.18 is open, $COP_{(r)}$ is as in (3-23b):

$$COP_{(r)} = \frac{(h_{Eo} - h_{ECIo}) - \frac{m_{(r)HG}}{m_{(r)EX2}} \cdot (h_{HGi} - h_{Eo})}{(h_{Po} - h_{Eo}) \cdot \left(1 + \frac{m_{(r)HG}}{m_{(r)EX2}}\right) + A(h_{Po} - h_{ECvo})} \qquad \text{(A7-2b)}$$

where A is as in (A7-2a) above. Here, $m_{(r)HG}/m_{(r)EX2}$ is the ratio of mass flow of bypassing hot gas to that through the *second* expansion valve (the final one that feeds the evaporator). Some machines are equipped with two hot gas bypass valves, the second one bypassing hot gas from the condenser to the economiser. Formula (A7-2b) can readily be modified accordingly. For such machines, particular care must be taken to note *which* hot gas bypass valves (one or possibly both) are open.

A7.3 Machines with a Three-Stage Centrifugal Compressor and Two Economisers

The refrigerant circuit of such machines is illustrated in Figure A7.1 below.

---

[2] Again, this liquid may come directly from the condenser, or from a subcooler following or built into the condenser.

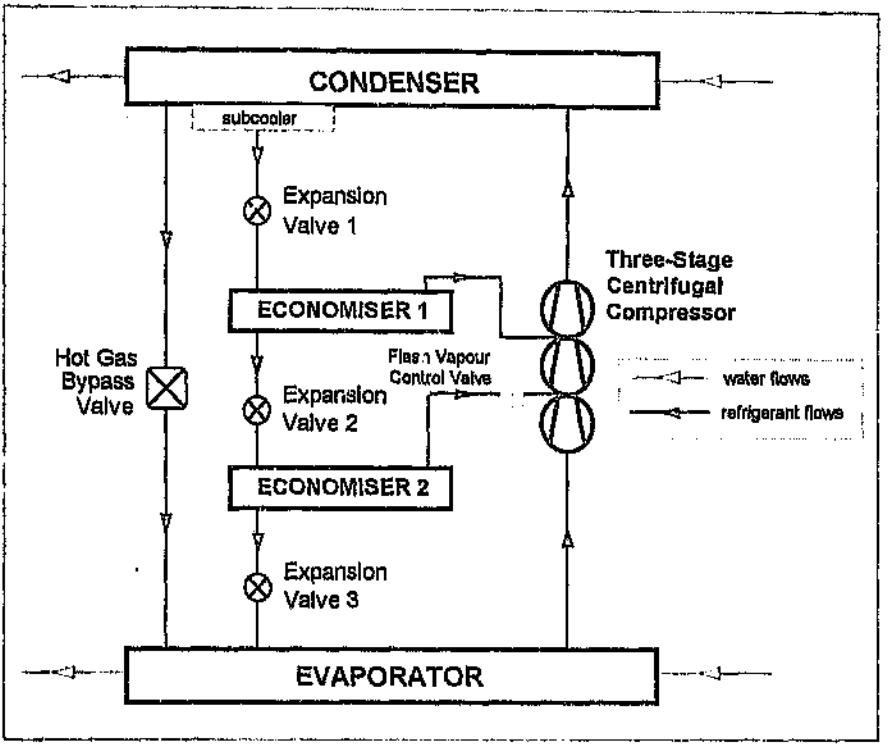

Figure A7.1 Conventional Machine with Three-Stage Centrifugal Compressor and Two Economisers

A7.3.1 Machine Operating Normally

If no hot gas is being bypassed,

$$COP_{(r)} = \frac{h_{Eo} - h_{EC2fo}}{(h_{Po} - h_{Eo}) + A_1(h_{Po} - h_{EC1vo}) + A_2(h_{Po} - h_{EC2vo})}$$

where $$A_1 = \frac{(h_{EX1f} - h_{EC1fo})(h_{EC2vo} - h_{EC2fo})}{(h_{EC1vo} - h_{EX1f})(h_{EC2vo} - h_{EC1fo})} \qquad \text{(A7-3a)}$$

and $$A_2 = \frac{h_{EC1fo} - h_{EC2fo}}{h_{EC2vo} - h_{EC1fo}}$$

where h_{EC1fo} and h_{EC1vo} are the enthalpies of liquid and vapour, respectively, leaving the *first* (higher-pressure) economiser, and h_{EC2fo}

and h_{EC2vo} are the corresponding enthalpies for the second (lower-pressure) economiser. The enthalpy h_{EX1i} is that of the liquid entering the first expansion valve from either the condenser or a subcooler following or built into the condenser.

A7.3.2 Machine Bypassing Hot Gas

Again, this formula is for hot gas bypassing directly from condenser to evaporator.

$$COP_{(r)} = \frac{\left(h_{Eo} - h_{EC2vo}\right) - \dfrac{m_{(r)HG}}{m_{(r)EX3}} \cdot \left(h_{HGi} - h_{Eo}\right)}{\left(h_{Po} - h_{Eo}\right) \cdot \left(1 + \dfrac{m_{(r)HG}}{m_{(r)EX3}}\right) + A_1\left(h_{Po} - h_{EC1vo}\right) + A_2\left(h_{Po} - h_{EC2vo}\right)} \quad \text{(A7-3b)}$$

where A_1 and A_2 are as in (A7-3a) above. $m_{(r)HG}/m_{(r)EX3}$ is the ratio of mass flow of bypassing hot gas to that through the *third* expansion valve (the final one feeding the evaporator). Again, some machines may be equipped with additional hot gas bypass valves, bypassing hot gas to the first or second economisers. In such cases, (A7-3b) can be modified accordingly, and the remarks for (A7-2b) above also apply.

APPENDIX 8

CORRECTING REFRIGERANT-CIRCUIT COP TO REFLECT ACTUAL COP

From (3-11c), (3-9) and (3-10), the refrigerant-circuit COP $COP_{(r)}$ of the generalised water chilling machine is

$$COP_{(r)} \equiv \frac{-\sum m_{(r)EB} h_{(r)EB}}{-\sum m_{(r)VCB} h_{(r)VCB}} = \frac{\sum Q_{(w)EB} + \sum Q_{(w)EB(VCB)} + \sum Q_{(s)EB}}{\sum W_{VCB} - \sum Q_{(w)EB(VCB)} - \sum Q_{(w)CB(VCB)} + \sum Q_{(w)VCB(Ms)} + \sum Q_{(s)VCB}} \quad \text{(A8-1)}$$

As seen from comparing this with (3-11a), $COP_{(r)}$ is not identical to actual COP. It is corrected to reflect actual COP as follows.

In determining $COP_{(r)}$, it is sometimes convenient not to include certain auxiliary *refrigerant* flows circulating between the vapour-compression block and the evaporator or condenser blocks. Such flows, for example, may be those passing through oil-to-refrigerant heat exchangers cooling compressor oil. Let the heat loads passing into the evaporator and condenser blocks due to such auxiliary refrigerant flows be $\sum Q_{(r.aux)EB(VCB)}$ and $\sum Q_{(r.aux)CB(VCB)}$ respectively, defined as:

$$\sum Q_{(r.aux)EB(VCB)} \equiv \left(\sum m_{(r.aux)EB} h_{(r.aux)EB}\right)_{(VCB)}$$
$$\sum Q_{(r.aux)CB(VCB)} \equiv \left(\sum m_{(r.aux)CB} h_{(r.aux)CB}\right)_{(VCB)} \quad \text{(A8-2)}$$

$\sum m_{(r)EB} h_{(r)EB}$ and $\sum m_{(r)VCB} h_{(r)VCB}$ in (3-9) and (3-10) are accordingly defined as follows:

$$\begin{aligned}\sum m_{(r)EB}h_{(r)EB} &\equiv \left(\sum m_{(r)EB}h_{(r)EB}\right)_{\text{non-aux}} + \left(\sum m_{(r,\text{aux})EB}h_{(r,\text{aux})EB}\right)_{(VCB)} \\ &= \left(\sum m_{(r)EB}h_{(r)EB}\right)_{\text{non-aux}} + \sum Q_{(r,\text{aux})EB(VCB)}\end{aligned} \tag{A8-3a}$$

$$\begin{aligned}\sum m_{(r)VCB}h_{(r)VCB} &\equiv \left(\sum m_{(r)VCB}h_{(r)VCB}\right)_{\text{non-aux}} \\ &\quad -\left(\sum m_{(r,\text{aux})EB}h_{(r,\text{aux})EB}\right)_{(VCB)} - \left(\sum m_{(r,\text{aux})CB}h_{(r,\text{aux})CB}\right)_{(VCB)} \\ &= \left(\sum m_{(r)VCB}h_{(r)VCB}\right)_{\text{non-aux}} \\ &\quad -\sum Q_{(r,\text{aux})EB(VCB)} - \sum Q_{(r,\text{aux})CB(VCB)}\end{aligned} \tag{A8-3b}$$

Hence, if it is convenient to consider the refrigerant-circuit COP $COP_{(r)}$ as the ratio of flows of heat and work absorbed by the main (non-auxiliary) flows of refrigerant - given by $\left(\sum m_{(r)EB}h_{(r)EB}\right)_{\text{non-aux}} \Big/ \left(\sum m_{(r)VCB}h_{(r)VCB}\right)_{\text{non-aux}}$ - then from (A8-1),

$$\begin{aligned}COP_{(r)} &= \frac{-\left(\sum m_{(r)EB}h_{(r)EB}\right)_{\text{non-aux}}}{-\left(\sum m_{(r)VCB}h_{(r)VCB}\right)_{\text{non-aux}}} \\ &= \frac{\sum Q_{(w)EB} + \sum Q_{(w)EB(VCB)} + \sum Q_{(s)EB} + \sum Q_{(r,\text{aux})EB(VCB)}}{\left[\begin{array}{l}\sum W_{VCB} - \sum Q_{(w)EB(VCB)} - \sum Q_{(w)CB(VCB)} + \sum Q_{(w)VCB(Ms)} \\ +\sum Q_{(s)VCB} - \sum Q_{(r,\text{aux})EB(VCB)} - \sum Q_{(r,\text{aux})CB(VCB)}\end{array}\right]}\end{aligned} \tag{A8-4}$$

Let the following ratios of energy flows be defined:

$$\begin{aligned}R_{(EB)} &\equiv \frac{\sum Q_{(w)EB(VCB)} + \sum Q_{(s)EB} + \sum Q_{(r,\text{aux})EB(VCB)}}{\sum Q_{(w)EB}} \\ R_{(VCB)} &\equiv \frac{\left[\begin{array}{l}-\sum Q_{(w)EB(VCB)} - \sum Q_{(w)CB(VCB)} + \sum Q_{(w)VCB(Ms)} + \sum Q_{(s)VCB} \\ -\sum Q_{(r,\text{aux})EB(VCB)} - \sum Q_{(r,\text{aux})CB(VCB)}\end{array}\right]}{\sum W_{VCB}}\end{aligned} \tag{A8-5}$$

The rightmost side of (A8-4) accordingly becomes

$$COP_{(r)} = \frac{\left(1+R_{[EB]}\right)\sum Q_{(w)EB}}{\left(1+R_{[VCB]}\right)\sum W_{VCB}} = \frac{1+R_{[EB]}}{1+R_{[VCB]}} \cdot COP \qquad \text{(A8-6)}$$

If $\sum Q_{(s)EB}$ and $\sum Q_{(s)VCB}$ are negligible compared to the sums of the other terms in the respective numerators of (A8-5), then

$$R_{[EB]} \cong \frac{\sum Q_{(w)EB(VCB)} + \sum Q_{(r.aux)EB(VCB)}}{\sum Q_{(w)EB}}$$

$$R_{[VCB]} \cong \frac{\left[\begin{array}{l} -\sum Q_{(w)EB(VCB)} - \sum Q_{(w)CB(VCB)} + \sum Q_{(w)VCB(Me)} \\ -\sum Q_{(r.aux)EB(VCB)} - \sum Q_{(r.aux)CB(VCB)} \end{array}\right]}{\sum W_{VCB}} \qquad \text{(A8-7)}$$

A8.1 All Water or Auxiliary Refrigerant Flows Circulating between Evaporator and Vapour-Compression Blocks

If all water flows passing through the vapour-compression block, or all such auxiliary refrigerant flows, circulate between the vapour-compression and evaporator blocks,

$$R_{[VCB]} = -\left(\sum Q_{(w)EB(VCB)} + \sum Q_{(r.aux)EB(VCB)}\right) \Big/ \sum W_{VCB} \qquad \text{(A8-8a)}$$

and so it follows from the definition of COP (see (3-11a)) that

$$R_{[EB]} \cong \frac{-R_{[VCB]}}{COP} \qquad \text{(A8-8b)}$$

Substituting (A8-8b) into (A8-6) and solving for COP,

$$COP \cong COP_{(r)}\left(1+R_{[VCB]}\right) + R_{[VCB]} \qquad \text{(A8-8c)}$$

with $R_{[VCB]}$ given by (A8-8a). In reality, $R_{[VCB]}$ has to be estimated from the ratio $-\left(\sum Q_{(w)EB(VCB)} + \sum Q_{(r.aux)EB(VCB)}\right) \Big/ \sum W_{VCBp}$, where $\sum W_{VCBp}$ is the

apparent value of total mechanical input power, calculated from the principal measurements. For centrifugal compressors, $\left(\sum Q_{(w)EB(VCB)} + \sum Q_{(r,aux)EB(VCB)}\right)$ may be estimated approximately, as it is small (but generally not negligible) compared to $\sum W_{VCB}$. For screw compressors whose oil is cooled in oil-to-water or oil-to-refrigerant heat exchangers, the oil cooling load is a significant fraction of $\sum W_{VCB}$, so it is important to measure $\left(\sum Q_{(w)EB(VCB)} + \sum Q_{(r,aux)EB(VCB)}\right)$ in order to accurately estimate $R_{[VCB]}$.

A8.2 All Water or Auxiliary Refrigerant Flows Circulating between Vapour-Compression Block and Condenser Block or outside Machine Boundary

Where all water flows passing through the vapour-compression block circulate between this block and either the condenser block or sources outside the machine boundary - or where all auxiliary refrigerant flows not included in the determination of $COP_{(r)}$ pass between the vapour-compression and condenser blocks, it is seen from (A8-7) that

$$R_{[VCB]} \cong \frac{\sum Q_{(w)VCB(Ms)} - \sum Q_{(w)CB(VCB)} - \sum Q_{(r,aux)CB(VCB)}}{\sum W_{VCB}} \qquad \text{(A8-9a)}$$

$$R_{[EB]} \cong 0$$

Hence, from (A8-6),

$$COP \cong COP_{(r)}\left(1 + R_{[VCB]}\right) \qquad \text{(A8-9b)}$$

with $R_{[VCB]}$ being given by (A8-9a). In reality, $R_{[VCB]}$ has to be estimated from the ratio $\left(\sum Q_{(w)VCB(Ms)} - \sum Q_{(w)CB(VCB)} - \sum Q_{(r,aux)CB(VCB)}\right)/\sum W_{VCBp}$, where $\sum W_{VCBp}$ is the *apparent* value of total mechanical input power,

calculated from the principal measurements. The concluding remarks of Section A7.1 above also apply here.

A8.3 No Water Flows through Vapour-Compression Block; all Refrigerant Flows Included in Determination of Refrigerant-Circuit COP

If no water flows pa: through the vapour-compression block, and if *all* refrigerant flows passing between blocks are included in the determination of the refrigerant-circuit COP, $R_{[VCB]} \cong 0$ and $R_{[EB]} \cong 0$ in (A8-7) and hence

$$COP \cong COP_{(r)} \qquad \text{(A8-10)}$$

APPENDIX 9

RELATIONSHIPS BETWEEN RELATIVE ERRORS IN APPARENT CONSTITUENTS OF HEAT BALANCE

A9.1 Error in Apparent Evaporator-Load COP

The first apparent COP, $COP_{[EB]p}$, of (5-9c) is that calculated from apparent evaporator block load and input power. Let $\delta COP_{[EB]p}$ be the difference between this apparent COP and the actual COP. $\delta COP_{[EB]p}$ is thus the error in $COP_{[EB]p}$:

$$\delta COP_{[EB]p} \equiv COP_{[EB]p} - COP \tag{A9-1a}$$

From (5-9c) and (5-6) respectively,

$$\delta COP_{[EB]p} = \frac{\sum Q_{EBp}}{\sum W_{VCBp}} - \frac{\sum Q_{(w)EB}}{\sum W_{VCB}} \tag{A9-1b}$$

From the definitions of the relative errors in (5-3), it can be shown that

$$\sum Q_{(w)EB} = \frac{\sum Q_{EBp}}{1+n_{EBp}} \qquad \sum W_{VCB} = \frac{\sum W_{VCBp}}{1+n_{VCBp}}$$
$$\sum Q_{(w)JB} = \frac{\sum Q_{JBp}}{1+n_{JBp}} \tag{A9-2}$$

Substituting the first two relations of (A9-2) into (A9-1b) and manipulating,

$$\delta COP_{[EB]p} = \frac{\sum Q_{EBp}}{\sum W_{VCBp}} - \frac{\sum Q_{EBp}(1+n_{VCBp})}{\sum W_{VCBp}(1+n_{EBp})} = \frac{\sum Q_{EBp}(n_{EBp}-n_{VCBp})}{\sum W_{VCBp}(1+n_{EBp})}$$
$$= COP_{[EB]p} \cdot \frac{n_{EBp}-n_{VCBp}}{1+n_{EBp}} \tag{A9-3a}$$

Recalling the definition of $\delta COP_{[EB]p}$ in (A9-1a), it follows that

$$\frac{COP_{[EB]p} - COP}{COP_{[EB]p}} = \frac{n_{EBp} - n_{VCBp}}{1 + n_{EBp}} \qquad \text{(A9-3b)}$$

Solving (A9-3b) for n_{EBp} yields the first relation in (5-11).

A9.2 Error in Apparent Rejection-Load COP

The second apparent COP, $COP_{[JB]p}$, of (5-9c) is that calculated from apparent joint rejection load and input power. The error $\delta COP_{[JB]p}$ in this apparent COP is, from (5-9c) and (5-6) respectively:

$$\delta COP_{[JB]p} \equiv COP_{[JB]p} - COP = \frac{-\left(\sum Q_{JBp} + \sum W_{VCBp}\right)}{\sum W_{VCBp}} - \frac{\sum Q_{(w)EB}}{\sum W_{VCB}} \qquad \text{(A9-4)}$$

From (3-7c) and (5-1a), $\sum Q_{(w)EB} \approx -\left(\sum W_{VCB} + \sum Q_{(w)JB} + \sum Q_{(Ms)}\right)$. Substituting into (A9-4) and using the second and third relations of (A9-2), it follows after manipulation that

$$\frac{COP_{[JB]p} - COP}{1 + COP_{[JB]p}} + \frac{\sum Q_{(Ms)} \cdot \left(1 + n_{VCBp}\right)}{\sum Q_{JBp}} = \frac{n_{JBp} - n_{VCBp}}{1 + n_{JBp}} \qquad \text{(A9-5)}$$

Solving (A9-5) for n_{JBp} yields, after manipulation,

$$n_{JBp} = \frac{\left(1 + COP_{[JB]p}\right)\left(1 - \sum Q_{(Ms)} / \sum Q_{JBp}\right)\left(1 + n_{VCBp}\right) - \left(1 + COP\right)}{\left(1 + COP\right) + \left(1 + COP_{[JB]p}\right)\left(\sum Q_{(Ms)} / \sum Q_{JBp}\right)\left(1 + n_{VCBp}\right)} \qquad \text{(A9-6)}$$

For large-capacity machines, the ratio $\sum Q_{(Ms)} / \sum Q_{JBp} << 1$ and so, if this ratio is negligible, n_{JBp} reduces to the second relation in (5-11).

APPENDIX 10

EXPERIMENTAL TECHNIQUE IN SURVEYS OF PERFORMANCE OF WATER CHILLING MACHINES

A10.1 Temperature-Measuring Instruments

In all cases, portable mercury-in-glass thermometers with graduations of 0,1°C commencing above their specified immersion length of 100 mm were employed, having the following ranges:

-10°C to +20°C
+15°C to +45°C
+40°C to +70°C
+60°C to +90°C

These thermometers were calibrated by the South African Bureau of Standards after purchase, and certified to have uncertainties not exceeding ±0,04°C after applying the corrections determined during calibration.

A10.2 Other Instruments

With one exception, all other instruments were the normal ones fitted to the machines on site, and thus yielding the accuracies given in the rightmost column of Table 4.8 at best. The exception was Case Study B of Chapter 5. Here, it was possible to fit refrigerant pressure gauges of semi-master quality, purchased immediately beforehand and certified by their manufacturer as having uncertainty not exceeding ±1 kPa.

A10.3 Measurement Technique

The abovementioned thermometers were inserted into the available temperature-measuring wells in the piping or components of the machine. To ensure good thermal contact between well and thermometer, vertical

or inclined wells were first filled with water or light oil; horizontal wells were first filled with aluminium-based heat-conductive paste.

All measurements were recorded manually at 5-minute intervals, using enough observers (with synchronised watches) to record all required measurements simultaneously. The initial sets of measurements were carefully scrutinised for sufficient steadiness, that is, for the absence of variations rapid and substantial enough to introduce significant dynamic effects into machine performance. Apart from key input variables such as water flow-rates, quantities particularly scrutinised for such steadiness were positions of compressor capacity-regulating devices[1] and observable state variables, such as liquid levels in all refrigerant vessels and oil levels and foaming in compressor oil reservoirs.

Recording these sets of simultaneous measurements was continued until at least four consecutive sets with no variations capable of causing significant dynamic effects, and thus representative of static machine performance, were obtained. More than four such sets were obtained wherever possible, but this was not possible with machines in some installations - for example, the surface installation of Case Study A, Chapter 5 - where conditions varied considerably from hour to hour.

Once the measurements from these consecutive sets had been plotted and checked for obvious absurdities,[2] they were averaged and the mean values used to calculate the apparent constituents of the heat balance and the apparent measures of performance. An example of how this was done, and how the mean values of the confirming measurements were used to verify apparent performance by the enhanced Thorp method, is set out in detail in Appendix 11.

---

[1] For example, openings of variable inlet guide vanes on centrifugal compressors.

[2] For example, the evaporator outlet water temperature being lower than the evaporating refrigerant temperature!

APPENDIX 11

CASE STUDY A: MEASUREMENTS AND CALCULATIONS FOR ENHANCED THORP METHOD

Figure A11.1 reproduces Figure 5.8, showing in addition the available measuring points for water flows and temperatures, and refrigerant pressures and temperatures. The connections of the oil-to-water compressor oil cooler are also shown. As there was a separate subcooler following the condenser, this machine's condenser block comprised both of these components, as shown. The oil cooler obtained its water from the water lines *within the condenser block's thermodynamic boundary* - that is, closer to the condenser than the points at which water flow and temperatures were measured.

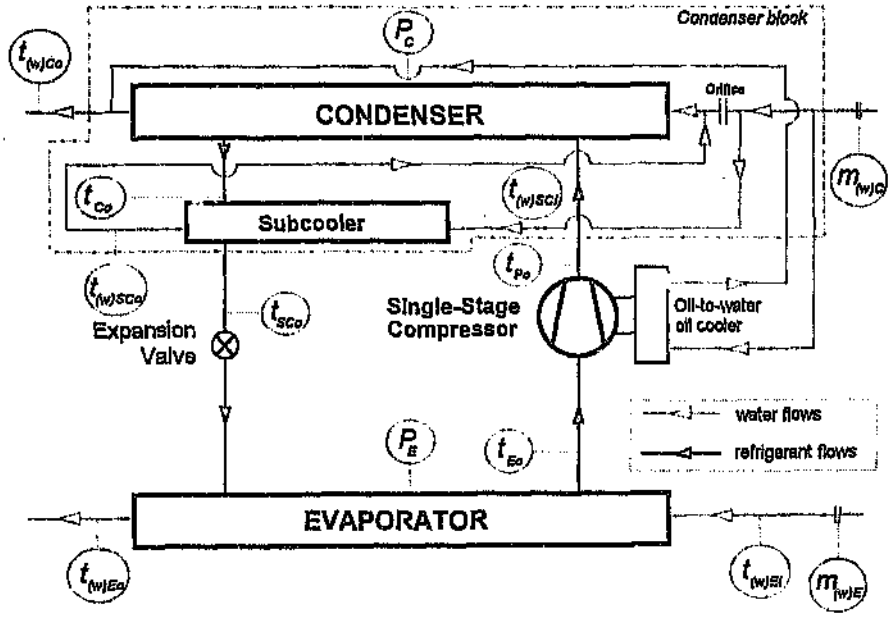

Figure A11.1 Case Study A: Measuring Points on Machine

The averaged principal and confirming measurements taken during the performance survey of this machine are given in Table A11.1 below.

Table A11.1 Case Study A: Averaged Measurements Taken During Survey of Machine

QUANTITY	UNIT	VALUE
EVAPORATOR		
Water flow-rate $m_{f(w)Ep}$	l/s	150,0
Inlet water temperature $t_{(w)Ei,p}$	°C	15,25
Outlet water temperature $t_{(w)Eo,p}$	°C	5,12
Refrigerant pressure P_{Ep}	kPaa	335,4
Outlet refrigerant temperature $t_{Eo,p}$	°C	4,29
Refrigerant level		normal
CONDENSER		
Water flow-rate $m_{(w)Cp}$	l/s	384,4
Inlet water temperature	°C	21,7[1]
Outlet water temperature $t_{(w)Co,p}$	°C	27,21
Refrigerant pressure P_{Cp}	kPaa	761,2
Outlet refrigerant temperature $t_{Co,p}$	°C	26,80
SUBCOOLER		
Inlet water temperature $t_{(w)SCi,p}$	°C	22,45
Outlet water temperature $t_{(w)SCo,p}$	°C	22,85
Outlet refrigerant temperature $t_{SCo,p}$	°C	23,56
COMPRESSOR		
Vane opening	degrees	38,9
Discharge temperature $t_{Po,p}$	°C	40,85
Motor current	A	98
Motor electrical input power	kW	988

A11.1 Apparent Constituents of Heat Balance

Let $m_{(w)Ep}$ be the apparent evaporator water flow, $c_{(w)}$ the specific heat of water, and $t_{(w)Ei,p}$ and $t_{(w)Eo,p}$ the measured water temperatures at evaporator inlet and outlet. The apparent evaporator block water load was calculated without difficulty:

[1] Value indicated on control panel; there was no thermometer well enabling manual measurement. This value was obviously erroneous; it could not be lower than the inlet water temperature of the subcooler.

$$Q_{EBp} = m_{(w)Ep}c_{(w)}\left(t_{(w)Ei,p} - t_{(w)Eo,p}\right)$$
$$= 150{,}0 \cdot 4{,}19 \cdot (15{,}25 - 5{,}12) = 6\,362 \text{ kW(R)} \qquad \text{(A11-1)}$$

Let $m_{(w)Cp}$, $t_{(w)Ci,p}$ and $t_{(w)Co,p}$ be the corresponding quantities for the apparent condenser water load. From Figure A11.1, it is seen that there was no measuring point for $t_{(w)Ci}$; however, this was identical to $t_{(w)SCi}$, for which a measuring point was available. Hence apparent condenser block water load Q_{CBp} was given by

$$Q_{CBp} = m_{(w)Cp}c_{(w)}\left(t_{(w)SCi,p} - t_{(w)Co,p}\right)$$
$$= 384{,}4 \cdot 4{,}19 \cdot (22{,}45 - 27{,}21) = -7\,665 \text{ kW(R)} \qquad \text{(A11-2)}$$

From (5-1a), as $\sum Q_{(w)VCB(Ms)} = 0$, apparent *rejection* load $Q_{JBp} = Q_{CBp}$. Finally, from manufacturers' data, the full-load efficiency $\eta_{P,motor}$ of the compressor drive motor was 96 per cent,[2] and the full-load efficiency $\eta_{P,gearbox}$ of the speed-increasing gearbox was 97,5 per cent. Denoting apparent electrical power input to the compressor motor by $W_{P,motor,p}$, the apparent input power W_{VCBp} was

$$W_{VCBp} = W_{P,motor,p} \cdot \eta_{P,motor} \cdot \eta_{P,gearbox}$$
$$= 988 \cdot 0{,}96 \cdot 0{,}975 = 925 \text{ kW} \qquad \text{(A11-3)}$$

A11.2 Relative Heat Imbalance

From (5-8),

$$\varepsilon = \frac{6\,362 + 925}{-7\,665} + 1 = +4{,}92\% \qquad \text{(A11-4)}$$

---

[2] The motor was operating close to full load, because its rated output power was 1 100 kW. Hence its efficiency could be assumed to be its rated full-load efficiency with negligible error.

A11.3 Apparent Evaporator-Load and Rejection-Load COPs

From (5-9c),

$$COP_{[EB]p} = \frac{6\,362}{925} = 6{,}878 \qquad COP_{[JB]p} = \frac{-(-7\,665 + 925)}{925} = 7{,}286 \quad \text{(A11-5)}$$

A11.4 Refrigerant-Circuit COP

From (3-14b), the refrigerant-circuit COP for a machine with a single-stage centrifugal compressor is

$$COP_{(r)} = \frac{h_{Eo} - h_{EXI}}{h_{Po} - h_{Eo}} \quad \text{(A11-6)}$$

where h_{Eo} is enthalpy of vapour at evaporator outlet, h_{EXI} is entnalpy of liquid entering the expansion valve (identical here to h_{SCo}, enthalpy of refrigerant liquid leaving the subcooler), and h_{Po} is enthalpy of vapour at compressor discharge.

The calibrated thermometers described in Appendix 10 were used for all temperature measurements; the systematic uncertainty in these temperature measurements was thus assumed to be ±0,2°C. The site-fitted pressure gauges were not calibrated; they were therefore assumed to have systematic uncertainties of ±2 per cent of their full-scale values - that is, ±20 kPa for P_{Ep} and ±30 kPa for P_{Cp}.

A difficulty arose here. Whereas the measured refrigerant temperatures $t_{Eo,p}$, $t_{SCo,p}$ and $t_{Po,p}$ were available, the refrigerant pressures at these points were not. Only the measured evaporating and condensing pressures P_{Ep} and P_{Cp} were available. The required refrigerant pressures P_{Eo}, P_{SCo} and P_{Po} differed from P_E and P_C by the pressure differences $\Delta P_{E \to Eo}$, $\Delta P_{C \to SCo}$ and $\Delta P_{Po \to C}$ respectively:

$$P_{Eo} \equiv P_E + \Delta P_{E\to Eo} \qquad P_{SCo} \equiv P_C + \Delta P_{C\to SCo}$$
$$P_{Po} \equiv P_C + \Delta P_{Po\to C} \qquad \text{(A11-7)}$$

Nothing was known of $\Delta P_{E\to Eo}$, $\Delta P_{C\to SCo}$ and $\Delta P_{Po\to C}$. All that was known is that they were greater than zero and less than or equal to the design (full-duty) pressure drops between the ends of the pipelines concerned. These design pressure drops were 9 kPa between evaporator and compressor and 21 kPa between compressor and condenser. Now the measuring points of $t_{Eo,p}$ and $t_{Po,p}$ were relatively close (compared to the total lengths of piping) to the outlets of the evaporator and compressor respectively, and all bends[3] in the piping were after these measuring points. Hence most of whatever pressure drop there was would have occurred after these measuring points. Hence $\Delta P_{E\to Eo}$ and $\Delta P_{Po\to C}$ - the pressure drops between the physical outlets and the temperature measuring points - would have been small compared to the above uncertainties in P_{Ep} and P_{Cp}. Regarding $\Delta P_{C\to SCo}$, the maximum value of this would have been 12 kPa, corresponding to the static liquid refrigerant head over the approximately 1-metre difference in elevation between the condenser liquid outlet and the expansion valve inlet;[4] as will be seen in Table A11.3, such an elevational difference had a negligible effect on the calculated enthalpy. All these pressure drops, $\Delta P_{E\to Eo}$, $\Delta P_{C\to SCo}$ and $\Delta P_{Po\to C}$, were thus ignored.

Next, before calculating the three enthalpies in (A11-6), it had to be established whether the refrigerant at these three key points was saturated, subcooled (for liquid) or superheated (for vapour). This was done as in Table A11.2 below.

---

[3] One 90° long-radius bend in the piping between evaporator and compressor, and four 90° short-radius bends in the piping between compressor and condenser!

[4] The actual pressure rise would have been somewhat less, as some pressure drop had to occur in the pipe between the condenser and subcooler, and in the subcooler itself.

Table A11.2 Case Study A: Establishing Refrigerant State at Key Points in Refrigerant Circuit

Measuring point	Abs. pressure (kPa)	Corresponding sat. temp. from tables (°C)	Temp. reading (°C)	Conclusions on difference between temperatures
Evaporator outlet	335,4 ± 20	2,57 ± 1,8	4,29 ± 0,2	The refrigerant vapour was slightly superheated. It was thus a function of both pressure and temperature.
Expansion valve inlet	761,2 ± 30	30,84 ± 1,5	23,56 ± 0,2	The liquid was considerably subcooled. Again, it was a function of both pressure and temperature.
Compressor outlet	761,2	30,84 ± 1,5	40,85 ± 0,2	The vapour was superheated by approximately 10 degrees.

The enthalpies h_{Eo}, h_{SCo} and h_{Po} were then functions of the measured temperatures and pressures as follows:

$$\begin{aligned} h_{Eo} &= h_{Eo}(P_E, t_{Eo}) \\ h_{SCo} &= h_{SCo}(P_C, t_{SCo}) \\ h_{Po} &= h_{Po}(P_C, t_{Po}) \end{aligned} \qquad \text{(A11-8)}$$

Using the values of P_{Ep}, P_{Cp}, $t_{Eo,p}$, $t_{SCo,p}$ and $t_{Po,p}$ from Table A11.1, and using tables of properties of Refrigerant 12 (IIR, 1981), these enthalpies, except h_{SCo}, were found by interpolation to be as in Table A11.3 below. The exception was the enthalpy of the subcooled liquid h_{SCo}; this was estimated by (see Gosney, 1982 : 217)

$$h_{SCo} = h_{(f)}(t_{SCo}) + v_{(f)}(t_{SCo}) \cdot \left[P_C - P_{sat}(t_{SCo})\right] \qquad \text{(A11-9)}$$

where $h_{(f)}(t_{SCo})$, $v_{(f)}(t_{SCo})$ and $P_{sat}(t_{SCo})$ were obtained from the abovementioned tables.

Table A11.3 Case Study A: Enthalpies of Refrigerant at Key Points in Refrigerant Circuit

Location	Pressure, kPaa	Temperature, °C	Aux. Quantities	Enthalpy, kJ/kg
Evaporator outlet	335,4	4,29		353,707
Compressor outlet	761,2	40,85		371,294
Expansion valve inlet	761,2	$t_{sCo,p} = 23,56$	$h_{(f)}(t_{sCo,p}) =$ 222,253 kJ/kg $v_{(f)}(t_{sCo,p}) =$ 0,000760 m³/kg $P_{sat}(t_{sCo,p}) =$ 626,191 kPaa	From (A11-9), $h_{sCo} = 222,356$. It can be seen that a difference of 12 kPa in $P_{sat}(t_{sCo,p})$ made negligible difference to this value.

Hence, from (A11-6),

$$COP_{(r)} = \frac{353,707 - 222,356}{371,294 - 353,707} = 7,468 \qquad \text{(A11-10)}$$

A11.5 Correcting Refrigerant-Circuit COP to Reflect Actual COP

The compressor was equipped with an oil-to-water oil cooler, obtaining its water from the *condenser* water lines. Hence the estimate of actual COP was obtained from (5-10c):

$$COP \cong COP_{(r)}\left(1 + R_{(VCB)}\right)$$
$$\text{where } R_{(VCB)} = \frac{-\sum Q_{(w)CB(VCB)}}{\sum W_{VCBp}} \qquad \text{(A11-11a)}$$

Here, $-\sum Q_{(w)CB(VCB)}$ was just the apparent load $Q_{(w)OCp}$ in the single oil cooler, and $\sum W_{VCBp}$ was just W_{VCEp}. From data supplied by the manufacturer, $Q_{(w)OCp}$ was approximately -35 kW(R). Hence

$$COP \cong COP_{(r)}\left(1 + \frac{Q_{(w)OCp}}{W_{VCBp}}\right) = 7,468 \cdot \left(1 + \frac{-35}{925}\right) = 7,185 \qquad \text{(A11-11b)}$$

A11.6 Plotting Load Error Lir s on the Acceptability Plot

From (5-11), the relationships between the relative errors n_{EBp}, n_{JBp} and n_{VCBp} in apparent evaporator load, rejection load and input power were then given by

$$n_{EBp} = \frac{6{,}878\left(1+n_{VCBp}\right)}{7{,}185} - 1 \qquad n_{JBp} = \frac{\left(1+7{,}286\right)\left(1+n_{VCBp}\right)}{1+7{,}185} - 1 \quad \text{(A11-12)}$$

The corresponding load error lines on the acceptability plot were then plotted without difficulty.

APPENDIX 12

CASE STUDY A: UNCERTAINTY IN CORRECTED REFRIGERANT-CIRCUIT COP

As noted in Appendix 4, the uncertainty $\delta\Theta$ in a function Θ of multiple variables $z_1, z_2, \ldots z_n$ can be expressed in terms of the uncertainties $\delta z_1, \delta z_2, \ldots \delta z_n$ in these variables, provided that they are all independent:

$$\delta\Theta = \sqrt{\sum_{k=1}^{n}\left(\frac{\partial\Theta}{\partial z_k}\cdot\delta z_k\right)^2} \qquad \text{(A12-1)}$$

For Case Study A, the estimate of actual COP was given by (A11-11b):

$$COP = COP_{(r)}\left(1 + \frac{Q_{(w)OCp}}{W_{VCBp}}\right) \qquad \text{(A12-2)}$$

where $COP_{(r)}$ is the refrigerant-circuit COP; W_{VCBp} is the apparent input power; and $Q_{(w)OCp}$ is the cooling load in the oil-to-water oil cooler.

A12.1 Uncertainty in Refrigerant-Circuit COP

The measurements of refrigerant pressures and temperatures were made at the points shown in Figure A11.1. The refrigerant-circuit COP was given by, from (A11-6) and (A11-8)

$$COP_{(r)} = \frac{h_{Eo}(P_E, t_{Eo}) - h_{SCo}(P_C, t_{SCo})}{h_{Po}(P_C, t_{Po}) - h_{Eo}(P_E, t_{Eo})} \qquad \text{(A12-3)}$$

where each enthalpy is expressed as a function of the independent measurements. It was thus necessary to evaluate the derivative of $COP_{(r)}$ with respect to each one of these independent measurements.

As all the measurements in (A12-3) were independe. ıe uncertainty in $COP_{(r)}$, (from A12-1), was as follows:

$$\delta COP_{(r)} = \sqrt{\left(\frac{\partial COP_{(r)}}{\partial P_E}\delta P_E\right)^2 + \left(\frac{\partial COP_{(r)}}{\partial t_{Eo}}\delta t_{Eo}\right)^2 + \left(\frac{\partial COP_{(r)}}{\partial P_C}\delta P_C\right)^2 + \left(\frac{\partial COP_{(r)}}{\partial t_{SCo}}\delta t_{SCo}\right)^2 + \left(\frac{\partial COP_{(r)}}{\partial t_{Po}}\delta t_{Po}\right)^2} \qquad \text{(A12-4)}$$

The partial derivatives were readily evaluated using finite-difference approximations from adjacent tabulated values in tables of refrigerant properties (IIR, 1981). (A12-4) was then evaluated as shown in Table A12.1 below.

Table A12.1 Case Study A: Evaluation of Uncertainty in Refrigerant-Circuit COP

Measurement z	Partial derivative $\partial COP_{(r)}/\partial z$	Uncertainty δz in measurement (see Sect. A11.4, Appendix 11)	Square of product $\frac{\partial COP_{(r)}}{\partial z}\cdot\delta z$	Square root of sum of squared products
t_{Eo}	0,31478	± 0,2°C	0,003963	
P_E	-0,01002	± 20 kPa	0,040187	
t_{Po}	-0,30793	± 0,2°C	0,003793	
P_C	0,007018	± 30 kPa	0,044329	
t_{SCo}	-0,05431	± 0,2°C	0,000118	
		Total:	0,092391	0,303959

The refrigerant-circuit COP was thus (7,468 ± 0,304), or 7,468 ± 4,07%. Most of the uncertainty, as seen in Table A12.1, was due to the uncertainties in the apparent refrigerant evaporating and condensing pressures, due to the pressure gauges not being calibrated.[1]

[1] If the evaporator and condenser pressure gauges had been calibrated for accuracies of ±1% of their full scale values - that is, ±10 kPa and ±15 kPa respectively - the uncertainty in refrigerant-circuit COP would have shrunk to ±2,3 per cent.

A12.2 Uncertainty in Apparent Input Power

The electrical energy ΔE consumed by a compressor motor and measured by an electrical energy meter during a time interval $\Delta\tau = \tau_2 - \tau_1$ is given by

$$\Delta E = f' \int_{\tau_1}^{\tau_2} W_m \cdot d\tau \qquad \text{(A12-5a)}$$

where f' is the meter multiplying factor (the product of the ratios of the isolating voltage and current transformers whose secondary windings are connected to the meter) and W_m is the electrical power measured by the meter from the voltages and currents generated in these secondary windings. If W_m is constant over $(\tau_2 - \tau_1)$, then

$$\Delta E = f' W_m \Delta\tau \qquad \text{(A12-5b)}$$

Let the uncertainties in f' and W_m be $\delta f'$ and δW_m respectively. The relative uncertainties $n_{f'}$ and $n_{W.m}$ in these two quantities are then

$$n_{f'} = \delta f'/f' \qquad n_{W.m} = \delta W_m/W_m \qquad \text{(A12-6)}$$

It is assumed that there is negligible uncertainty in $\Delta\tau$. As f' and W_m are independent, the overall relative uncertainty $n_{\Delta E}$ in the apparent energy input to the compressor motor is, from A12-1:

$$n_{\Delta E} = \sqrt{n_{f'}^2 + n_{W.m}^2} \qquad \text{(A12-7)}$$

A12.2.1 Uncertainty in Electrical Power Measured by Meter

$n_{W.m}$ is considered first. Consider the phasor diagram of Figure A12.1 for a three-phase balanced load. The three phases are named A, B and C. θ is the phase angle; I_{Am} and I_{Cm} are the currents in the secondary

circuits of the separate current transformers in phases A and C; V_{ABm} and V_{CBm} are the voltages in the secondary circuit of the three-phase voltage transformer; $\phi_{V.ABm}$ and $\phi_{V.CBm}$ are the phase-shift errors in the three-phase voltage transformer; and $\phi_{I.Am}$ and $\phi_{I.Cm}$ are the phase-shift errors in the separate current transformers in phases A and C.[2] All phase-shift angles ϕ have zero mean, and maximum limits on their variance.

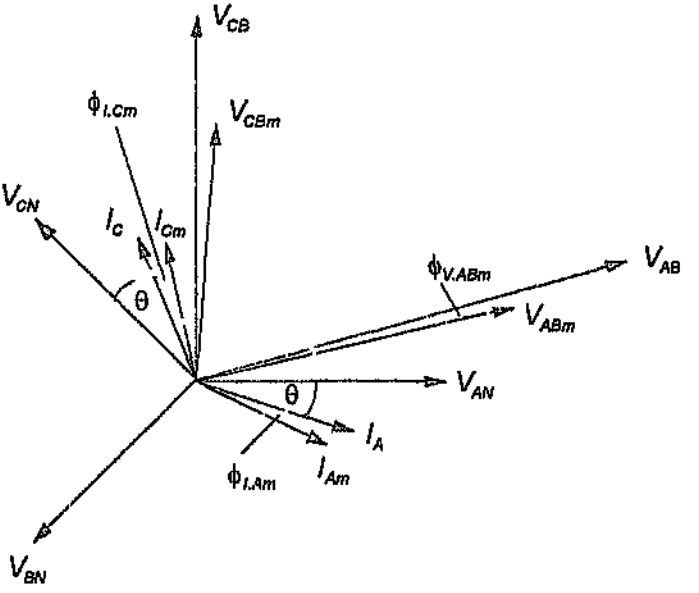

Figure A12.1 Phasor Diagram for Three-Phase Balanced Electrical Load

In the measurement of three-phase power by the two-wattmeter method (i.e. a two-element watt-hour meter),

$$W_{Am} = V_{ABm} I_{Am} \cos\left[30° + (\theta - \phi_{V.ABm} + \phi_{I.Am})\right]$$

and (A12-8a)

$$W_{Cm} = V_{CBm} I_{Cm} \cos\left[30° - (\theta - \phi_{V.CBm} + \phi_{I.Cm})\right]$$

---

[2] In reality, secondary quantities are opposite in phase to primary quantities; for the sake of clarity, this is ignored here.

Hence total power W_m is

$$\begin{aligned} W_m &= W_{Am} + W_{Cm} \\ &= V_{ABm} I_{Am} \cos\left[30° + (\theta - \phi_{V.ABm} + \phi_{I.Am})\right] \\ &\quad + V_{CBm} I_{Cm} \cos\left[30° - (\theta - \phi_{V.CBm} + \phi_{I.Cm})\right] \end{aligned} \qquad \text{(A12-8b)}$$

As the voltage transformer is a three-phase, magnetically-coupled type, it is assumed that $V_{ABm} = V_{CBm} = V_m$ and $\phi_{V.ABm} = \phi_{V.CBm} = \phi_{V.m}$. Hence

$$W_m = V_m \left\{ \begin{aligned} &I_{Am} \cos\left[30° + (\theta - \phi_{V.m} + \phi_{I.Am})\right] \\ &+ I_{Cm} \cos\left[30° - (\theta - \phi_{V.m} + \phi_{I.Cm})\right] \end{aligned} \right\} \qquad \text{(A12-8c)}$$

Now taking the partial derivatives of W_m with respect to each one of these quantities, which are independent,

$$\frac{\partial W_m}{\partial V_m} = I_{Am} \cos\left[30° + (\theta - \phi_{V.m} + \phi_{I.Am})\right] + I_{Cm} \cos\left[30° - (\theta - \phi_{V.m} + \phi_{I.Cm})\right]$$

$$\frac{\partial W_m}{\partial I_{Am}} = V_m \cos\left[30° + (\theta - \phi_{V.m} + \phi_{I.Am})\right]$$

$$\frac{\partial W_m}{\partial I_{Cm}} = V_m \cos\left[30° - (\theta - \phi_{V.m} + \phi_{I.Cm})\right]$$

$$\frac{\partial W_m}{\partial \phi_{V.m}} = V_m \left\{ I_{Am} \sin\left[30° + (\theta - \phi_{V.m} + \phi_{I.Am})\right] - I_{Cm} \sin\left[30° - (\theta - \phi_{V.m} + \phi_{I.Cm})\right] \right\}$$

$$\frac{\partial W_m}{\partial \phi_{I.Am}} = -V_m I_{Am} \sin\left[30° + (\theta - \phi_{V.m} + \phi_{I.Am})\right]$$

$$\frac{\partial W_m}{\partial \phi_{I.Cm}} = V_m I_{Cm} \sin\left[30° - (\theta - \phi_{V.m} + \phi_{I.Cm})\right]$$

Evaluating these partial derivatives at the *mean values* of the quantities concerned ($\bar{I}_{Am} = \bar{I}_{Cm} = I_m$, $\bar{\Phi}_{V.m} = \bar{\Phi}_{I.Am} = \bar{\Phi}_{I.Cm} = 0$),

$$\frac{\partial W_m}{\partial V_m} = I_m\left\{\cos\left[30°+\theta\right] + \cos\left[30°-\theta\right]\right\} = I_m\sqrt{3}\cos\theta$$

$$\frac{\partial W_m}{\partial I_{Am}} = V_m \cos\left[30°+\theta\right]$$

$$\frac{\partial W_m}{\partial I_{Cm}} = V_m \cos\left[30°-\theta\right]$$

$$\frac{\partial W_m}{\partial \phi_{V.m}} = V_m\left\{I_m \sin\left[30°+\theta\right] - I_m \sin\left[30°-\theta\right]\right\} = V_m I_m\sqrt{3}\sin\theta$$

$$\frac{\partial W_m}{\partial \phi_{I.Am}} = -V_m I_m \sin\left[30°+\theta\right]$$

$$\frac{\partial W_m}{\partial \phi_{I.Cm}} = V_m I_m \sin\left[30°-\theta\right]$$

From (A3-1), the uncertainty δW_m in W_m is

$$\delta W_m = \sqrt{\begin{aligned}&\left(I_m\sqrt{3}\cos\theta\right)^2\delta V_m^2\\&+\left[V_m\cos(30°+\theta)\right]^2\delta I_{Am}^2 + \left[V_m\cos(30°-\theta)\right]^2\delta I_{Cm}^2\\&+\left(V_m I_m\sqrt{3}\sin\theta\right)^2\delta\phi_{V.m}^2\\&+\left[V_m I_m\sin(30°+\theta)\right]^2\delta\phi_{I.Am}^2 + \left[V_m I_m\sin(30°-\theta)\right]^2\delta\phi_{I.Cm}^2\end{aligned}} \qquad \text{(A12-9)}$$

From (A12-6), the relative error $n_{W.m}$ in W_m is given by, after algebraic manipulation,

$$n_{W.m} = \sqrt{\frac{\delta V_m^2}{V_m^2} + \frac{\cos^2(30°+\theta)\delta I_m^2}{3I_m^2\cos^2\theta} + \frac{\cos^2(30°-\theta)\delta I_m^2}{3I_m^2\cos^2\theta} + \frac{\delta\phi_{V.m}^2\sin^2\theta}{\cos^2\theta} + \frac{\delta\phi_{I.Am}^2\sin^2(30°+\theta)}{3\cos^2\theta} + \frac{\delta\phi_{I.Cm}^2\sin^2(30°-\theta)}{3\cos^2\theta}} \quad \text{(A12-10a)}$$

It is easily shown that

$$\frac{\cos(30°+\theta)}{\cos\theta} = \tfrac{1}{2}\left(\sqrt{3} - \tan\theta\right) \qquad \frac{\cos(30°-\theta)}{\cos\theta} = \tfrac{1}{2}\left(\sqrt{3} + \tan\theta\right)$$

$$\frac{\sin(30°+\theta)}{\cos\theta} = \tfrac{1}{2}\left(1 + \sqrt{3}\tan\theta\right) \qquad \frac{\sin(30°-\theta)}{\cos\theta} = \tfrac{1}{2}\left(1 - \sqrt{3}\tan\theta\right)$$

Substituting these into (A12-10a) and assuming that $\phi_{I.Am} = \phi_{I.Cm} = \phi_{I.m}$,

$$n_{W.m} = \sqrt{\frac{\delta V_m^2}{V_m^2} + \frac{\delta I_m^2}{6I_m^2}\left(3 + \tan^2\theta\right) + \delta\phi_{V.m}^2\tan^2\theta + \frac{\delta\phi_{I.m}^2}{6}\left(1 + 3\tan^2\theta\right)} \quad \text{(A12-10b)}$$

The quantities $\delta V_m/V_m$ and $\delta I_m/I_m$ in (A12-10b) need to be expressed in terms of the ratio errors of their voltage and current transformers. For a voltage transformer, for example, let the rated transformation ratio be R_{vt}. The *relative* ratio error $n_{R.vt}$ is then (BSI, 1994), where V is the voltage on the primary side of the transformer,

$$n_{R.vt} = \frac{R_{vt}V_m - V}{V} = R_{vt}\frac{V_m}{V} - 1, \text{ whence}$$

$$V_m = \frac{V}{R_{vt}} + \frac{Vn_{R.vt}}{R_{vt}}$$

The true value of V_m is, of course, V/R_{vt}. Hence $\delta V_m = Vn_{R.vt}/R_{vt}$ and so

$$\frac{\delta V_m}{V_m} = \frac{Vn_{R.vt}/R_{vt}}{\dfrac{V}{R_{vt}} + \dfrac{Vn_{R.vt}}{R_{vt}}} = \frac{n_{R.vt}}{n_{R.vt}+1}$$

and similarly for the relative ratio error $n_{R.i}$ of a current transformer. Substituting in (A12-10b),

$$n_{W.m} = \sqrt{\left(\frac{n_{R.vt}}{n_{R.vt}+1}\right)^2 + \delta\phi_{V.m}^2 \tan^2\theta + \frac{1}{6}\left[\left(\frac{n_{R.it}}{n_{R.it}+1}\right)^2\left(3+\tan^2\theta\right) + \delta\phi_{I.m}^2\left(1+3\tan^2\theta\right)\right]} \qquad \text{(A12-10c)}$$

With $n_{R.vt} = \pm 0{,}01$ and $\delta\phi_{V.m} = 0{,}012$ radians for a Class 1 voltage transformer (BSI, 1994), and $n_{R.it} = \pm 0{,}015$ and $\delta\phi_{I.m} = 0{,}027$ radians for a Class 1 current transformer (BSI, 1973), the variation of $n_{W.m}$ with power factor ($\cos\theta$) is tabulated in Table A12.2 below.

Table A12.2 Variation of Uncertainty in Electric Power Measured by Energy Meter

Power factor	Uncertainty $n_{W.m}$ in measured elec. power
1,0	0,01793
0,8	0,02472
0,6	0,03516
0,5	0,04319
0,4	0,05498
0,3	0,07433
0,25	0,08967
0,2	0,11257

A12.2.2 Overall Uncertainty in Measured Electrical Energy Input to Compressor Motor

(A12-7) was then used to calculate the overall uncertainty $n_{\Delta E}$ in the apparent energy input to the compressor motor. It was assumed that the uncertainty in measurement due to the meter itself was ±2% for a Class 2 watt-hour meter (BSI, 1979)[3]. This uncertainty was assigned to n_r in

[3] For power factors greater than or equal to 0,5.

(A12-7). Values of $n_{\Delta E}$, yielded by (A12-7) for various power factors, are listed in Table A12.3 below.

Table A12.3 Overall Uncertainty in Electrical Energy Input to Compressor Motor

Power factor	$n_{W,m}$	$n_{f\cdot}$	$n_{\Delta E}$ (by (A12-7))
1,0	0,01793	0,02	0,02686
0,8	0,02472	0,02	0,03180
0,6	0,03516	0,02	0,04045
0,5	0,04319	0,02	0,04760
0,2	0,08967	0,085	0,12355

A12.2.4 Relative Uncertainty in Apparent Input Power

The apparent electrical power input to the compressor motor is given by

$$W_{\text{input to motor}} = \Delta E_p / \Delta \tau_p$$

where ΔE_p is the electrical energy recorded by the meter over a measured time interval $\Delta \tau_p$. The apparent power input to the compressor itself - that is, the apparent input power W_{VCBp} - is given by (A11-3), reproduced below:

$$W_{VCBp} = W_{P,\text{motor},p} \cdot \eta_{P,\text{motor}} \cdot \eta_{P,\text{gearbox}}$$

The uncertainties in $\Delta \tau_p$, $\eta_{P,\text{motor}}$ and $\eta_{P,\text{gearbox}}$ were assumed to be negligible in comparison to that in $W_{P,\text{motor},p}$. From Table A12.3 above, the overall uncertainty in apparent input power W_{VCBp} was thus taken as ±4%, provided that motor power factor was not less than 0 5.

A12.3 Uncertainty in Corrected Refrigerant-Circuit COP

Now the corrected refrigerant-circuit COP is given by (A12-2), and by (A12-1), since the quantities are again all independent,

$$\delta COP = \sqrt{\left(\frac{\partial COP}{\partial COP_{(r)}}\delta COP_{(r)}\right)^2 + \left(\frac{\partial COP}{\partial Q_{(w)oc}}\delta Q_{(w)oc}\right)^2 + \left(\frac{\partial COP}{\partial W_{vcs}}\delta W_{vcs}\right)^2} \quad \text{(A12-11a)}$$

From (A12-2), the partial derivatives are given by

$$\frac{\partial COP}{\partial COP_{(r)}} = 1 + \frac{Q_{(w)oc}}{W_{vcs}} \qquad \frac{\partial COP}{\partial Q_{(w)oc}} = \frac{COP_{(r)}}{W_{vcs}} \qquad \frac{\partial COP}{\partial W_{vcs}} = -\frac{COP_{(r)}Q_{(w)oc}}{W_{vcs}^2} \quad \text{(A12-11b)}$$

From Appendix 11, the values of $COP_{(r)}$, $Q_{(w)ocp}$ and W_{vcsp} were 7,468; -35 kW(R); and 925 kW. $\delta COP_{(r)}$ was ±0,303959 from Table A12.1; δW_{vcs} was taken as ±37 kW, ±4 per cent of W_{vcsp}, by Table A12.3 above; and $\delta Q_{(w)oc}$ was taken as ±5 kW(R). Substituting these quantities, (A12-11) was evaluated as in Table A12.4 below. As seen, the contributions of the uncertainties in $Q_{(w)ocp}$ and W_{vcsp} were negligible.

Table A12.4 Case Study A: Evaluation of Uncertainty in Corrected Refrigerant-Circuit COP

Quantity z	Partial derivative $\partial COP/\partial z$	Uncertainty δz in quantity	Square of product $\frac{\partial COP}{\partial z}\cdot\delta z$	Square root of sum of squared products
$COP_{(r)}$	0,962164	±0,303959	0,085532	
$Q_{(w)oc}$	-0,00807	±5	0,00163	
W_{vcs}	0,000305	±37,00142	0,000128	
		Total:	0,087289	0,295447

The estimate of actual COP was thus (7,186 ± 0,295), or 7,186 ± 4,11%. As seen, most of the uncertainty was in the refrigerant-circuit COP, and hence due to the uncertainties in the apparent refrigerant evaporating and condensing pressures, as recalled from Table A12.1 above.

APPENDIX 13

LIMITS OF ACCEPTABILITY OF APPARENT EVAPORATOR AND CONDENSER LOADS ON ACCEPTABILITY BAND PLOT

From (5-11),

$$n_{Ep} = \frac{COP_{[EB]p}\left(1+n_{VCBp}\right)}{COP} - 1 \qquad n_{JBp} = \frac{\left(1+COP_{[JB]p}\right)\left(1+n_{VCBp}\right)}{1+COP} - 1 \quad \text{(A13-1)}$$

Rearranging this pair of formulae to yield COP,

$$COP = \frac{COP_{[EB]p}\left(1+n_{VCBp}\right)}{1+n_{EBp}} \qquad COP = \frac{\left(1+COP_{[JB]p}\right)\left(1+n_{VCBp}\right)}{1+n_{JBp}} - 1 \quad \text{(A13-2)}$$

Substituting the acceptability limits of -7% and +7% for n_{EBp} in the first formula of (A13-2) yields the pair of formulae (5-13a). Doing likewise for n_{JBp} in the second formula of (A13-2) yields the corresponding pair of formulae (5-13b).

APPENDIX 14

CASE STUDY D: CONSTRUCTING ACCEPTABILITY BAND PLOTS

A14.1 Plot of Evaporator Load Acceptability Band

The plot of the evaporator load acceptability band in Figure 5.17 was constructed as follows. From Table 5.5, the apparent evaporator-load COP, $COP_{[EB]p}$, was 3,27. Accordingly, from (5-13a), the lines of the lower limit (-7%) and upper limit (+7%) of this band were given, respectively, by

$$COP = \frac{3{,}27\left(1+n_{VCBp}\right)}{0{,}93} \qquad COP = \frac{3{,}27\left(1+n_{VCBp}\right)}{1{,}07} \qquad \text{(A14-1)}$$

These lines could then be plotted without difficulty.

A14.2 Plot of Rejection Load Acceptability Band

The rejection load acceptability band was then plotted on Figure 5.18 as follows. From Table 5.5, the apparent rejection-load COP, $COP_{[JB]p}$, was 3,63 Accordingly, from (5-13b), the lines of the lower limit (-7%) and upper limit (+7%) of this band were given, respectively, by

$$COP = \frac{(1+3{,}63)\left(1+n_{VCBp}\right)}{0{,}93} - 1 \qquad COP = \frac{(1+3{,}63)\left(1+n_{VCBp}\right)}{1{,}07} - 1 \qquad \text{(A14-2)}$$

These lines could then be plotted without difficulty.

APPENDIX 15

THE CHILLER COMPUTER PROGRAM: MODELS OF WATER CHILLING MACHINE COMPONENTS

The functional forms of the equations for refrigerant properties are first presented. The models of the components of conventional water chilling machines employed in Version 1.01 of the CHILLER computer program are then described.

A15.1 Properties of Halocarbon Refrigerants

The equations for thermodynamic properties of Refrigerants 11, 12 and 22 are as given in Du Pont Freon Products Technical Bulletin X-88F (E.I. Du Pont de Nemours & Co., 1969), but converted to metric units. They are stated conceptually as functions of properties below.

Density of saturated liquid. $\rho_{(f)} \equiv \rho_{(f)}(T)$ (A15-1a)

Saturated vapour pressure. $P_{sat} \equiv P_{sat}(T)$ (A15-1b)

Equation of state of vapour. $P \equiv P(T,v)$ (A15-1c)

The specific volume of saturated vapour, $v_{(g)}$, is obtained by solving (A15-1c) for v at the given T and $P = P_{sat}$. P_{sat} is obtained from (A15-1b), and $v_{(g)}$ is thus a function of T only, i.e. $v_{(g)} = v_{(g)}(T)$.

Enthalpy of vapour. $h \equiv h(T,v)$ (A15-1d)

The enthalpy of saturated vapour, $h_{(g)}$, is given by $h_{(g)} \equiv h\left(T, v_{(g)}\right)$ and since $v_{(g)}$ is a function of T only, so is $h_{(g)}$, i.e. $h_{(g)} = h_{(g)}(T)$.

Entropy of vapour. $s \equiv s(T,v)$ (A15-1e)

Similarly, entropy $s_{(g)}$ of saturated vapour is a function of T only, i.e. $s_{(g)} = s_{(g)}(T)$.

Latent heat of vaporisation. $h_{(f)(g)} \equiv h_{(f)(g)}\left((dP_{sat}/dT),T,v_{(f)},v_{(g)}\right)$ (A15-1f)

where dP_{sat}/dT is given by the differentiated form of (A15-1b); $v_{(f)} = 1/\rho_{(f)}$; and $v_{(g)}$ is obtained as above.

Enthalpy of saturated liquid. $h_{(f)} = h_{(g)} - h_{(f)(g)}$ (A15-1g)

A15.2 The Shell-and-Tube Evaporator

A15.2.1 Assumptions

1. There is no refrigerant pressure drop through the evaporator.
2. The evaporating refrigerant covers all evaporator tubes and wets them thoroughly.
3. Refrigerant evaporating temperature and refrigerant-side heat transfer coefficient are the same for all horizontal tube rows in the evaporator.
4. Refrigerant leaves the evaporator as saturated vapour.
5. Entering refrigerant is uniformly distributed along the length of the evaporator.
6. No oil or other contaminants are present in the refrigerant.

Denoting refrigerant temperature in the evaporator by $t_{(f)E}$, corresponding saturation pressure by $P_{sat}\left(T_{(f)E}\right)$ and outlet refrigerant enthalpy by h_{Eo}, assumptions 1, 2 and 4 can be expressed as

$$t_{(r)Ei} = t_{(r)Eo} = t_{(r)E} \qquad P_{Ei} = P_{Eo} = P_{sat}\left(T_{(r)E}\right) \qquad h_{Eo} = h_{(g)}\left(T_{(r)E}\right) \qquad \text{(A15-2)}$$

A15.2.2 Constraints

Denoting the heat transferred through the evaporator from the water to the refrigerant by Q_E, the constraints on the performance of the evaporator are

$$Q_E = -Q_{(w)E} \qquad Q_{(r)E} = -Q_{(w)E} \qquad \text{(A15-3)}$$

A15.2.3 Energy and Heat Transfer Relationships

The evaporator water load is given without difficulty by

$$Q_{(w)E} = m_{(w)E}c_{(w)}\left(t_{(w)Eo} - t_{(w)Ei}\right) \qquad \text{(A15-4)}$$

The evaporator refrigerant load $Q_{(r)E}$ is the product of the refrigerant mass flow-rate and enthalpy change through the evaporator:

$$Q_{(r)E} = m_{(r)E}\left(h_{Eo} - h_{Ei}\right) \qquad \text{(A15-5)}$$

From (3-19), the heat transferred through the evaporator, Q_E, is

$$Q_E = UA_E \cdot LMTD_E \qquad \text{(A15-6a)}$$

where, from (3-20) and (3-21) respectively

$$LMTD_E = \frac{t_{(w)Eo} - t_{(w)Ei}}{\ln\left(\dfrac{t_{(w)Eo} - t_{(r)E}}{t_{(w)Ei} - t_{(r)E}}\right)} \qquad \text{(A15-6b)}$$

$$\frac{1}{UA_E} = \frac{1}{h'_{[w]E}A_{T[w]E}} + \frac{1}{h'_{[w]E}A_{T[w]E}} + \frac{y_{TE}}{k_{TE}A_{TE}} + \frac{1}{h'_{[r]E}A_{T[r]E}} \qquad \text{(A15-6c)}$$

Expressions for the water- and refrigerant-side coefficients $h'_{[w]E}$ and $h'_{[r]E}$ of heat transfer, and the mean heat-transferring area $\overline{A}_{TE}$, are now given.

Water-Side Coefficient of Heat Transfer

For water flowing turbulently inside a tube, the coefficient $h'_{[w]}$ of heat transfer to or from water by forced convection is given by the well-known relationship (see, for example, ASHRAE, 1992 : 36.2)

$$h'_{[w]}k_w/D_T = 0{,}023(\mathrm{Re})^{0{,}8}(\mathrm{Pr})^{0{,}4}$$

where k_w is the thermal conductivity of water, D_T is the internal diameter of a tube, Re is the Reynolds number of the water flow in this tube, and Pr is the Prandtl number for water. Whillier (1982) simplifies this relationship into the more useful form

$$h'_{[w]} = \frac{5\,680\left[1+0{,}015\left(t_{(w)i}+t_{(w)o}\right)/2\right]\upsilon_{(w)}^{0{,}8}}{d_T^{0{,}2}} \qquad \text{(A15-7a)}$$

where $t_{(w)i}$ and $t_{(w)o}$ are the inlet and outlet water temperatures; d_T is the internal tube diameter *in millimetres;* and $\upsilon_{(w)}$ is the water velocity through the tube, given by

$$\upsilon_{(w)} \equiv \frac{N_{pa}m_{(w)}}{N_T a_T \rho_{(w)}} \qquad \text{(A15-7b)}$$

where N_{pa} and N_T are the amounts of passes and tubes respectively; a_T is the internal cross-sectional area of a tube, and $\rho_{(w)}$ is the density of water.

Mean of Water-Side and Refrigerant-Side Heat-Transferring Areas

For shell-and-tube heat exchangers, $A_{T[w]}$ is the total inside wall area of the tubes, while $A_{T[r]}$ is the total *outside* wall area, which is obviously greater than $A_{T[w]}$. The question then arises of how to calculate the mean area $\overline{A}_T$, needed to calculate the thermal resistance of the tube material. For plain tubes, where inside and outside walls are smooth cylindrical surfaces, it is well known (see, for example, Whillier, 1982) that the correct mean area is the logarithmic mean area. However, as tube wall thicknesses are small (rarely exceeding 2 mm), and thermal resistance of the tube material is thus likely to be the smallest of all four resistances in (A15-6c), it is sufficiently accurate to use the arithmetic mean for $\overline{A}_T$:

$$\overline{A}_T \cong \left(A_{T[w]} + A_{T[r]}\right)/2 \qquad \text{(A15-8)}$$

Coefficient of Heat Transfer to Evaporating Refrigerant

In flooded shell-and-tube evaporators, refrigerant boils outside the tubes at low fluid velocities. In a comprehensive review of completed and ongoing research into heat transfer from tubes to refrigerant in flooded evaporators, Webb (1991) points out that this is by a combination of nucleate boiling - where bubbles of vapour form on the outside walls of the tubes, break away, and reach the free surface of the liquid - and two-phase forced convection. Accurately modelling this combined process requires iterative calculations for each horizontal tube row, because the effect of forced convection increases for the upper rows. The heat transferred by nucleate boiling also depends very strongly on the nucleating characteristics of the tube surfaces. Tubes with enhanced surfaces have far better nucleating characteristics than integral-fin tubes (Webb, 1991).

Earlier, less accurate models of heat transfer from tubes to refrigerant, yielding an average heat transfer coefficient for all the tubes, are based upon correlations for a single, horizontal tube where heat transfer is by nucleate boiling only. As ASHRAE (1993 : 4.5) states, these merely approximate heat transfer rates in flooded evaporators with bundles of tubes. Such a correlation is employed here: it is the 1951 one of Rohsenow for nucleate boiling, as reported by ASHRAE (1993 : 4.3):

$$(\mathrm{Nu})_b = (\mathrm{Re})_b^{2/3} \cdot (\mathrm{Pr}_{,\ell}{}^{7}) / C_{sf} \qquad \text{(A15-9a)}$$

where C_{sf} is a constant depending on the material of the heating surface and the refrigerant. The bubble Nusselt and Reynolds numbers $(\mathrm{Nu})_b$ and $(\mathrm{Re})_b$, and the Prandtl number $(\mathrm{Pr})_\ell$ for the liquid refrigerant are given by

$$(\mathrm{Nu})_b = h' D_b / k_\ell \qquad (\mathrm{Re})_b = Q D_b / A h_{(\ell)(g)} \mu_\ell$$
$$(\mathrm{Pr})_\ell = \left[\mu c_p / k\right]_\ell \qquad \text{(A15-9b)}$$

where the maximum diameter D_b of a bubble as it leaves the surface is given by

$$D_b = \sqrt{\sigma_\ell / (\rho_\ell - \rho_v) g} \qquad \text{(A15-9c)}$$

and h' is the heat transfer coefficient; k_ℓ, μ_ℓ and $c_{p\ell}$ are the thermal conductivity, absolute viscosity and specific heat at constant pressure, respectively, of the liquid refrigerant; Q/A is the heat flux passing through the heating surface of area A; $h_{(\ell)(g)}$ is the latent heat of evaporation of the refrigerant; σ_ℓ is the surface tension of the liquid at the temperature of evaporation, and ρ_ℓ and ρ_v are the densities of the liquid and vapour respectively.

Rohsenow's correlation is used in several reported models of conventional water chilling machines (customarily termed "centrifugal chillers"); see, for example, Chi (1979) and Wong and Wang (1989). Substituting (A15-9b) into (A15-9a) and solving for the heat transfer coefficient h',

$$h' = \left(\frac{Q}{A}\right)^{2/3} \cdot \frac{k_\ell}{D_b}\left(\frac{D_b}{h_{(f)(g)}\mu_\ell}\right)^{2/3}\left(\frac{\mu c_p}{k}\right)_\ell^{-0,7} \Big/ C_{sf} \qquad \text{(A15-9d)}$$

with D_b given by (A15-9c).

Examining (A15-9d), it is seen that the correlation for the heat transfer coefficient h' is a function of the heat flux Q/A; the local gravitational acceleration g; the material of the heating surface and the particular refrigerant employed; and the properties of the refrigerant at the prevailing evaporation temperature, combined into a dimensional "refrigerant factor" $\frac{k_\ell}{D_b}\left(\frac{D_b}{h_{(f)(g)}\mu_\ell}\right)^{2/3}\left(\frac{\mu c_p}{k}\right)_\ell^{-0,7}$. Table A15.1 lists values of this "refrigerant factor", calculated from tabulated properties (IIR, 1981), for Refrigerants 11, 12 and 22 at different evaporating temperatures.

Table A15.1 Dimensional "Refrigerant Factor" of Rohsenow's Correlation for Heat Transfer to Boiling Refrigerant in Flooded Evaporators

Evaporating Temperature, °C	Refrigerant Factor $\frac{k_\ell}{D_b}\left(\frac{D_b}{h_{(f)(g)}\mu_\ell}\right)^{2/3}\left(\frac{\mu c_p}{k}\right)_\ell^{-0,7}$ *(figures below must be multiplied by 10^{-9})*		
	Refrigerant 11	Refrigerant 12	Refrigerant 22
0	1,152	6,652	6,804
4	1,271	7,124	7,166
10	1,475	7,898	7,660

For Refrigerant 11, the "refrigerant factors" at 4°C and 10°C are 110% and 128% of that at 0°C. The variation is less for Refrigerant 12 (107% and 119%) and Refrigerant 22 (105% and 107%).

As refrigerant evaporating temperatures in most water chilling machines are within the range of Table A15.1, this suggests that, *for a particular flooded shell-and-tube evaporator employing a particular refrigerant,* the refrigerant-side coefficient of heat transfer may be adequately expressed as a function of a constant C and the heat flux through the tubes:

$$h'_{r|E} = C \cdot \left(Q_E / A_{T|r|}\right)^{0,7}$$

This is the approach adopted by Howes (1976), who, on the basis of a survey of reported performance of flooded shell-and-tube evaporators of water chilling machines on South African gold mines, uses the following correlation:

$$h'_{r|E} = C \cdot \left(Q_E / A_{T|w|}\right)^{0,7} \qquad \text{W/m}^{2\circ}\text{C} \qquad \text{(A15-10)}$$

where $A_{T|w|}$ is the total *inside* wall area of the tubes. $C = 200$ for Refrigerant 11 and $C = 290$ for Refrigerants 12 and 22.

A15.3 The Shell-and-Tube Condenser

A15.3.1 Assumptions

1. There is no refrigerant pressure drop through the condenser.
2. There is no refrigerant liquid in the condenser apart from condensed liquid (condensate) draining off the tubes.
3. Refrigerant condensing temperature and refrigerant-side heat transfer coefficient are the same throughout the condenser.
4. Refrigerant leaves the condenser as saturated liquid.

5. Entering refrigerant is uniformly distributed along the length of the condenser.

6. No oil or other contaminants are present in the refrigerant.

Denoting refrigerant condensing temperature by $t_{(r)c}$, corresponding saturation pressure by $P_{sat}(T_{(r)c})$ and outlet refrigerant enthalpy by h_{co}, assumptions 1, 3 and 4 can be expressed as

$$t_{(r)co} = t_{(r)c} \qquad P_{ci} = P_{co} = P_{sat}(T_{(r)c}) \qquad h_{co} = h_{(f)}(T_{(r)c}) \qquad \text{(A15-11)}$$

A15.3.2 Constraints

Denoting the heat transferred through the condenser from the refrigerant to the water by Q_c, the constraints on the performance of the condenser are

$$Q_c = -Q_{(w)c} \qquad Q_{(r)c} = -Q_{(w)c} \qquad \text{(A15-12)}$$

A15.3.3 Energy and Heat Transfer Relationships

Similarly to the shell-and-tube evaporator,

$$Q_{(w)c} = m_{(w)c}c_{(w)}(t_{(w)co} - t_{(w)ci}) \qquad \text{(A15-13)}$$

$$Q_{(r)c} = m_{(r)c}(h_{co} - h_{ci}) \qquad \text{(A15-14)}$$

The heat transferred through the condenser, Q_c, is

$$Q_c = UA_c \cdot LMTD_c \qquad \text{(A15-15a)}$$

and similarly to (A15-6b) and (A15-6c)

$$LMTD_C = \frac{t_{(w)Co} - t_{(w)Ci}}{\ln\left(\frac{t_{(w)Co} - t_{(r)C}}{t_{(w)Ci} - t_{(r)C}}\right)} \qquad \text{(A15-15b)}$$

$$\frac{1}{UA_C} = \frac{1}{h'_{[w]C}A_{T[w]C}} + \frac{1}{h'_{f[w]C}A_{T[w]C}} + \frac{y_{TC}}{k_{TC}\overline{A}_{TC}} + \frac{1}{h'_{[r]C}A_{T[r]C}} \qquad \text{(A15-15c)}$$

$h'_{[w]C}$ and $\overline{A}_{TC}$ are given by exactly analogous versions of (A15-7a) and (A15-7b), and (A15-8) respectively. The coefficient $h'_{[r]C}$ of heat transfer from condensing refrigerant is now given.

Coefficient of Heat Transfer from Condensing Refrigerant

Refrigerant is first de-superheated and then condensed in the shell-and-tube water-cooled condenser. Because the tube wall temperature is normally lower than the condensing temperature everywhere in the condenser, condensation takes place throughout the condenser. The effect of changes in the entering gas superheat are typically insignificant due to an inversely proportional relationship between temperature differences and heat transfer coefficients. As a result, an average overall heat transfer coefficient and the mean temperature difference (calculated from the saturated condensing temperature corresponding to the condensing pressure, and the entering and leaving water temperatures) give reasonably accurate predictions of performance (ASHRAE, 1992).

A correlation is again sought which will have reasonable applicability to the range of horizontal shell-and-tube condensers used in large-capacity water chilling machines. For laminar filmwise condensation on finned tubes, the 1948 correlation of Beatty and Katz, as reported by ASHRAE (1993 : 4.8) is used:

$$h' = 0{,}689 \cdot \left(\frac{k_{lf}^3 \rho_{lf}^2 g}{\mu_{lf}} \right)^{0{,}25} \cdot \left(\frac{h_{(r)(g)}}{D_{eq} \Delta t} \right)^{0{,}25} \qquad \text{(A15-16a)}$$

where $\Delta t = t_{(r)sat} - \bar{t}_{(w)}$; $t_{(r)sat}$ is the saturation temperature at the refrigerant *pressure* (assumed constant) in the condenser, and $\bar{t}_{(w)}$ is the average temperature of the water flowing through the tubes. k_{lf}, μ_{lf} and ρ_{lf} are thermal conductivity, absolute viscosity and density of the refrigerant liquid *at the temperature* t_f *of the liquid film on the tubes*, given by $t_f = t_{(r)sat} - 0{,}75\Delta t$. The equivalent diameter D_{eq} depends on the external tube diameter; the *primary* outside wall area of one tube (i.e. the area without fins); the area of one side of one fin; the surface area of all fins on one tube; and the fin efficiency.

The Beatty and Katz correlation is used in several models of centrifugal chillers reported; see, for example, Chi (1979), Braun et al (1987), and Wong and Wang (1989). However, as Webb (1984) points out in a detailed survey of the state of knowledge of shell-side refrigerant condensation in shell-and-tube condensers, the Beatty and Katz model assumes that no condensate is retained between the tube fins due to capillary forces, and that the force of gravity drains the condensate from the fins and the tube between the fins. Tests have shown that these assumptions are incorrect; a significant fraction of the tube surface may be flooded with condensate, and surface tension rather than gravity controls condensate drainage from the tubes.

The Beatty and Katz model also does not account for row effects, i.e. differences in performance of successive horizontal tube rows. These are primarily due to vapour velocity within the tube bundle, and "inundation" of lower tube rows by condensate draining from upper tube rows (Webb, 1984). The thermal resistance of the liquid film on inundated tubes reduces the condensation coefficient; however, vapour velocity disturbs

the condensate drainage pattern from tube to tube, and hence reduces this inundation effect. The summary of ASHRAE (1993 : 36.3) concludes that these and other compensating effects make actual row effect uncertain.

Examining (A15-16a), the correlation for the heat transfer coefficient h' is a function of (a) the prevailing refrigerant pressure, which determines the saturation temperature $t_{(r)sat}$ and the latent heat $h_{(r)(g)}$; (b) the temperature difference Δt; (c) the properties of the refrigerant at the film temperature t_f; (d) the local gravitational acceleration g; and (e) the construction and arrangement of tubes within the condenser. This suggests that, *for a particular horizontal shell-and-tube condenser condensing a particular refrigerant,* the refrigerant-side coefficient of heat transfer may be expressed as

$$h' = C \cdot \left(\frac{k_{tf}^3 \rho_{tf}^2 g}{\mu_{tf}}\right)^{0,25} \cdot h_{(r)(g)}^{0,25} \cdot \left(\frac{1}{\Delta t}\right)^{0,25} \qquad \text{(A15-16b)}$$

For Refrigerants 11, 12 and 22, Table A15.2 shows how the condensing coefficient factor $\left(\frac{k_{tf}^3 \rho_{tf}^2 g}{\mu_{tf}}\right)^{0,25}$ and the latent heat factor $h_{(r)g}^{0,25}$ vary over the range of refrigerant temperatures encountered in condensers in water chilling machines on mines.

For Refrigerant 11, the variations in these factors are 1 and 2 per cent respectively. This suggests that the refrigerant-side coefficient of heat transfer may be adequately expressed as a function of a constant C and the temperature difference Δt:

$$h'_{(r)c} = \frac{C}{(\Delta t)^{0,25}} = \frac{C}{\left[t_{(r)c} - \left(t_{(w)ci} + t_{(w)co}\right)/2\right]^{0,25}} \qquad \text{(A15-17)}$$

This is the approach adopted by Howes (1976), who gives values for C as $C = 3\ 350$ for Refrigerant 12, and $C = 4\ 355$ for Refrigerants 11 and 22. This approach is not as valid for Refrigerants 12 and 22, though because the variations in the factors in Table A15.2 for these refrigerants are of the order of 16 and 8 per cent respectively.

Table A15.2 Condensing Coefficient Factors and Latent Heat Factors for Halocarbon Refrigerants (ASHRAE, 1993 : 4.9)

Film Temperature t_{film}, °C	Condensing Coefficient Factor $\left(k_{rl}^3 \rho_{rl}^2 g/\mu_{rl}\right)^{0,25}$	Saturation Temperature $t_{(r)sat}$, °C	Latent Heat Factor $h_{(r)(g)}^{0,25}$
Refrigerant 11			
24	80,7	24	20,60
38	80,3	38	20,45
68	79,2	68	20,06
Refrigerant 12			
24	69,8	24	19,30
38	64,0	38	18,99
68	58,7	68	18,06
Refrigerant 22			
24	80,3	24	20,71
38	75,5	38	20,28
68	69,2	68	18,89

A15.4 The Centrifugal Compressor Stage

Version 1.01 of CHILLER utilises isentropic analysis in modelling individual stages of a centrifugal compressor, for the reasons cited on page 77, Chapter 3. Because manufacturers generally do not release detailed characteristic performance curves of their compressors, such modelling has the definite advantage that isentropic work and efficiency can be directly ascertained from the thermodynamic properties of the refrigerant employed.

A centrifugal compressor stage, assumed to be equipped with variable inlet guide vanes, is modelled in the form of *maps* of curves of fraction-of-design isentropic head and fraction-of-design isentropic efficiency, both

being functions of fraction-of design volumetric flow-rate and inlet guide vane (or diffuser vane) opening. The map of artificial curves used in CHILLER for a compressor stage with inlet guide vanes is shown in Figure A15.1. The curves therein are approximate, polynomial curve fits to those reported by Grollius, Meyer, Rautenberg and Bailey-McEwan (1987). The *design point* (100% of volumetric flow-rate, 100% of isentropic head) is always defined to be on the curve for a guide vane angle of 0° (i.e. when the guide vanes are fully open). As seen, for each position of the vanes, different curves of isentropic head and efficiency obtain. Each such curve has a surge point, and the locus of the surge points produces the surge line shown.

The accuracy of modelling a centrifugal compressor stage in this way depends on the accuracy of the shape of each curve, and on the accuracy of the changes in position of the curves as the vane opening changes. The curves in Figure A15.1 of per unit (i.e. fraction-of-design) isentropic head $\Delta h|_s / \Delta h|_{s.des}$ and per unit isentropic efficiency $\eta|_s / \eta|_{s.des}$ are expressed as functions of vane opening ψ and per unit (fraction-of-design) volumetric flow-rate $\dot{V}_{PI} / \dot{V}_{PI.des}$ as follows.

$$\frac{\Delta h|_s}{\Delta h|_{s.des}} \equiv \frac{\Delta h|_s}{\Delta h|_{s.des}} \left(\psi, \frac{\dot{V}_{PI}}{\dot{V}_{PI.des}} \right) \qquad \text{(A15-18a)}$$

$$\frac{\eta|_s}{\eta|_{s.des}} \equiv \frac{\eta|_s}{\eta|_{s.des}} \left(\psi, \frac{\dot{V}_{PI}}{\dot{V}_{PI.des}} \right) \qquad \text{(A15-18b)}$$

One of the more important aspects in which characteristic curves of compressors may differ is the overall slope of the design curve, expressed relatively in terms of "steepness" or "flatness". CHILLER Version 1.01 allows seven different slopes of the design curve, named as in Table A15.3 below.

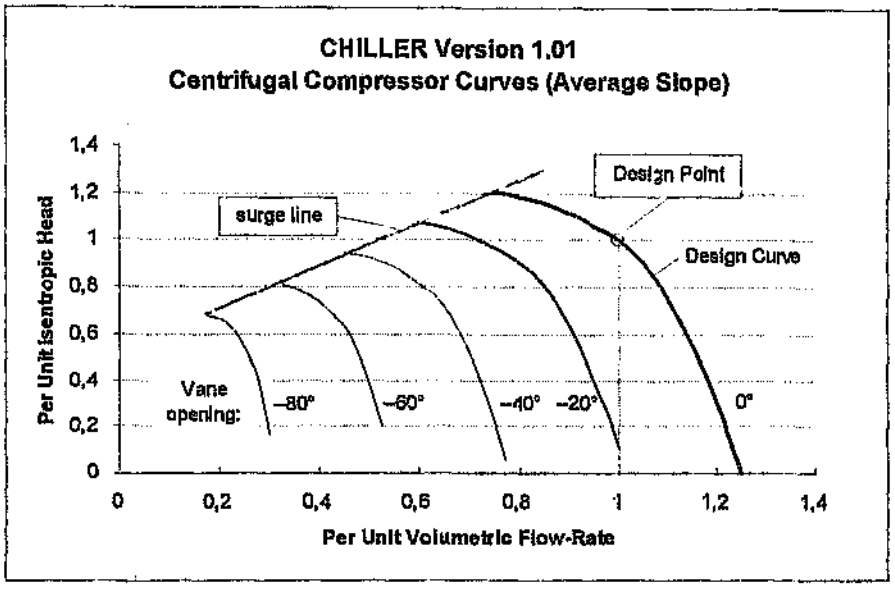

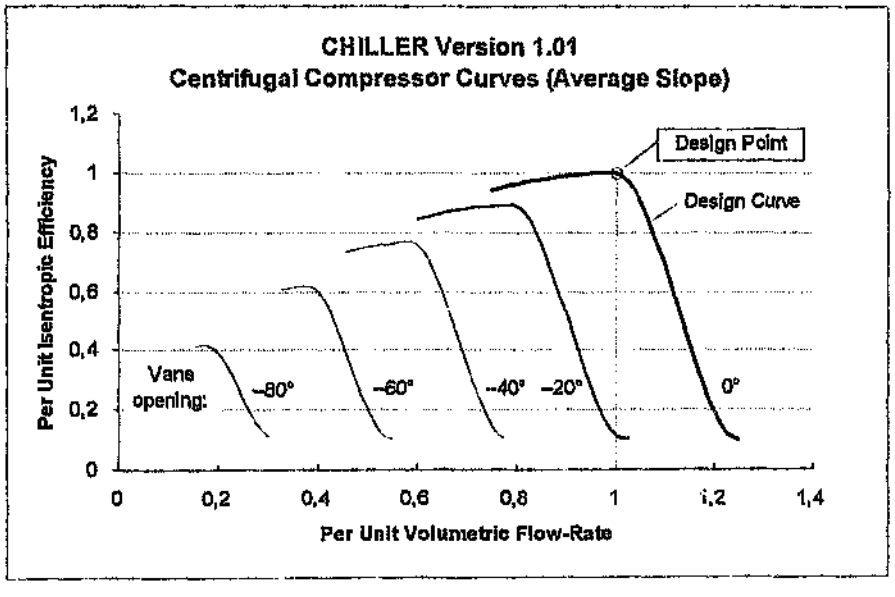

Figure A15.1 CHILLER Version 1.01: Isentropic Head and Efficiency Curve Maps for Centrifugal Compressor Stage with Inlet Guide Vanes

Table A15.3 CHILLER Version 1.01: Family of Design Curves of Per Unit Isentropic Head versus Per Unit Volumetric Flow-Rate

Name of slope	Per unit volumetric flow-rate at:		
	surge point	design point	choke point
very flat	60	100	140
flat	65	100	135
fairly flat	70	100	130
average slope	75	100	125
fairly steep	80	100	120
steep	85	100	115
very steep	90	100	110

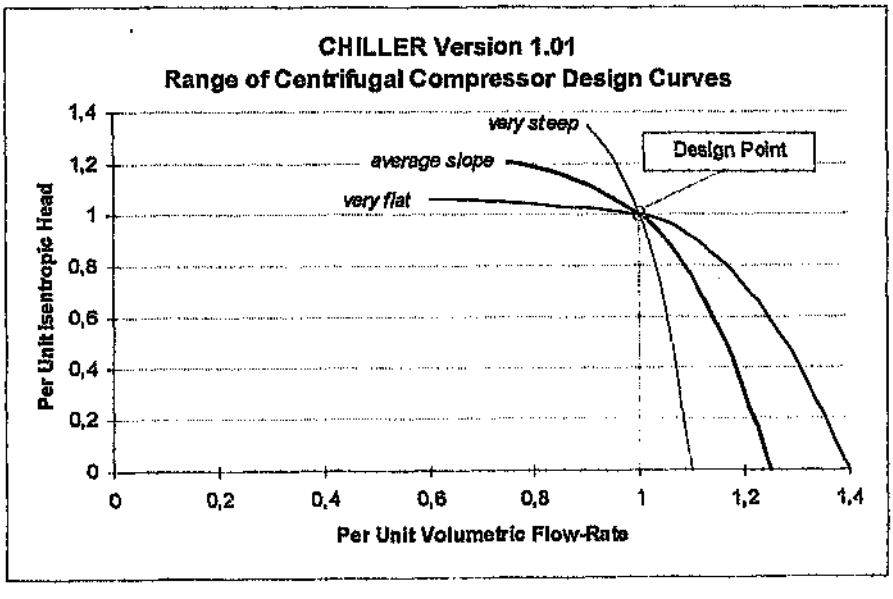

Figure A15.2 CHILLER Version 1.01: Range of Design Curves of Per Unit Isentropic Head versus Per Unit Volumetric Flow-Rate

The "very flat", "average slope" and "very steep" design curves are shown in Figure A15.2.

Each stage of a multi-stage centrifugal compressor is modelled separately, which allows the interactions between the stages and the other components in the refrigerant circuit to be taken into account.

A15.5 The Economiser

An open-flash economiser, depicted in Figure A15.3 below, serves to separate the liquid and vapour in an incoming two-phase stream of refrigerant from an expansion valve.

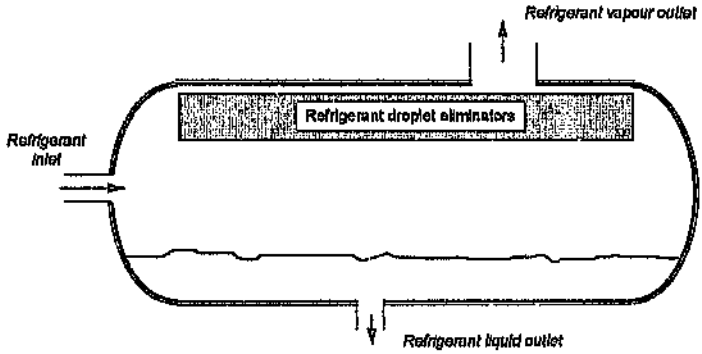

Figure A15.3 Open-Flash Economiser

A15.5.1 Assumptions

Saturated conditions prevail in the economiser, and there is no pressure drop therein.

A15.5.2 Constraints

Denoting the temperature of the saturated refrigerant in the economiser by $t_{(r)EC}$, and the enthalpies at the inlet, liquid outlet and vapour outlet by h_{ECi}, h_{EClo} and h_{ECvo} respectively,

$$t_{(r)ECi} = t_{(r)ECto} = t_{(r)ECvo} = t_{(r)EC} \qquad P_{ECi} = P_{ECto} = P_{ECvo} = P_{sat}\left(T_{(r)EC}\right) \text{ (A15-19a)}$$

$$h_{ECi} = h_{(f)}\left(T_{(r)EC}\right) \qquad h_{ECvo} = h_{(g)}\left(T_{(r)EC}\right) \text{ (A15-19b)}$$

A15.5.3 Energy and Heat Transfer Relationships

Denoting the refrigerant mass flows at the inlet, liquid outlet and vapour outlet by m_{ECi}, m_{ECto} and m_{ECvo} respectively, mass and energy balances over the economiser yield without difficulty

$$m_{ECto} = m_{ECi}\frac{h_{ECi} - h_{ECvo}}{h_{ECto} - h_{ECvo}} \qquad m_{ECvo} = m_{ECi} - m_{ECto} \text{ (A15-20)}$$

A15.6 The Expansion Valve

Here, the constraint is simply

$$h_{EXo} = h_{EXi} \text{ (A15-21)}$$

APPENDIX 16

THE CHILLER COMPUTER PROGRAM TO PREDICT PERFORMANCE OF MINE WATER CHILLING INSTALLATIONS

The CHILLER computer program was developed by the Chamber of Mines of South Africa for the South African mining industry (Bailey-McEwan and Penman, 1987). As noted in Chapter 4, it has two key features making it more generally applicable than other programs developed during the same period.

1) It models the single- or multi-stage centrifugal compressor of conventional water chilling machines more fundamentally, using artificial compressor characteristic curves for *each* stage. The principal features of these artificial curves, as explained later, are specifiable in order to match the actual curves of each compressor stage as closely as possible;

2) It can predict the performance of complete water chilling installations, consisting of multiple conventional water chilling machines, cooling towers, and reservoirs interconnected in any user-specified configuration.

The second feature is utilised only once in this thesis, and therefore deserves brief elaboration. As explained in Section 2.4, Chapter 2, most water chilling installations experience significant variations in duty due to both daily and seasonal climatic changes, and the unpredictable nature of mining. While such installations must be able to provide their peak cooling capacity under full-duty design conditions, their performance under all significantly off-design conditions, where energy-efficiency and adaptability are desirable, is equally important. To assess the quality of energy-efficiency and adaptability, and hence optimally design an installation, it is therefore desirable to predict off-design performance. A computer program is required to make this practicable, though, in view of

the complex interactions between the water chilling, heat-rejection and other plants in such installations, and between the components within these plants.

Two other uses for such a program are immediately evident. The effects of changes to existing or envisaged installations can be simulated and assessed. Case studies of such use of CHILLER are reported by Bailey-McEwan (1991). It is also of use in ascertaining and assessing performance of and detecting faults in conventional water chilling machines, as demonstrated in Chapters 5 and 6.

A16.1 Representation of Installation Being Simulated

CHILLER is an interactive program, running on any IBM-PC-compatible microcomputer, and has been designed for user-friendliness. Bailey-McEwan and Penman (1987) give a complete description of the features and facilities of Version 1.01 of this program. Here, the manner in which the installation is represented is outlined, and the program's two principal facilities, termed "Catalogues" and "Installation", are described.

A water chilling installation is represented as a chilled water circuit; a condenser water circuit; and the water chilling plant, consisting of a group of conventional water chilling machines CHILLER represents each refrigerant circuit and water circuit separately, as described below.

A16.1.1 Refrigerant Circuits of Conventional Water Chilling Machines

Version 1.01 of CHILLER can simulate only conventional, packaged water chilling machines with a single- or two-stage centrifugal compressor.

Up to ten conventional water chilling machines are permitted in the installation simulated. A directory of machines permits access to any one in the installation. Each machine is represented as a closed refrigerant circuit, consisting of an evaporator, a condenser, a single- or two-stage centrifugal compressor, the corresponding amount of expansion valves,

and an economiser in the case of a two-stage compressor. The refrigerant employed - R11, R12, or R22 - must be specified.

A16.1.2 Chilled Water Circuit

Components permitted in the chilled water circuit are evaporators (of conventional machines), cooling towers, reservoirs, links, and entrances to and exits from the installation. The user builds a circuit interactively, through a highlighting window which is moved to where a component must be inserted or deleted. Components can be inserted or deleted at any location, and can be connected to any neighbouring component in series or parallel fashion. Water flows through links and reservoirs can be directed backwards if required, thus permitting feedback streams between any two points.

A16.1.3 Condenser Water Circuit

This is represented as for the chilled water circuit. The same range of components is allowed except that condensers of conventional machines are substituted for evaporators.

A16.2 Built-In Catalogues of Installation Components

The "Catalogues" facility allows the user to create and modify the built-in catalogues containing the specifications of up to 15 different models of evaporators, condensers, cooling towers, and centrifugal compressor stages. Each component in the installation is identified as a particular model in the appropriate catalogue.

For each type of component, there is a range of available *classes*. For example, centrifugal compressor stages may be regulated by variable inlet guide vanes or variable diffuser vanes. The user may select the class, whereupon a corresponding specification sheet is displayed. Individual specifications in this sheet, initially set to default values, may then be modified.

For example, Table A16.1a shows the specification sheet for a centrifugal compressor stage. The specification process is listed in Table A16.1b.

Table A16.1a CHILLER Version 1.01: Specification Sheet for Centrifugal Compressor Stage

Class: vane-regulated Name: Description of Attributes	Unit	Min.	Value	Max.
Max. guide vane setting (fully open)	degr.	0,00		20,00
Min. guide vane setting (fully closed)	degr.	-80,00		-40,00
Design refrigerant		R12		
Compressor curve family		Chamber of Mines		
Slope of full-capacity curve		average slope		
Design suction vol. flow-rate	m³/s	0,10		20,00
Design isentropic head	kJ/kg	1,00		25,00
Design isentropic efficiency	%	10,00		90,00

Table A16.1b CHILLER Version 1.01: Specifying a Centrifugal Compressor Stage

Attribute	Selection
Max. and min. guide vane settings	The desired values are entered in the corresponding "Value" fields.
Design Refrigerant	R11, R12 or R22 is selected.
Compressor Curve Family	The "Chamber of Mines" option (the only option available in Version 1.01) accesses CHILLER's family of artificial curves.
Slope of full-capacity curve	One of the seven slopes listed in Table A15.3, Appendix 15 is selected.
Design suction vol. flow-rate; isentropic head; and isentropic efficiency	The desired values are entered in the corresponding "Value" fields.

A16.3 Simulation of Installation Performance

In the "Installation" facility, the installation is first built as described above. Next, the specifications of all evaporators, condensers, cooling towers and centrifugal compressors are set by specifying each as a particular model in the appropriate built-in catalogue.

Next, all inputs and internal process parameters which the user is required to specify are entered. These comprise barometric pressure, air mass flow-rate and inlet air wet-bulb temperature for each cooling tower;

volume and temperature of water stored in each reservoir; water flow-rates and inlet water temperatures for the chilled and condenser water circuits; and, for each conventional water chilling machine, water-side fouling factors for the evaporator and condenser, and inlet guide vane (or diffuser vane) angle settings on each centrifugal compressor stage. Water flow-rates are then checked for balance at each node of the chilled and condenser water circuits.

A16.3.1 Master Simulation Algorithm

The static performance of the installation is then simulated, using the master algorithm depicted in Figure A16.1. Initial estimates of the unknown water temperatures in the chilled and condenser water circuits are first obtained, by a simple guessing sub-algorithm if values from a previous simulation are not available. Using these estimates as inputs, the performance of each installation component is calculated. The values of the unknown water temperatures so calculated are compared with their estimated values. Unless calculated and estimated values of all unknown water temperatures agree within 0,001°C, the latter are refined by the multi-dimensional Newton-Raphson method until this is the case.

A16.3.2 Models and Simulation Algorithms for Installation Components

As mentioned above, permitted installation components in CHILLER Version 1.01 are conventional water chilling machines, cooling towers, water reservoirs, links, and water entrances to or exits from the installation. All interconnecting water piping, including links, between installation components is assumed to be frictionless and without heat gain or loss. The models employed in CHILLER Version 1.01 for a cooling tower and a conventional water chilling machine with a single- or two-stage centrifugal compressor are now described. The models employed for the components of these machines are fully described and justified in Appendix 15, to which reference is made as appropriate.

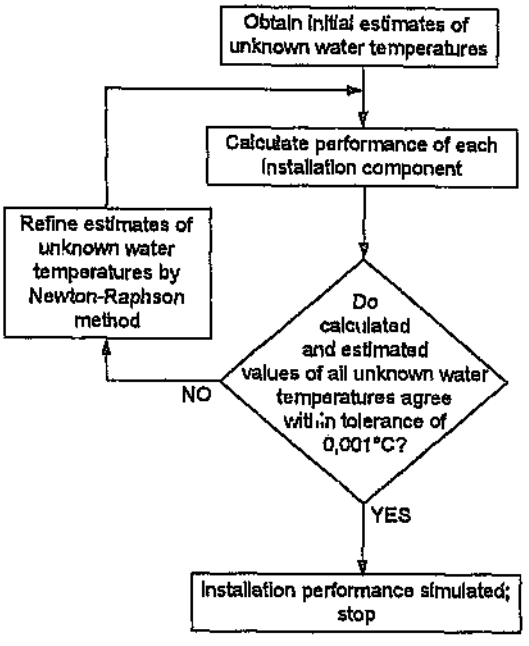

Figure A16.1 CHILLER Version 1.01: Master Algorithm to Simulate Installation Performance

Cooling Tower

The performance of a cooling tower is simulated by the factor-of-merit method described by Whillier (1977). The only specification required for a cooling tower is thus its factor of merit. Inputs required are barometric pressure, inlet wet-bulb temperature and flow-rate (on a dry mass basis) of the air; and mass flow-rate and inlet temperature of the water.

Conventional Machine with Single-Stage Centrifugal Compressor

Components. These are an interconnected shell-and-tube evaporator, single-stage centrifugal compressor, shell-and-tube condenser and expansion valve as in Figure A16.2. The interconnecting piping between these components is assumed to be frictionless, so changes in refrigerant pressure and other properties along this piping are ignored. Mechanical

inefficiencies in the compressor and the effect of its oil cooler are also ignored. The machine is assumed to have no hot gas bypass valve.

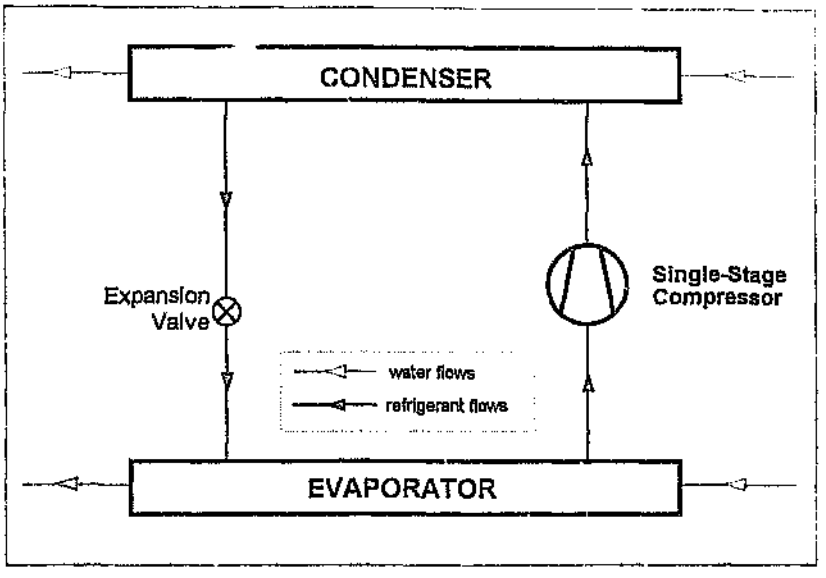

Figure A16.2 CHILLER Version 1.01: Model of Conventional Water Chilling Machine with Single-Stage Centrifugal Compressor

User-Supplied Specifications. These specifications (entered into the appropriate built-in catalogues) and their corresponding symbols are listed in Table A16.2 below.

Inputs and Internal Process Parameters. These are listed in Table A16.3 below with their corresponding symbols.

Properties of Refrigerant. These are given by (A15-1a) through (A15-1g) in Section A15.1, Appendix 15.

Model of Evaporator. The refrigerant mass flow-rate and properties at the inlet are given by the constraints

$$m_{(r)E} = m_{(r)EX} \qquad h_{EI} = h_{EXo} \qquad \text{(A16-1a)}$$

Table A16.2 CHILLER Version 1.01: Specifications for Conventional Machine with Single-Stage Centrifugal Compressor

Machine Component	Specification	Symbol
Evaporator	Amount of passes	$N_{pa,E}$
	Amount of tubes	N_{TE}
	Internal tube diameter, mm	d_{TE}
	Tube wall thickness, m	y_{TE}
	Total inside wall area of tubes, m²	$A_{T[w]E}$
	Total outside wall area of tubes, m²	$A_{T[r]E}$
	Thermal conductivity of tube material, W/m.K	k_{TE}
Condenser	Amount of passes	$N_{pa,C}$
	Amount of tubes	N_{TC}
	Internal tube diameter, mm	d_{TC}
	Tube wall thickness, m	y_{TC}
	Total inside wall area of tubes, m²	$A_{T[w]C}$
	Total outside wall area of tubes, m²	$A_{T[r]C}$
	Thermal conductivity of tube material, W/m.K	k_{TC}
Compressor	Max. guide vane setting (fully open), ° Min. guide vane setting (fully closed), ° Design refrigerant Slope of full-capacity curve Design suction volumetric flow-rate, m³/s	$\dot{V}_{Pl,des}$
	Design isentropic head, kJ/kg	$\Delta h\|_{s,P,des}$
	Design isentropic efficiency, %	$\eta\|_{s,P,des}$

Table A16.3 CHILLER Version 1.01: Inputs and Internal Process Parameters for Conventional Machine with Single-Stage Centrifugal Compressor

Machine Component	Input or Internal Process Parameter	Symbol
Evaporator	Water flow-rate, kg/s	$m_{(w)E}$
	Inlet water temperature, °C	$t_{(w)Ei}$
	Water-side fouling factor, m²°C/W	$1/h'_{f[w]E}$
Compressor	Inlet guide vane opening, °	Ψ_P
Condenser	Water flow-rate, kg/s	$m_{(w)C}$
	Inlet water temperature, °C	$t_{(w)Ci}$
	Water-side fouling factor, m²°C/W	$1/h'_{f[w]C}$

The evaporator model described in Section A15.2, Appendix 15 is used. The assumptions, constraints and energy and heat-transfer relationships are accordingly as follows.

⇒ Assumptions: as in (A15-2) and so in addition

$$v_{Eo} = v_{(g)}\left(T_{(r)E}\right) \qquad s_{Eo} = s_{(g)}\left(T_{(r)E}\right) \tag{A16-1b}$$

⇒ Constraints: as in (A15-3);

⇒ Energy and heat-transfer relationships: as in (A15-4) through (A15-8), and (A15-10).

Model of Single-Stage Centrifugal Compressor. The refrigerant mass flow-rate and properties at the inlet are given by the constraints

$$\begin{aligned} &m_{(r)P} = m_{(r)E} && P_{Pl} = P_{Eo} \\ &h_{Pl} = h_{Eo} \qquad s_{Pl} = s_{Eo} && v_{Pl} = v_{Eo} \qquad \dot{V}_{Pl} = m_{(r)P} v_{Pl} \end{aligned} \tag{A16-2a}$$

The model of a centrifugal compressor stage described in Section A15.4, Appendix 15 is used. The isentropic head $\Delta h|_{s,P}$ and isentropic efficiency $\eta|_{s,P}$ are accordingly given in terms of the design values $\Delta h|_{s,P,des}$ and $\eta|_{s,P,des}$ and the per unit relationships (A15-18a) and (A15-18b):

$$\Delta h|_{s,P} = \Delta h|_{s,P,des} \cdot \left[\frac{\Delta h|_{s}}{\Delta h|_{s,des}} \left(\psi_P, \frac{\dot{V}_{Pl}}{\dot{V}_{Pl,des}} \right) \right] \tag{A16-2b}$$

$$\eta|_{s,P} = \eta|_{s,P,des} \cdot \left[\frac{\eta|_{s}}{\eta|_{s,des}} \left(\psi_P, \frac{\dot{V}_{Pl}}{\dot{V}_{Pl,des}} \right) \right] \tag{A16-2c}$$

where ψ_P is inlet guide vane opening. Actual head Δh_P, outlet enthalpy h_{Po} and power input W_P are then given by

$$h_{Po} - h_{Pi} = \Delta h_P = \frac{\Delta h|_{s,P}}{\eta|_{s,P}} \qquad h_{Po} = h_{Pi} + \Delta h_P \qquad W_P = m_{(r)P}\Delta h_P \qquad \text{(A16-2d)}$$

Enthalpy $h|_{s,Po}$ and entropy $s|_{s,Po}$ at the end of the ideal, hypothetical isentropic compression are obtained by

$$h|_{s,Po} = h_{Pi} + \Delta h|_{s,P} \qquad s|_{s,Po} = s_{Pi} \qquad \text{(A16-2e)}$$

Ideal, isentropic discharge temperature $T|_{s,Po}$ and specific volume $v|_{s,Po}$ are obtained by solving (A15-1d) and (A15-1e) simultaneously, with h and s given by (A16-2e). Outlet refrigerant pressure P_{Po} is then given by (A15-1c):

$$P_{Po} = P\left(T|_{s,Po}, v|_{s,Po}\right) \qquad \text{(A16-2f)}$$

The real discharge temperature T_{Po} and specific volume v_{Po} are then obtained by solving (A15-1c) and (A15-1d) simultaneously, with P and h being P_{Po} and h_{Po}.

Model of Expansion Valve. The refrigerant mass flow-rate and properties at the inlet are given by the constraints

$$m_{(r)EX} = m_{(r)C} \qquad h_{EXi} = h_{Co} \qquad \text{(A16-3a)}$$

and outlet refrigerant properties are given by

$$h_{EXo} = h_{Co} \qquad P_{EXo} = P_{Ei} \qquad \text{(A16-3b)}$$

Model of Conderser. The refrigerant mass flow-rate and properties at the inlet are given by the constraints

$$m_{(r)C} = m_{(r)P} \qquad h_{Ci} = h_{Po} \qquad P_{Ci} = P_{Po} \qquad \text{(A16-4a)}$$

The condenser model described in Section A15.3, Appendix 15 is used. The assumptions, constraints and energy and heat-transfer relationships are accordingly as follows.

⇒ Assumptions: as in (A15-11);

⇒ Constraints: as in (A15-12);

⇒ Energy and heat-transfer relationships: as in (A15-13) through (A15-15c); exactly analogous versions of (A15-7b) and (A15-8); and (A15-17).

Overall Mass And Energy Balances. These are the constraints

$$m_{(r)E} = m_{(r)P} = m_{(r)C} = m_{(r)EX} = m_{(r)} \qquad Q_E + W_P + Q_C = 0 \qquad \text{(A16-5)}$$

Simulation Algorithm. This model of the machine is solved by the multi-dimensional Newton-Raphson method.

Conventional Machine with Two-Stage Centrifugal Compressor

Components. These are an interconnected shell-and-tube evaporator, a two-stage centrifugal compressor, an economiser, a shell-and-tube condenser and two expansion valves interconnected as in Figure 5.10. As for the single-stage machine, the interconnecting piping is assumed to be frictionless; mechanical inefficiencies in the compressor and the effect of its oil cooler are ignored; and no hot gas bypass valve is assumed.

User-Supplied Specifications. These are as in Table A16.2, except that the two compressor stages are specified separately as in Table A16.4 below.

Inputs and Internal Process Parameters. These are as in Table A16.3, except that the vane openings ψ_{P1} and ψ_{P2} of the two compressor stages are input quantities.

Table A16.4 CHILLER Version 1.01: Compressor Stage Specifications for Conventional Machine with Two-Stage Centrifugal Compressor

Machine Component	Specification	Symbol
Compressor Stage 1	Max. guide vane setting (fully open), ° Min. guide vane setting (fully closed), ° Design refrigerant Slope of full-capacity curve Design suction volumetric flow-rate, m³/s Design isentropic head, kJ/kg Design isentropic efficiency, %	$\dot{V}_{P1l,des}$ $\Delta h\|_{s,P1,des}$ $\eta\|_{s,P1,des}$
Compressor Stage 2	Max. guide vane setting (fully open), ° Min. guide vane setting (fully closed), ° Design refrigerant Slope of full-capacity curve Design suction volumetric flow-rate, m³/s Design isentropic head, kJ/kg Design isentropic efficiency, %	$\dot{V}_{P2l,des}$ $\Delta h\|_{s,P2,des}$ $\eta\|_{s,P2,des}$

Properties of Refrigerant. These are as in Section A15.1, Appendix 15.

Model of Evaporator. The refrigerant mass flow-rate and properties at the inlet are given by the constraints

$$m_{(r)E} = m_{(r)EX2} \qquad h_{Ei} = h_{EX2o} \tag{A16-6}$$

The same evaporator model as for the single-stage machine is used.

Model of Two-Stage Centrifugal Compressor: Stage 1. The refrigerant mass flow-rate and properties at the inlet are given by the constraints

$$\begin{aligned} &m_{(r)P1} = m_{(r)E} && P_{P1i} = P_{Eo} \\ &h_{P1i} = h_{Eo} \qquad s_{P1i} = s_{Eo} && v_{P1i} = v_{Eo} \qquad \dot{V}_{P1i} = m_{(r)P1} v_{Pi} \end{aligned} \tag{A16-7a}$$

The centrifugal compressor stage model of Section A15.4, Appendix 15 is again used. The isentropic head $\Delta h|_{s,P1}$, isentropic efficiency $\eta|_{s,P1}$, actual head Δh_{P1}, outlet enthalpy h_{P1o}, power input W_{P1}, and outlet pressure

P_{P1o}, temperature T_{P1o} and specific volume v_{P1o} are obtained in the same way as for the single-stage machine.

Model of Economiser. The refrigerant mass flow-rate and properties at the inlet are given by the constraints

$$m_{(r)ECI} = m_{(r)C} \qquad h_{ECI} = h_{EX1o} \qquad P_{ECI} = P_{Co} \tag{A16-8a}$$

The economiser model in Section A15.5, Appendix 15 is used. The constraints and energy and heat-transfer relationships are accordingly as in (A15-19a) through (A15-20).

Model of Two-Stage Centrifugal Compressor: Stage 2. The refrigerant mass flow-rate and properties at the inlet are given by the constraints

$$\begin{aligned} &m_{(r)P2} = m_{(r)C} = m_{(r)P1} + m_{(r)ECVo} \qquad P_{P2I} = P_{P1o} \\ &h_{P2I} = \frac{m_{(r)P1}h_{P1o} + m_{(r)ECVo}h_{ECVo}}{m_{(r)P1} + m_{(r)ECVo}} \end{aligned} \tag{A16-9a}$$

The inlet temperature T_{P2I} and specific volume v_{P2I} are obtained by solving (A15-1c) and (A15-1d) simultaneously, with P and h being P_{P2I} and h_{P2I}. Then

$$s_{P2I} = s\left(T_{P2I}, v_{P2I}\right) \qquad \dot{V}_{P2I} = m_{(r)C}v_{P2I} \tag{A16-9b}$$

The isentropic head $\Delta h|_{s,P2}$, isentropic efficiency $\eta|_{s,P2}$, actual head Δh_{P2}, outlet enthalpy h_{P2o}, power input W_{P2}, and outlet pressure P_{P2o}, temperature T_{P2o} and specific volume v_{P2o} are then obtained in the same way as before.

Model of Expansion Valve 1. The refrigerant mass flow-rate and properties at the inlet are given by the constraints

$$m_{(r)EX1} = m_{(r)C} \qquad h_{EX1i} = h_{Co} \tag{A16-10a}$$

and outlet refrigerant properties are given by

$$h_{EX1o} = h_{Co} \qquad P_{EX1o} = P_{ECi} \tag{A16-10b}$$

Model of Expansion Valve 2. The refrigerant mass flow-rate and properties at the inlet are given by the constraints

$$m_{(r)EX2} = m_{(r)ECLo} \qquad h_{EX2i} = h_{ECLo} \tag{A16-11a}$$

and outlet refrigerant properties are given by

$$h_{EX2o} = h_{ECLo} \qquad P_{EX2o} = P_{Ei} \tag{A16-11b}$$

Model of Condenser. The refrigerant mass flow-rate and properties at the inlet are given by the constraints

$$m_{(r)C} = m_{(r)P2o} \qquad h_{Ci} = h_{P2o} \qquad P_{Ci} = P_{P2o} \tag{A16-12}$$

The same condenser model as for the single-stage machine is used.

Overall Mass And Energy Balances. These are the constraints

$$m_{(r)C} = m_{(r)E} + m_{(r)ECvo} \qquad Q_E + W_{P1} + W_{P2} + Q_C = 0 \tag{A16-13}$$

Simulation Algorithm. As for that of the single-stage machine, this model is solved by the multi-dimensional Newton-Raphson method.

APPENDIX 17

USE OF CHILLER PROGRAM TO OBTAIN INPUTS AND INTERNAL PROCESS PARAMETERS WHEN THESE ARE UNKNOWN

Version 1.01 of CHILLER does not solve this inverse type of problem directly. When simulating a conventional water chilling machine, it assumes that the inputs and internal process parameters are known. CHILLER then calculates the resulting outputs, including outlet water temperatures and all refrigerant properties.

If, instead, some of these outputs are known and some of the inputs or internal process parameters are not, the program has to be used indirectly. The user must supply initial estimates of the unknown inputs or internal process parameters, and use CHILLER to predict the corresponding performance. The user must then manually refine these estimates of the unknown inputs or internal process parameters until the predicted values of the known outputs match the actual values. This refining must be done carefully, preferably with the aid of an iterative solution-finding mathematical technique, as each known output will generally be influenced by more than one of the unknown inputs or internal process parameters. When using CHILLER in this way, each water chilling machine must be simulated individually, *not* as part of its complete installation.

As an example, the use of CHILLER to estimate the unknown water flow-rates and fouling factors in Case Study G, Section 5.4.1, Chapter 5 is described.

Three inputs were known: inlet water temperatures of evaporator and condenser, and vane opening of the first, regulated compressor stage. The two unknown inputs were evaporator and condenser water flow-rates. The important internal process parameters - water-side fouling factors in

the evaporator and condenser - were also unknown. However, four measurable outputs relating to the evaporator and condenser were known: evaporating refrigerant temperature, evaporator outlet water temperature, and condenser outlet refrigerant and water temperatures. The unknown water flow-rates and fouling factors were thus estimated and refined until the predicted values of these outputs agreed satisfactorily with the measured ones.

Excellent initial estimates of water flow-rates were the values estimated by the Thorp method (in the third column of Table 5.11). For initial estimates of the water-side fouling factors, the design values were used. The process of refining these estimates is portrayed in Table A17.1 below.

Table A17.1 Case Study G: Refinement of Estimates of Unknown Water Flow-Rates and Fouling Factors

Unknown inputs, int. process parameters				Known outputs			
Evaporator		Condenser		Evaporator		Condenser	
Water flow, l/s	Fouling factor, m²°C/w	Water flow, l/s	Fouling factor, m²°C/w	Outlet water temp., °C	Refrig. temp., °C	Outlet water temp., °C	Outlet refrig. temp., °C
				Actual values (from Table 5.11)			
				8,4	5,2	42,3	48,0
				Values predicted by CHILLER:			
Initial set of estimates:							
77,9	0,00007	333,5	0,00031	7,69	6,24	42,51	47,83
First refinement:							
80,0	0,00020	375,0	0,00040	8,30	5,67	42,05	48,50
Second refinement:							
79,9	0,00029	360,3	0,00035	8,50	4,97	42,11	47,80
Third refinement:							
79,8	0,00026	341,4	0,00035	8,41	5,22	42,30	48,01

The third refinement satisfactorily matched all actual values of the known outputs. The corresponding performance predicted by CHILLER is given in the fourth column of Table 5.11.

APPENDIX 18

CASE STUDY C: MODELLING OF REAL THREE-STAGE COMPRESSOR AS VIRTUAL TWO-STAGE COMPRESSOR

In Case Study C, both water chilling machines employed a three-stage centrifugal compressor and two interstage economisers. Such a vapour-compression block, illustrated in Figure A7.1, Appendix 7, is not modelled by Version 1.01 of CHILLER. Accordingly, in each machine of Case Study C, the real three-stage compressor and two economisers were represented as a virtual two-stage compressor and single economiser, *equivalent at full-duty design conditions.* That is, the virtual two-stage vapour-compression block was modelled to produce exactly the same effects in the evaporator and condenser under design conditions.

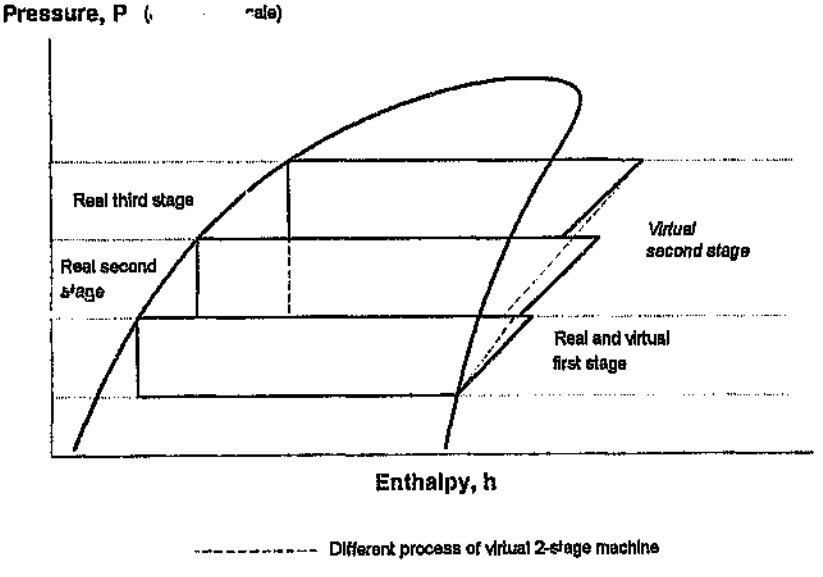

Figure A18.1 Representation of Real Three-Stage Water Chilling Machine as Virtual Two-Stage Machine at Design Conditions

The virtual two-stage vapour-compression block was therefore modelled as follows:

(i) design economiser pressure was made identical to that of Economiser 2 in the real three-stage block (see Figure A7.1), to ensure identical effects in the evaporator; that is, the same flash vapour fraction and refrigerating effect;

(ii) design isentropic efficiency of both stages in the two-stage virtual compressor had to be higher than those of all three stages of the real compressor, to ensure the same discharge temperature of the vapour leaving the compressor, and hence identical effects in the condenser.

The refrigerating cycles for both real three-stage machine and virtual two-stage machine are shown in the pressure-enthalpy diagram in Figure A18.1. The steeper slopes of the compression processes of the virtual two-stage compressor indicate the greater efficiencies required.

Obviously, perfect equivalence will not occur under off-design conditions, and this is reflected, for example, in the differences between predicted and measured temperatures of vapour leaving the economisers in Table 5.12.

APPENDIX 19

CASE STUDY A: MODELLING OF WATER CHILLING MACHINE WITH PARTIALLY FLOODED CONDENSER

This machine, depicted schematically in Figure 5.8 and of 7 350 kW(R) design capacity, was the largest-capacity machine modelled in this thesis. Modelling of it was different from that of other conventional machines in the following aspects:

- "typical" compressor characteristic curves were available from the manufacturer; these were therefore used instead of the artificial curves of the CHILLER program;
- the separate subcooler also had to be modelled;
- the pressure drops in the compressor suction and discharge piping were significant and thus were modelled for greater accuracy;
- the partial flooding in the condenser had to be modelled.

These four aspects are therefore considered in turn, following which the modelling of the complete machine is described.

A19.1 Modelling of Compressor

The "typical" curves furnished by the manufacturer are reproduced in Figure A19.1 below. As seen, percentage of full-duty pressure ratio is plotted as a function of inlet guide vane position and percentage of full-duty suction volumetric flow. Denoting pressure ratio by R_{press}, this function is denoted by $\frac{R_{press}}{R_{press.des}}\left(\psi_P, \frac{\dot{V}_{Pl}}{\dot{V}_{Pl.des}}\right)$. Curves of percentage of full-duty isentropic efficiency are superimposed; these are more conveniently expressed as a function of vane opening and percentage of design pressure ratio, so these are denoted by $\frac{\eta|_s}{\eta|_{s.des}}\left(\psi_P, \frac{R_{press.P}}{R_{press.P.des}}\right)$.

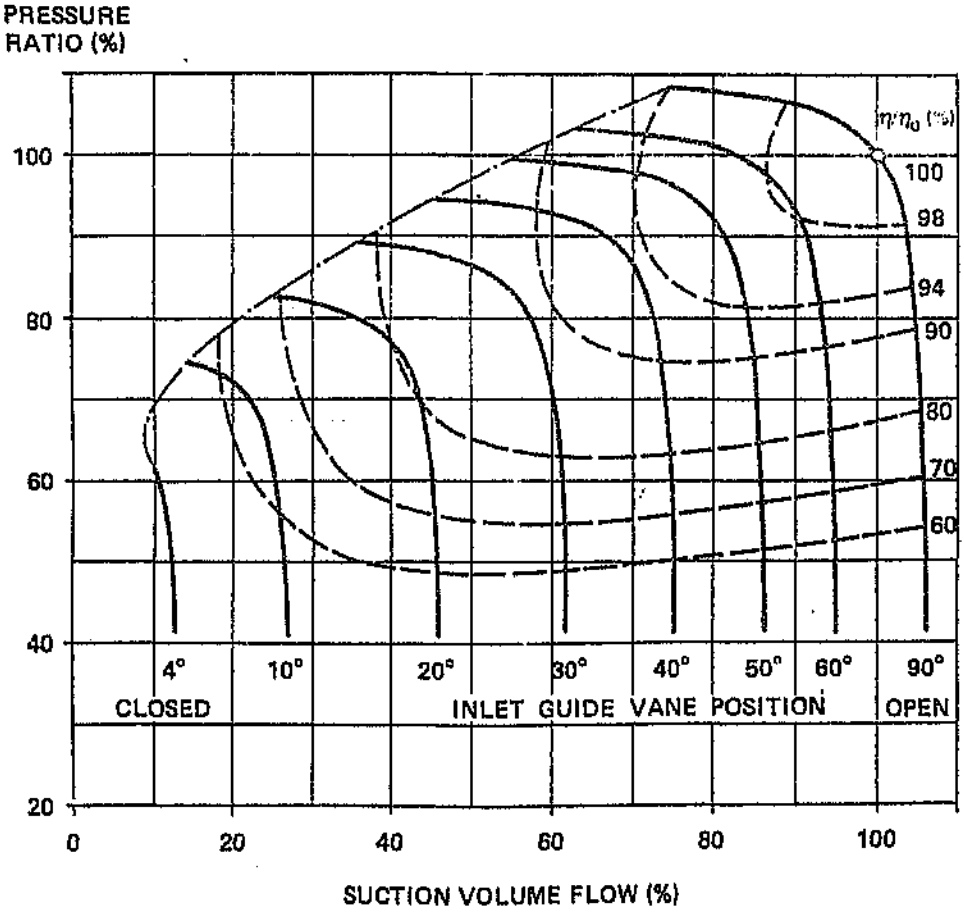

Figure A19.1 Case Study A. Typical Compressor Characteristic Curves Furnished by Manufacturer of Machine

Pressure ratio and isentropic efficiency of the compressor are thus expressed as

$$R_{press,P} = R_{press,P,des} \cdot \left[\frac{R_{press}}{R_{press,des}} \left(\psi_{P,} \frac{\dot{V}_{Pl}}{\dot{V}_{Pl,des}} \right) \right] \qquad \text{(A19-1a)}$$

$$\eta|_{s,P} = \eta|_{s,P,des} \cdot \left[\frac{\eta|_s}{\eta|_{s,des}} \left(\psi_P, \frac{R_{press,P}}{R_{press,P,des}} \right) \right] \qquad \text{(A19-1b)}$$

A19.2 Modelling of Subcooler

This is as depicted in Figure 3.15 and is denoted by the subscript *SC*.

A19.2.1 Assumptions

1. There is no refrigerant pressure drop through the subcooler.
2. The refrigerant-side heat transfer coefficient is the same throughout the subcooler.
3. No oil or other contaminants are present in the refrigerant.

A19.2.2 Constraints

Analogously to the condenser considered in Section A15.3, Appendix 15, the constraints are

$$Q_{sc} = -Q_{(w)sc} \qquad Q_{(r)sc} = -Q_{(w)sc} \qquad \text{(A19-2)}$$

A19.2.3 Energy and Heat Transfer Relationships

The relationships for water and refrigerant heat loads are exactly analogous to (A15-13) and (A15-14). The heat Q_{sc} transferred through the subcooler is

$$Q_{sc} = UA_{sc} \cdot LMTD_{sc} \qquad \text{(A19-3a)}$$

where $LMTD_{sc}$, assuming counterflow configuration (as in Figure 3.15) is given by

$$LMTD_{sc} = \frac{\left(t_{(r)sco} - t_{(w)sci}\right) - \left(t_{(r)sci} - t_{(w)sco}\right)}{\ln\left(\frac{t_{(r)sco} - t_{(w)sci}}{t_{(r)sci} - t_{(w)sco}}\right)} \qquad \text{(A19-3b)}$$

and

$$\frac{1}{UA_{sc}} = \frac{1}{h'_{[w]sc}A_{T[w]sc}} + \frac{1}{h'_{t[w]sc}A_{T[w]sc}} + \frac{y_{T.sc}}{k_{T.sc}\overline{A}_{T.sc}} + \frac{1}{h'_{[r]sc}A_{T[r]sc}} \qquad \text{(A19-3c)}$$

$h'_{[w]c}$ and $\overline{A}_{Tc}$ are given by exactly analogous versions of (A15-7a) and (A15-7b), and (A15-8) respectively. If the tubes are at least ten rows deep and in a staggered arrangement, and if normal leakage in a baffled heat exchanger is assumed, the refrigerant-side heat transfer coefficient $h'_{[r]sc}$ is given by the dimensional relation (Perry and Green, 1984 : 10-18)

$$h'_{[r]sc} = \frac{C}{D_{To.sc}^{0,4}} \cdot \left(\frac{c_p^{1/3} \rho^{0,6} k^{2/3}}{\mu^{0,287}} \right)_{(r)} \cdot \upsilon_{T.sc.max}^{0,6} \qquad \text{(A19-3d)}$$

where the constant $C = 0{,}198$; $D_{To.sc}$ is the outside diameter of the tubes; and $\upsilon_{T.sc.max}$ is the maximum inter-tube velocity of the refrigerant.

A19.3 Compressor Suction and Discharge Piping

A19.3.1 Assumptions

It is assumed that the piping consists of various lengths of straight pipe, and one or more bends.

A19.3.2 Energy and Heat Transfer Relationships

Suction and discharge piping in a conventional water chilling machine is designed for small pressure drops, as the compressor has to develop extra pressure rise to overcome these. Thus the changes in refrigerant vapour density along compressor suction and discharge piping are small. According to Perry and Green (1984 : 5-23), flow of a gas can be considered incompressible if its density within the system through which it is flowing changes by no more than 10 per cent. In this event, if the inlet

density is employed, the resulting error in computed pressure drop will generally not exceed the uncertainty limits in the friction factor.

Accordingly, the pressure drop $\Delta P_{(r)pipe}$ along suction or discharge piping is assumed to be given by the well-known relation for viscous, incompressible flow in conduits (see, for example, Welty, Wicks and Wilson, 1976 : 205-211):

$$\Delta P_{(r)pipe} = \left[\rho_{(r)l} v_{(r)l}^2 \cdot 2(FL/D + K/4)\right]_{pipe} \qquad \text{(A19-4a)}$$

where F and L are the Fanning friction factor and length of straight piping respectively, and K is the total friction coefficient for all bends and fittings that may be in the piping. For a particular suction or discharge pipe, $2(FL/D + K/4)$ is constant, and noting that $v_{(r)pipe,l} = \left(m_{(r)}/\rho_{(r)l}\, a\right)_{pipe}$, (A19-4a) becomes

$$\Delta P_{(r)pipe} = \left(C \cdot m_{(r)}^2/\rho_{(r)l}\right)_{pipe} = \left(C \cdot m_{(r)}^2 v_{(r)l}\right)_{pipe}$$
$$\text{where } C = \left[2(FL/D + K/4)/a^2\right]_{pipe} \qquad \text{(A19-4b)}$$

A19.4 Modelling of Partially Flooded Shell-and-Tube Condenser

Partial flooding is when one or more bottom rows of tubes are submerged in liquid refrigerant, as shown in Figure A19.2 below.

If the flooding in the condenser is known to be confined to the bottom pass of tubes, such a situation can be modelled by regarding the condenser as three interconnected heat exchangers as in Figure A19.3 below.

The bottom pass is modelled as an unflooded portion, "Condenser 1", and a flooded portion, "Subcooler 1", connected in parallel on the water side and in series on the refrigerant side. The other passes are modelled as a normal shell-and-tube condenser, termed "Condenser 2". On the water

side, this is connected in series with the bottom pass. On the refrigerant side, it is connected in parallel with the unflooded portion of the bottom pass.

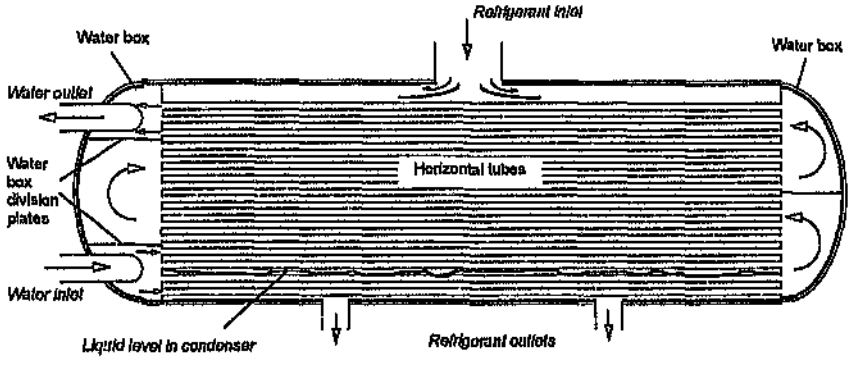

Figure A19.2 Partially Flooded Shell-and-Tube Condenser

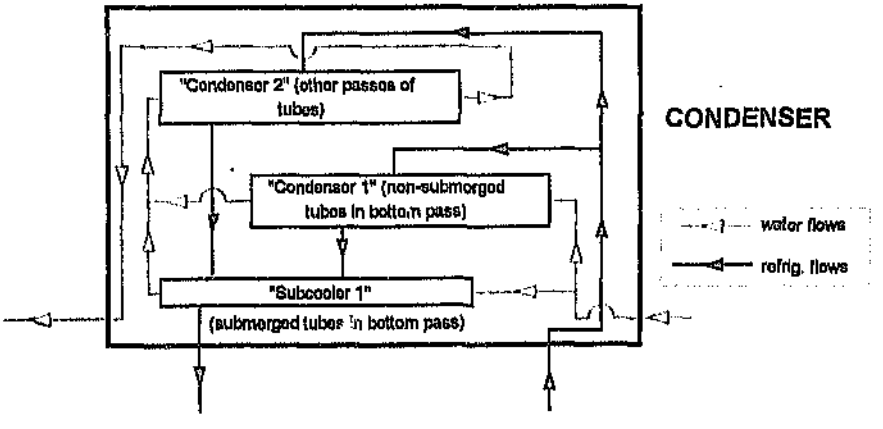

Figure A19.3 Case Study A: Modelling of Partially Flooded Shell-and-Tube Condenser

A19.4.1 Assumptions

For "Condenser 1", the unflooded portion of the bottom pass, and "Condenser 2", the other passes of tubes, the assumptions are as in

Section A15.3.1, Appendix 15. For "Subcooler 1", the flooded portion of the bottom pass, it is assumed that:

1) there is no refrigerant pressure drop;

2) heat transfer from refrigerant to tubes is by natural convection[1] and refrigerant-side heat transfer coefficient is the same for all tubes;

3) entering refrigerant is uniformly distributed along the length of the tubes;

4) no oil or other contaminants are present in the refrigerant.

A19.4.2 Constraints

Denoting the whole condenser by the subscript C, and "Condenser 1", "Subcooler 1" and "Condenser 2" by the subscripts *"C1", "SC1"* and *"C2"* respectively the constraints are as follows.

Flows of Water and Refrigerant

If N_{TC} and $N_{pa,C}$ are the amounts of tubes and passes, respectively, in the condenser, let the amount of *flooded* tubes be $N_{T,"SC1"}$. The amount of tubes per pass in the condenser is $N_{TC}/N_{pa,C}$. The water flows $m_{(w)"SC1"}$ and $m_{(w)"C1"}$ though the flooded and unflooded portions of the bottom pass are thus

$$m_{(w)"SC1"} = m_{(w)C}\frac{N_{T,"SC1"}}{N_{TC}/N_{pa,C}} \qquad m_{(w)"C1"} = m_{(w)C} - m_{(w)"SC1"} \qquad \text{(A19-5a)}$$

Also, the respective refrigerant flows $m_{(r)"C1"}$ and $m_{(r)"C2"}$ through "Condenser 1" and "Condenser 2" are related by

---

[1] Following the observation of ASHRAE (1992 : 36.4) that "where *means* are provided to elevate the condensate level for the desired submergence of the subcooler tubes" (meaning the bottom-most rows of tubes in the condenser) "heat is transferred principally by natural convection."

$$m_{(r)"c1"} + m_{(r)"c2"} = m_{(r)c} \qquad \text{(A19-5b)}$$

and the water temperature $t_{(w)"c2"i}$ at the inlet of "Condenser 2" is given by

$$t_{(w)"c2"i} = \frac{m_{(w)"c1"}t_{(w)"c1"o} + m_{(w)"sc1"}t_{"sc1"o}}{m_{(w)c}} \qquad \text{(A19-5c)}$$

Heat Transfer

$$\begin{aligned} Q_{"sc1"} &= -Q_{(w)"sc1"} & \qquad Q_{(r)"sc1"} &= -Q_{(w)"sc1"} \\ Q_{"c1"} &= -Q_{(w)"c1"} & \qquad Q_{(r)"c1"} &= -Q_{(w)"c1"} \\ Q_{"c2"} &= -Q_{(w)"c2"} & \qquad Q_{(r)"c2"} &= -Q_{(w)"c2"} \end{aligned} \qquad \text{(A19-5d)}$$

$$\begin{aligned} Q_{(r)c} &= Q_{(r)"sc1"} + Q_{(r)"c1"} + Q_{(r)"c2"} \\ Q_{(w)c} &= Q_{(w)"sc1"} + Q_{(w)"c1"} + Q_{(w)"c2"} \end{aligned} \qquad \text{(A19-5e)}$$

A19.4.3 Energy and Heat Transfer Relationships

"Condenser 1" (Unflooded Portion of Bottom Pass) and "Condenser 2"

The relationships are exactly analogous to those in Section A15.3.3, Appendix 15, with the following exception. As Refrigerant 12 is employed, (A15-16b) instead of (A15-17) is used to predict the refrigerant-side heat transfer coefficient, in order to allow for the variation of the condensing coefficient and latent heat factors in Table A15.2. As described in Section A15.3.3 of Appendix 15, these factors are evaluated at the *film temperature* $t_f = t_{(r)sat} - 0{,}75\Delta t$, where $\Delta t = t_{(r)sat} - \left(t_{(w)ci} + t_{(w)co}\right)/2$.

"Subcooler 1" (Flooded Portion of Bottom Pass)

The relationships for water and refrigerant heat loads are exactly analogous to (A15-13) and (A15-14). This portion, like the rest of the condenser, constitutes a *crossflow* heat exchanger. Unlike the rest of the condenser, however, the refrigerant is sensibly cooled (subcooled in the

liquid phase), so the crossflow configuration must be taken into account. Some mixing of the refrigerant liquid will occur, as this liquid has to leave the condenser through one or more bottom outlets which are relatively small compared to the condenser length. It is prudent, therefore, to regard this flooded portion as a single-pass crossflow heat exchanger with the water unmixed, but the refrigerant mixed. The heat $Q_{"SC1"}$ transferred through this flooded portion is thus given by

$$Q_{"SC1"} = UA_{"SC1"} \cdot F' \cdot LMTD_{"SC1"} \qquad \text{(A19-6a)}$$

where $LMTD_{"SC1"}$ is calculated on the basis of counterflow:

$$LMTD_{"SC1"} = \frac{\left(t_{(r)"SC1"i} - t_{(w)"SC1"o}\right) - \left(t_{(r)"SC1"o} - t_{(w)"SC1"i}\right)}{\ln\left(\frac{t_{(r)"SC1"i} - t_{(w)"SC1"o}}{t_{(r)"SC1"o} - t_{(w)"SC1"i}}\right)} \qquad \text{(A19-6b)}$$

and F' is the well-known correction factor for the crossflow configuration, depending on the parameters Y and Z, these (see, for example, Welty, Wicks and Wilson, 1976 : 413-415) being here

$$Y = \frac{t_{(w)"SC1"o} - t_{(w)"SC1"i}}{t_{(r)"SC1"i} - t_{(w)"SC1"i}} \qquad Z = \frac{t_{(r)"SC1"i} - t_{(r)"SC1"o}}{t_{(w)"SC1"o} - t_{(w)"SC1"i}} \qquad \text{(A19-6c)}$$

$UA_{"SC1"}$ is given by

$$\frac{1}{UA_{"SC1"}} = \frac{1}{h'_{(w)"SC1"}A_{T(w)"SC1"}} + \frac{1}{h'_{f(w)"SC1"}A_{T(w)"SC1"}} + \frac{y_{TC}}{k_{TC}\overline{A}_{T,"SC1"}} + \frac{1}{h'_{(r)"SC1"}A_{T(r)"SC1"}} \qquad \text{(A19-6d)}$$

with $h'_{(w)"SC1"}$ and $\overline{A}_{T,"SC1"}$ given by exactly analogous versions of (A15-7a) and (A15-7b), and (A15-8) respectively. The coefficient $h'_{(r)"SC1"}$ of heat transfer by natural convection from refrigerant liquid to tubes is assumed

to be given by the general relationship presented in ASHRAE (1993 : 3.11,3.12):

$$h'_{(r)sc1} = C \cdot \frac{k_{(r)}}{L}(\mathrm{Gr} \cdot \mathrm{Pr})^n \qquad \text{(A19-6e)}$$

where Gr and Pr are the Grashof and Prandtl numbers for the liquid refrigerant, evaluated as described below; C and n are, respectively, 0,56 and 0,25 if $10^4 \leq (\mathrm{Gr} \cdot \mathrm{Pr}) \leq 10^8$, and 0,13 and 0,33 if $10^8 \leq (\mathrm{Gr} \cdot \mathrm{Pr}) \leq 10^{12}$; $k_{(r)}$ is the thermal conductivity of the liquid refrigerant, evaluated as described below; and L is the characteristic length of the heating or cooling surface. For a horizontal tube, $L = D_{To}$, the outside diameter of the tube.

The Grashof and Prandtl numbers for the liquid refrigerant are given by

$$\mathrm{Gr} = \left(\frac{L^3 \rho^2 \beta g(\Delta t)}{\mu^2}\right)_{(r)} \qquad \mathrm{Pr} = \left(\frac{\mu c_p}{k}\right)_{(r)} \qquad \text{(A19-6f)}$$

where the symbols not defined previously are β, the coefficient of thermal expansion of the liquid refrigerant, and Δt, the temperature difference between the outside surfaces of the tubes and the refrigerant. Here, Δt is assumed to be

$$\Delta t = \bar{t}_{(r)sc1} - \bar{t}_{To,sc1} \qquad \text{(A19-6g)}$$

where $\bar{t}_{(r)sc1}$ is the average or bulk temperature of the refrigerant, given by

$$\bar{t}_{(r)sc1} = \left(t_{(r)sc1i} + t_{(r)sc1o}\right)/2 \qquad \text{(A19-6h)}$$

and $\bar{t}_{To,"SC1"}$, the average temperature of the outside surfaces of the tubes, is that which yields a log-mean temperature difference $LMTD_{(To\rightarrow w),"SC1"}$ between the outside surfaces of the tubes and the water:

$$LMTD_{(To\rightarrow w),"SC1"} = \frac{\left(\bar{t}_{To,"SC1"} - t_{(w)"SC1"o}\right) - \left(\bar{t}_{To,"SC1"} - t_{(w)"SC1"i}\right)}{\ln\left(\frac{\bar{t}_{To,"SC1"} - t_{(w)"SC1"o}}{\bar{t}_{To,"SC1"} - t_{(w)"SC1"i}}\right)} \qquad \text{(A19-6i)}$$

This LMTD accomplishes the transfer of the heat load $Q_{"SC1"}$ in (A19-6a) between these outside surfaces and the water:

$$Q_{"SC1"} = UA_{(To\rightarrow w),"SC1"} \cdot LMTD_{(To\rightarrow w),"SC1"} \qquad \text{(A19-6j)}$$

where $1/UA_{(To\rightarrow w),"SC1"}$ is given by the first three terms in (A19-6d):

$$\frac{1}{UA_{(To\rightarrow w),"SC1"}} = \frac{1}{h'_{[w]"SC1"}A_{T[w]"SC1"}} + \frac{1}{h'_{i[w]"SC1"}A_{T[w]"SC1"}} + \frac{y_{Tc}}{k_{Tc}\bar{A}_{T,"SC1"}} \qquad \text{(A19-6k)}$$

It is customary (see, for example, Welty, Wicks and Wilson, 1976 : 335) to evaluate the Grashof and Prandtl numbers in (A19-6f) at the *film temperature* $t_{(r)f,"SC1"}$, defined as the arithmetic mean of the surface and bulk fluid temperatures. Here, therefore,

$$t_{(r)f,"SC1"} = \left(\bar{t}_{To,"SC1"} + \bar{t}_{(w)"SC1"}\right)/2 \qquad \text{(A19-6l)}$$

A19.5 Modelling of Complete Machine

A19.5.1 User-Supplied Specifications

These are listed with their corresponding symbols in Table A19.1 below.

Table A19.1 Case Study A: Specifications of Machine

Machine Component	Specification	Value	Symbol
Evaporator	Amount of passes	4	$N_{pa.E}$
	Amount of tubes	1 632	N_{TE}
	Internal tube diameter, mm	15,95	d_{TE}
	Tube wall thickness, m	1,24	y_{TE}
	Total inside wall area of tubes, m²	654,2	$A_{T[w]E}$
	Outside surface of tubes	Union Carbide "hi-flux"	
	Total outside wall area of tubes, m²	777	$A_{T[r]E}$
	Thermal conductivity of tube material, W/m.K	44	k_{TE}
Condenser	Amount of passes	2	$N_{pa.C}$
	Amount of tubes	2 340	N_{TC}
	Internal tube diameter, mm	13,8	d_{TC}
	Tube wall thickness, m	1,24	y_{TC}
	Total inside wall area of tubes, m²	811,6	$A_{T[w]C}$
	Outside surface of tubes	19 fins per 25 mm	
	Total outside wall area of tubes, m²	2 952	$A_{T[r]C}$
	Thermal conductivity of tube material, W/m.K	44	k_{TC}
Subcooler	Amount of passes	1	$N_{pa.SC}$
	Amount of tubes	237	$N_{T.SC}$
	Internal tube diameter, mm	16,52	$d_{T.SC}$
	Tube wall thickness, m	1,24	$y_{T.SC}$
	Total inside wall area of tubes, m²	61,5	$A_{T[w]SC}$
	Outside surface of tubes	Plain	
	Total outside wall area of tubes, m²	70,7	$A_{T[r]C}$
	Thermal conductivity of tube material, W/m.K	44	$k_{T.SC}$
Compressor	Max. guide vane setting (fully open), degrees	90	
	Min. guide vane setting (fully closed), degrees	4	
	Design refrigerant	R12	
	Design suction volumetric flow-rate, m³/s	4,31	$\dot{V}_{Pl.des}$
	Design pressure ratio	2,658	$R_{press.P.des}$
	Design isentropic efficiency, %	89,2	$\eta\|_{s.P.des}$

A19.5.2 Inputs and Internal Process Parameters

These are listed with their corresponding symbols in Table A19.2 below.

Table A19.2 Case Study A: Inputs and Internal Process Parameters of Machine

Machine Component	Quantity	Symbol
Evaporator	Water flow-rate, kg/s	$m_{(w)E}$
	Inlet water temperature, °C	$t_{(w)Ei}$
	Water-side fouling factor, m²°C/W	$1/h'_{f(w)E}$
Compressor	Inlet guide vane opening, degrees	Ψ_P
Condenser	Water flow-rate, kg/s	$m_{(w)C}$
	Water-side fouling factor, m²°C/W	$1/h'_{f(w)C}$
	Amount of flooded tubes	$N_{T:sc}$
Subcooler	Inlet water temperature, °C	$t_{(w)SCi}$
	Water-side fouling factor, m²°C/W	$1/h'_{f(w)SC}$

A19.5.3 Model of Evaporator

The refrigerant mass flow-rate and properties at the inlet are given by the constraints

$$m_{(r)E} = m_{(r)EX} \qquad h_{Ei} = h_{EXo} \tag{A19-7a}$$

The evaporator model described in Section A15.2, Appendix 15 is used. The assumptions, constraints and energy and heat-transfer relationships are accordingly as follows.

⇒ Assumptions: as in (A15-2) and so in addition

$$v_{Eo} = v_{(g)}\left(T_{(r)E}\right) \tag{A19-7b}$$

⇒ Constraints: as in (A15-3);

⇒ Energy and heat-transfer relationships: as in (A15-4) through (A15-8), and (A15-10). The constant C in (A15-10), though, is 2 436 in order for the evaporator to yield its specified performance at design conditions.

A19.5.4 Compressor Suction Piping

Denoting this piping by the subscript $E \rightarrow P$ (evaporator to compressor), from (A19-4b)

$$\Delta P_{(r)E\rightarrow P} = C \cdot m_{(r)}^2 v_{Eo} \qquad \text{(A19-8a)}$$

where $C = 0{,}04236\ m^{-2}$ to give the specified pressure drop at design conditions. The conditions at the outlet of this piping - that is, the compressor inlet, denoted by the subscript Pi - are then

$$h_{Pi} = h_{Eo} \qquad P_{Pi} = P_{Eo} - \Delta P_{E\rightarrow P} \qquad \text{(A19-8b)}$$

Temperature and specific volume T_{Pi} and v_{Pi} at the compressor inlet are next obtained by simultaneously solving (A15-1c) and (A15-1d), with P and h being P_{Pi} and h_{Pi}.

A19.5.5 Model of Single-Stage Centrifugal Compressor

Entropy and volumetric flow-rate at the inlet are:

$$s_{Pi} = s(T_{Pi}, v_{Pi}) \qquad \dot{V}_{Pi} = m_{(r)P} v_{Pi} \qquad \text{(A19-9a)}$$

Pressure ratio $R_{press,P}$ and isentropic efficiency $\eta|_{s,P}$ are given by (A19-1a) and (A19-1b). Outlet pressure is then

$$P_{Po} = P_{Pi} R_{press,P} \qquad \text{(A19-9b)}$$

Ideal, isentropic discharge temperature $T|_{s,Po}$ and specific volume $v|_{s,Po}$ are obtained by solving (A15-1c) and (A15-1e) simultaneously, with P given by (A19-9b) and $s = s_{Pi}$. Ideal, isentropic discharge enthalpy $h|_{s,Po}$ (by (A15-1d)) and enthalpy rise $\Delta h|_{s,Po}$ are then

$$h|_{s,Po} = h\left(T|_{s,Po}, v|_{s,Po}\right) \qquad \Delta h|_{s,P} = h|_{s,Po} - h_{Pi} \qquad \text{(A19-9c)}$$

Actual head Δh_P, outlet enthalpy h_{Po} and power input W_P are then given by

$$h_{Po} - h_{Pi} = \Delta h_P = \frac{\Delta h|_{s,P}}{\eta|_{s,P}} \qquad h_{Po} = h_{Pi} + \Delta h_P \qquad W_P = m_{(r)P}\Delta h_P \qquad \text{(A19-9d)}$$

The real discharge temperature T_{Po} and specific volume v_{Po} are then obtained by solving (A15-1c) and (A15-1d) simultaneously, with P and h being P_{Po} and h_{Po}.

A19.5.6 Compressor Discharge Piping

Denoting this piping by the subscript $P \rightarrow C$ (compressor to condenser), pressure drop $\Delta P_{P\rightarrow C}$ and refrigerant properties at the condenser inlet are computed identically to (A19-8a) and (A19-8b), except that in (A19-8a), the constant C = 0,36421 to give the specified pressure drop at design conditions.

A19.5.7 Model of Partially Flooded Condenser

The refrigerant mass flow-rate and properties at the inlet are given by the constraints

$$m_{(r)C} = m_{(r)P} \qquad h_{Ci} = h_{Po} \qquad P_{Ci} = P_{Po} - \Delta P_{P\rightarrow C} \qquad \text{(A19-10a)}$$

The condenser is modelled as in Section A19.4 above. For "Condenser 1" and "Condenser 2", the constant C in (A15-16b) is 3,21644 to give the specified condenser performance at design (unflooded) conditions.

A19.5.8 Model of Subcooler

This is modelled as in Section A19.2 above. The maximum inter-tube velocity $\upsilon_{T,SC,max}$ of the refrigerant in (A19-3d) is 5,355 m/s to give the specified subcooler performance at design conditions.

A19.5.9 Model of Expansion Valve

The refrigerant mass flow-rate and properties at the inlet are given by the constraints

$$m_{(r)EX} = m_{(r)SC} \qquad h_{EXi} = h_{SCo} \tag{A19-11a}$$

and outlet refrigerant properties are given by

$$h_{EXo} = h_{SCo} \qquad P_{EXo} = P_{EI} \tag{A19-11b}$$

A19.5.10 Overall Mass and Energy Balances

These are the constraints

$$m_{(r)E} = m_{(r)P} = m_{(r)C} = m_{(r)SC} = m_{(r)EX} = m_{(r)} \tag{A19-12a}$$

$$Q_E + W_P + Q_C = 0 \tag{A19-12b}$$

A19.5.11 Simulation Algorithm

As stated in Chapter 5, a spreadsheet program with numerical equation-solving capability, Microsoft Excel 4.0, was used to solve the model of this machine.

A19.5.12 Accuracy of Modelling

The question naturally arose of how accurate this modelling of the complete machine was. Fortunately, the manufacturer had furnished quoted performance at two sets of operating conditions: full-duty design or

"summer" conditions, where water had to be chilled from 15°C to 4,5°C and the inlet water temperature of the condenser block was 22°C; and "maximum" conditions, where water had to be chilled from 13,5°C to 4,5°C and the inlet water temperature of the condenser block was 27°C.

Table A19.3 Case Study A: Quoted and Predicted Performance of Machine

QUANTITY	UNIT	"SUMMER"		"MAXIMUM"	
		Quoted	Predicted	Quoted	Predicted
EVAPORATOR					
Water flow-rate	l/s	168	168	168	168
Inlet water temperature	°C	15,0	15,0	15,0/13,5	15,0/13,5
Outlet water temperature	°C	4,5	4,5	6,0/4,5	6,0/4,5
W. er chilling load	kW(R)	7 386	7 386	8 350	6 330
Fouling factor	m²°C/W	0,0003	0,00025	0,0003	0,00025
Refrigerant pressure	kPaa	339	336,3	337	355,3/338,5
Refrigerant temperature	°C	2,7	2,66	2,9	4,36/2,86
COMPRESSOR					
Vane opening	degr.	-	40,5	-	37,7/45,1
Isentropic efficiency	%	82,9	82,4	82,5	76,5/78,0
Input power	kW	1 043	1 052	1 043	1 031/1 075
Suction temperature	°C	3,0	2,4	3,2	4,2/2,7
Discharge temperature	°C	41	41,1	45	46,4/46,6
CONDENSER					
Water flow-rate	l/s	377	377	377	377
Inlet water temperature	°C	22,2	22,23	27,2	27,18/27,18
Outlet water temperature	°C	27,3	27,35	31,7	31,67/31,69
Water heating load	kW(R)	8 087	8 080	7 137	7 074/7 116
Fouling factor	m²°C/W	0,0003	0,0003	0,0003	0,0003
Refrigerant pressure	kPaa	759	753,3	834	832,4/833,4
Outlet refrigerant temperature	°C	30,4	30,44	34,3	34,3
SUBCOOLER					
Water flow-rate	l/s	125	125	125	125
Inlet water temperature	°C	22,0	22,0	27,0	27,0
Outlet water temperature	°C	22,6	22,68	27,2	27,55/27,55
Water heating load	kW(R)	303	357,6	253	286,8/289,7
Fouling factor	m²°C/W	0,0003	0,0003	0,0003	0,0003
Inlet refrigerant temperature	°C	30,4	30,44	34,3	34,3
Outlet refrigerant temperature	°C	24,9	23,91	29,3	28,4
Measures of perfor.nance					
Coeffici .nt of performance (COP)		7,08	7,02	6,09	6,14/5,89

For both "summer" and "maximum" conditions, quoted performance and that predicted by the model are listed in Table A19.3. Excellent

correspondence was achieved for "summer" (i.e. full-duty design) conditions. For "maximum" conditions, predicted compressor isentropic efficiency was slightly lower than quoted, so predicted input power and COP were 3 per cent higher and lower respectively.

The conditions of Case Study A corresponded closely to "summer" conditions. Therefore, the machine model could be considered at least reasonably accurate for the purpose of predicting actual performance with a flooded condenser, and sufficiently accurate for the purpose of predicting corresponding normal and optimal performance.

APPENDIX 20

SIMPLIFIED MODELLING OF CONVENTIONAL MACHINES BY OVERALL ENERGY BALANCE

From (3-7d), the overall energy balance for the generalised water chilling machine, neglecting heat exchange between the external surfaces of the machine and its surroundings,

$$\sum Q_{(w)EB} + \sum W_{VCB} + \sum Q_{(w)VCB(Ms)} + \sum Q_{(w)CB} \cong 0$$

For a conventional water chilling machine, this simplifies to (as in (3-12))

$$Q_{(w)E} + W_P + W_{OP} + Q_{(w)OC(Ms)} + Q_{(w)C} \cong 0 \qquad \text{(A20-1)}$$

where W_P and W_{OP} are the mechanical power inputs to the compressor and its oil pump respectively, and $Q_{(w)OC(Ms)}$ is the heat transferred *outside* the machine boundary by any oil-to water compressor oil coolers.

From (A15-4) and (A15-13), it follows without difficulty that

$$m_{(w)C} \cong \frac{-m_{(w)E}c_{(w)}\left(t_{(w)Eo} - t_{(w)Ei}\right) + W_P + W_{OP} + Q_{(w)OC(Ms)}}{c_{(w)}\left(t_{(w)Co} - t_{(w)Ci}\right)} \qquad \text{(A20-2a)}$$

Equally well, $m_{(w)E}$ is a function of $m_{(w)C}$ if (A20-2a) is transposed:

$$m_{(w)E} \cong \frac{m_{(w)C}c_{(w)}\left(t_{(w)Co} - t_{(w)Ci}\right) - W_P - W_{OP} - Q_{(w)OC(Ms)}}{-c_{(w)}\left(t_{(w)Eo} - t_{(w)Ei}\right)} \qquad \text{(A20-2b)}$$

Therefore, if all other quantities in (A20-2a) and (A20-2b) are known, either mass flow-rate of water is a function of the other.

For Case Study E, one or both apparent water flow-rates were unacceptably erroneous, but all water temperatures had been accurately

measured. Therefore, assuming that the apparent input power of 871 kW was acceptably accurate, (A20-2a) and (A20-2b) were used[1] to determine the *implied* -

- evaporator water flow-rate corresponding to the apparent condenser water flow-rate of 85,5 l/s;
- condenser water flow-rates corresponding to the apparent and design evaporator water flow-rates of 51,6 and 60,6 l/s respectively.

These implied, corresponding flow-rates are tabulated with other relevant corresponding quantities in the shaded portions of Table A20.1. The corresponding water-side fouling factors therein were calculated from (A21-2) or (A21-4) in Appendix 21.

Table A20.1 Case Study E: Implied Quantities Corresponding to Apparent and Design Water Flow-Rates

Evaporator			Condenser			
Water flow-rate, l/s	Chilling load, kW(R)	Fouling factor, m²°C/W	Water flow-rate, l/s	Heating load, kW(R)	Fouling factor, m²°C/W	COP
35,0	1 404	0,00061	85,5 *(apparent value)*	2 275	0,00171	1,61
51,6 *(apparent value)*	2 070	0,00037	110,4	2 941	0,00128	2,37
60,6 *(design value)*	2 407	0,00030	123,1	3 277	0,00113	2,79

[1] For the machine in this case study, the compressor oil cooler was an oil-to-water heat exchanger, obtaining its water from the chilled water circuit of the installation, outside the machine boundary, and thus appearing as $Q_{(w)OC(Ms)}$ in (A20-2a) and (A20-2b). This term was neglected, though, in order to be consistent with the use of the CHILLER program to predict the performance of this machine (the available version of this program neglected the effect of compressor oil coolers). As the rating of the oil cooler was 12 kW(R), its effect could be ignored for the purpose of estimating condenser water flow-rate corresponding to evaporator water flow-rate, or vice versa. The power input of the compressor oil pump, rated at 1,5 kW, was also ignored.

APPENDIX 21

ESTIMATION OF WATER-SIDE FOULING FACTORS IN HEAT EXCHANGERS OF CONVENTIONAL MACHINES

As water-side fouling factors are not directly measurable, they have to be estimated by modelling. It can be shown that the water-side fouling factor in the evaporator or condenser of a conventional machine, where these heat exchangers are modelled as in Appendix 15, is a function of the water flow-rate and the water and refrigerant temperatures as follows.

For an evaporator, from (A15-3), (A15-4) and (A15-6a),

$$UA_E = \frac{-m_{(w)E}c_{(w)}\left(t_{(w)Eo} - t_{(w)Ei}\right)}{LMTD_E} \qquad \text{(A21-1a)}$$

From (A15-6c),

$$\frac{1}{UA_E} = \frac{1}{h'_{[w]E}A_{T[w]E}} + \frac{1}{h'_{r[w]E}A_{T[w]E}} + \frac{y_{TE}}{k_{TE}\overline{A}_{TE}} + \frac{1}{h'_{[r]E}A_{T[r]E}} \qquad \text{(A21-1b)}$$

Equating the reciprocal of (A21-1a) with (A21-1b) and solving for the water-side fouling factor $1/h'_{r[w]E}$,

$$\frac{1}{h'_{r[w]E}} = A_{T[w]E}\left(\frac{LMTD_E}{-m_{(w)E}c_{(w)}\left(t_{(w)Eo} - t_{(w)Ei}\right)} - \frac{1}{h'_{[w]E}A_{T[w]E}} - \frac{y_{TE}}{k_{TE}\overline{A}_{TE}} - \frac{1}{h'_{[r]E}A_{T[r]E}}\right) \qquad \text{(A21-2)}$$

From (A15-7a) and (A15-7b), $h'_{[w]E}$ is a function of $m_{(w)E}$, $t_{(w)Ei}$, $t_{(w)Eo}$ and evaporator specifications. From (A15-3), (A15-4) and (A15-10)

$$h'_{[r]E} = C\cdot\left(-Q_{(w)E}/A_{T[w]}\right)^{0,7} = C\cdot\left(-m_{(w)E}c_{(w)}\left(t_{(w)Eo} - t_{(w)Ei}\right)/A_{T[w]}\right)^{0,7} \qquad \text{(A21-3)}$$

and so $h'_{(r)E}$ is also a function of $m_{(w)E}$, $t_{(w)Ei}$, $t_{(w)Eo}$ and evaporator specifications. Hence the water-side fouling factor $1/h'_{f(w)E}$ in (A21-2) is a function of these and of evaporating refrigerant temperature $t_{(r)E}$ (this appears in $LMTD_E$, as seen from (A15-6b)).

A similar relationship holds for the water-side fouling factor in the condenser:

$$\frac{1}{h'_{f(w)C}} = A_{T(w)C}\left(\frac{LMTD_C}{-m_{(w)C}c_{(w)}\left(t_{(w)Co}-t_{(w)Ci}\right)} - \frac{1}{h'_{(w)C}A_{T(w)C}} - \frac{y_{TC}}{k_{TC}\bar{A}_{TC}} - \frac{1}{h'_{(r)C}A_{T(r)C}}\right) \qquad \text{(A21-4)}$$

and $1/h'_{f(w)C}$ is likewise a function of $m_{(w)C}$, $t_{(w)Ci}$, $t_{(w)Co}$, $t_{(r)C}$ and condenser specifications because $h'_{(w)C}$ is also given by (A15-7a) and (A15-7b), and $h'_{(r)C}$ by (A15-17).

The accuracy of the fouling factor estimated by (A21-2) or (A21-4) is at least moderately sensitive to the accuracy of the measured water flow-rate through the evaporator or condenser in question. The reasons are as follows. First, as seen from (A21-1a), the estimated thermal conductance (UA) of the heat exchanger depends directly on this water flow-rate. Second, the heat transfer coefficient $h'_{(w)}$ of the water boundary layer - appearing in (A21-2) and (A21-4) - depends on the water velocity in the tubes, and hence on the water flow-rate, as seen from (A15-7a) and (A15-7b) in Appendix 15.

(A21-2) and (A21-4) mean that if refrigerant temperatures and inlet and outlet water temperatures of the evaporator and condenser are known, their water-side fouling factors are functions of their water flow-rates.

REFERENCES

ALEFELD, G. (1987) Efficiency of Compressor Heat Pumps and Refrigerators Derived from the Second Law of Thermodynamics, *International Journal of Refrigeration,* Vol. 10, November 1987, pp. 331-341.

ANDERSON, S.A. and DIECKERT, J.C. (1990) On-Site Chiller Testing, *ASHRAE Journal,* Vol. 32, No. 4, April 1990, pp. 54-59.

ARI (1992) *Standard for Centrifugal and Rotary Water-Chilling Packages,* Air-Conditioning and Refrigeration Institute, Arlington, Virginia, USA, 1992 (Standard 550-92).

ASHRAE (1978) *Methods of Testing Liquid Chilling Packages,* American Society of Heating, Refrigerating and Air-Conditioning Engineers, New York, USA, 1978 (Standard 30-78).

ASHRAE (1990) Handbook: (Refrigeration), Chapter 8: Lubricants in Refrigerant Systems, *American Society of Heating, Refrigerating and Air-Conditioning Engineers* (ASHRAE), Inc., Atlanta, Georgia, USA, 1990.

ASHRAE (1992) Handbook (HVAC Systems and Equipment), *American Society of Heating, Refrigerating and Air-Conditioning Engineers* (ASHRAE), Inc., Atlanta, Georgia, USA, 1992.

ASHRAE (1993) Handbook (Fundamentals), *American Society of Heating, Refrigerating and Air-Conditioning Engineers* (ASHRAE), Inc., Atlanta, Georgia, USA, 1993.

ASHRAE (1995) *Method of Testing Liquid-Chilling Packages,* American Society of Heating, Refrigerating and Air-Conditioning Engineers, Inc., Atlanta, Georgia, USA, 1995 (ANSI/ASHRAE Standard 30-1995).

AUSTIN, S.A. (1991) Optimum Chiller Loading, *ASHRAE Journal,* Vol. 33, No. 7, July 1991, pp. 40-43.

BAILEY-McEWAN, M. and PENMAN, J.C. (1987) An Interactive Computer Program for Simulating the Performance of Water Chilling Installations on Mines, in: *APCOM 87: Proceedings of the 20th International Symposium on the Application of Computers and Mathematics in the Mineral Industries,* Vol. 1: Mining, Johannesburg, South African Institute of Mining and Metallurgy, 1987, pp. 291-305.

BAILEY-McEWAN, M. (1990) Advantages and Limitations of the Thorp Method of Cross-Checking Water Chiller Performance, in: *Proceedings of ASHRAE-FRIGAIR 90 Conference,* Pretoria, South Africa, 23-25 April 1990; Vol. 2, Mine Cooling Papers, S A. Institute of Refrigeration & Air-Conditioning (SAIRAC), Pretoria, South Africa; Paper M.14, 16p.

BAILEY-McEWAN, M. (1991) Use of the CHILLER Computer Program with Conventional Water Chilling Installations on South African Gold Mines, *Journal of the Mine Ventilation Society of South Africa,* Vol. 44, No. 1, January 1991, pp. 2-12.

BAILEY-McEWAN, M. and ROMAN, W.N. (1992) Assessment of Performance of Conventional Water Chilling Machines using Thorp Method and Machine Modelling, *Journal of the Mine Ventilation Society of South Africa,* Vol. 45, No. 5, May 1992, pp. 74-91.

BAILEY-McEWAN, M. (1995a) An Enhanced Version of the Thorp Method of Verifying Surveys of Performance of Conventional Water Chilling Machines, *Journal of the Mine Ventilation Society of South Africa,* Vol. 48, No. 1, January 1995, pp. 2-21.

BAILEY-McEWAN, M. (1995b) Extension of the Enhanced Thorp Method beyond Conventional Machines Operating Normally, *Journal of the Mine Ventilation Society of South Africa*, Vol. 48, No. 2, February 1995. pp. 30-46.

BAKER-DULY, H.C., RAMSDEN, R. and MACKAY, J.G. (1993) Water Systems Management and the Implications on Energy Use and Cost, *The South African Mechanical Engineer*, Vol. 43, No. 2, February 1993, pp. 49-51.

BEYENE, A., GUVEN, H., JAWDAT, Z. and LOWREY, P. (1994) Conventional Chiller Performances: Simulation and Field Data, *International Journal of Energy Research*, Vol. 18, 1994, pp. 391-399.

BLUHM, S.J. and LANCASTER, G.J. (1987) Optimum Use of Daily Changes in Wet-Bulb Temperature in the Operation of Surface Pre-Cooling Towers, *Journal of the Mine Ventilation Society of South Africa*, Vol. 40, No. 5, May 1987, pp. 64-70.

BRAIN, T.J.S. and SCOTT, R.W.W. (1982) Survey of Pipeline Flowmeters, *Journal of Physics, E: Instrument Science and Technology*, Vol. 15, 1982, pp. 967-980.

BRAUN, J.E., MITCHELL, J.W., KLEIN, S.A. and BECKMAN, W.A. (1987) Models for Variable-Speed Centrifugal Chillers, *ASHRAE Transactions*, Vol. 93, Part 1, 1987, pp. 1794-1813.

BSI (1973) *Current Transformers*, London: British Standards Institution, 1973 (BS 3938).

BSI (1979) *Specification for Class 0,5, 1 and 2 Single-Phase and Polyphase, Single-Rate and Multi-Rate Watt-Hour Meters*, London: British Standards Institution, 1979 (BS 5685, Part 1).

BSI (1989) *Specification for Rating and Performance of Air to Liquid and Liquid to Liquid Chilling Packages,* London: British Standards Institution, 1989 (BS 7120).

BSI (1994) *Instrument Transformers - Three-Phase Voltage Transformers Voltage Levels Having U_m up to 52 kV,* London: British Standards Institution, 1994 (BS 7729).

BURROWS, J.H.J. (1982) Refrigeration - Theory and Operation, in: *Environmental Engineering in South African Mines,* The Mine Ventilation Society of South Africa, Johannesburg, South Africa, 1982, pp. 613-652.

BURTON, R.C., KIELBLOCK, A.J., SHEER, T.J. and BLUHM, S.J. (1986) The Future Implications of Controlling the Thermal Environment in Deep Gold Mines, *GOLD 100: Proceedings, International Conference on Gold,* Vol. 1: Gold Mining Technology, Johannesburg, South African Institute of Mining and Metallurgy, 1986, pp.

CAHILL, J.A. (1974) Selecting Centrifugal Compressors for Maximum Energy Efficiency, *Specifying Engineer,* August/September 1974, pp. 13-16.

CARRIER CORPORATION (USA) (1981) Helical Screw Compressor Systems Components, *Form PREP-7, 1/81, Catalogue No. 817-095,* Syracuse, New York, USA, 1981.

CASEY, M.V. and MARTY, F. (1986) Centrifugal Compressors - Performance at Design and Off-Design, *Proceedings of the Institute of Refrigeration,* Vol. 82, 1985-1986, pp. 71-80.

CHAMBER OF MINES OF SOUTH AFRICA (1991a) *Statistical Tables, 1990;* Johannesburg, South Africa, 1991.

CHAMBER OF MINES OF SOUTH AFRICA (1991b) Internal documentation.

CHAMBER OF MINES OF SOUTH AFRICA (1997) *Statistical Tables, 1996;* Johannesburg, South Africa, 1997.

CHI, J. (1979) DEPAC - A Computer Model for Design and Performance Analysis of Centrifugal Chillers, *Winter Annual Meeting, Heat Transfer Division of American Society of Mechanical Engineers (ASME)*, December 1979, 9p.

CLELAND, A.C. and CLELAND, D.J. (1989) Development of Generalised Software for Simulation of Refrigeration System Performance, *Proceedings, The Impact of Technology on the Refrigeration/Heat Pump Industries*, 4-7 July 1989, Bristol, U K; International Institute of Refrigeration (IIR), Paris, France, 1989, pp. 73-78.

CSIR (Council for Scientific and Industrial Research), South Africa (1994) Internal documentation.

DEL CASTILLO, D.O. (1987) An Examination of the Air-Cycle for Cooling Deep Mines, *The South African Mechanical Engineer*, Vol. 37, No. 6, June 1987, pp. 252-259.

E.I. DU PONT DE NEMOURS & CO. (1969) Freon Products Technical Bulletin X-88F, 1969.

FANNIN, T. and HUNDY, G.F. (1987) Methods of Measurement and Instrumentation for Refrigeration Sy[illegible]s, *Proceedings, Joint Seminar on Performance Testing and Evaluation of Refrigeration Plant*, Institute of Refrigeration and Institution of Mechanical Engineers (UK), 13 May 1987 (Institute of Refrigeration, UK, 1987).

FATHI, Z., RAMIREZ, W.F. and KORBICZ, J. (1993) Analytical and Knowledge-Based Redundancy for Fault Diagnosis in Process Plants, *AIChE Journal*, Vol. 39, No. 1, January 1993, pp. 42-56.

GLUCKMAN, R. (1986) Inefficient Operation of Refrigeration Plant, *Proceedings, Joint Seminar on Cutting Refrigeration Energy Costs,* Institute of Refrigeration and Institution of Mechanical Engineers (UK), 19 November 1986 (Institute of Refrigeration (UK), 1986).

GLUCKMAN, R. and HART, D. (1992) The Development of Refrigeration Expert Systems, *Proceedings of the Institute of Refrigeration,* Vol. 88, 1991-1992, pp. 11-18.

GLUCKMAN, R. (1993) Optimisation of Refrigeration Plants for Off-Design Operating Conditions, *Proceedings of the Institute of Refrigeration,* Vol. 89, 1992-1993, pp. 81-90.

GORDON, J.M. and NG, K.C. (1994) Thermodynamic Modelling of Reciprocating Chillers, *Journal of Applied Physics,* Vol. 75, No. 6, 15 March 1994, pp. 2769-2774.

GORDON, J.M. and NG, K.C. (1995) Predictive and Diagnostic Aspects of a Universal Thermodynamic Model for Chillers, *International Journal of Heat and Mass Transfer,* Vol. 38, No. 5, 1995, pp. 807-818.

GORDON, J.M., NG, K.C. and CHUA, H.T. (1995) Centrifugal Chillers: Thermodynamic Modelling and a Diagnostic Case Study, *International Journal of Refrigeration,* Vol. 18, No. 4, July 1995, pp. 253-257.

GOSNEY, W.B. (1982) Principles of Refrigeration, Cambridge University Press, New York, USA, 1982.

GRIMMELIUS, H.T., KLEIN WOUD, J. and BEEN, G. (1995) On-Line Failure Diagnosis for Compression Refrigeration Plants, *International Journal of Refrigeration,* Vol. 18, No. 1, January 1995, pp. 31-41.

GROLLIUS, H., MEYER, C., RAUTENBERG, M. and BAILEY-McEWAN, M. (1987) Computer Modelling of the Performance of Centrifugal Water Chillers in Mine Refrigeration Installations, *International Journal of Refrigeration,* Vol. 10, No. 1, January 1987, pp. 49-52.

GUNDERSEN, R.E. (1991). New Technologies an Mining Methods to Benefit Hot Mines, *The South African Mechanical Engineer,* Vol. 41, No. 1, January 1991, pp. 23-26.

HALL, A.E. and UNSTED, A.D. (1976) Computer Modelling of Underground Refrigeration Equipment, in: *Proceedings of the Second IFAC Symposium on Automation in Mining, Mineral and Metal Processing,* Johannesburg, South Africa, 1976; South African Council for Automation and Computation, Pretoria, South Africa, 1977, pp 75-80.

HEMP, R. (1981) The Assessment and Prediction of Cooling Plant Performance, *Journal of the Mine Ventilation Society of South Africa,* Vol. 34, No. 5, May 1981, pp. 81-98, and Vol. 34, No. 6, June 1981, pp. 101-118.

HEMP, R. (1982) Sources of Heat in Mines, in: *Environmental Engineering in South African Mines,* The Mine Ventilation Society of South Africa, Johannesburg, South Africa, 1982, pp. 569-612.

HEMP, R., CILLIERS, P.F., STARFIELD, A.M. and FALLON, P. (1986) Computer Analysis of Underground Refrigeration Plant Performance, *Journal of the Mine Ventilation Society of South Africa,* Vol. 39, No. 6, June 1986, pp. 77-85.

HOWES, M.J. (1976) A Review of Current Mine Cooling Practice in South African Gold Mines, in: *Proceedings, First International Mine Ventilation Congress,* Johannesburg, South Africa, 15-19 September 1975; The Mine Ventilation Society of South Africa, Johannesburg, 1976, pp. 289-298.

HOWES, M.J. (1990) The Design and Control of Mine Refrigeration Systems in Australia Using Modelling Techniques, in: *Proceedings of ASHRAE-FRIGAIR 90 Conference,* Pretoria, South Africa, 23-25 April 1990; Vol. 2, Mine Cooling Papers, S A. Institute of Refrigeration & Air-Conditioning (SAIRAC), Pretoria, South Africa; Paper M.11, 12p.

HOWES, M.J. (1992) Control Strategies for Refrigeration Systems in Australian Mines, in: *Proceedings, Fifth International Mine Ventilation Congress,* Johannesburg, South Africa, 25-30 October 1992; Hemp, R., ed., The Mine Ventilation Society of South Africa, Johannesburg, 1992, pp. 251-258.

HUGHES, D.W., McMULLAN, J.T., MAWHINNEY, K.A. and MORGAN, R. (1982) Pressure-Enthalpy Charts for Mixtures of Oil and Refrigerant 12, *International Journal of Refrigeration,* Vol. 5, No. 4, July 1982.

HUNTINGTON, R.A. (1985) Evaluation of Polytropic Calculation Methods for Turbomachinery Performance, *ASME Journal of Engineering for Gas Turbines and Power,* Vol. 107, October 1985, pp. 872-876.

IIR (International Institute of Refrigeration) (1981) *Thermodynamic and Physical Properties of Refrigerant 11; Refrigerant 12; Refrigerant 22; and Refrigerant 717,* IIR, Paris, France, 1981.

ISO (1968) *Recommendation R916: Testing of Refrigerating Systems,* Switzerland, International Organisation for Standardisation, 1968 (ISO R916).

ISO (1992) *Draft International Standard: Refrigerating Systems - Test Methods - Part 1: Testing of Systems for Cooling Liquids and Gases Using a Positive Displacement Compressor,* Switzerland, International Organisation for Standardisation, 1992 (ISO/DIS 916-1).

ISO (1994) *Draft International Standard: Refrigerating Systems - Test Methods - Part 3: Testing of Systems for Cooling Liquids and Gases Using a Turbocompressor,* Switzerland, International Organisation for Standardisation, 1994 (ISO/DIS 916-3).

ISERMANN, R. (1982) Process Fault Detection Based on Modelling and Estimation Methods, *Proceedings, IFAC Conference on Identification and System Parameter Estimation,* Washington, DC, USA, 1982, pp. 7-30.

JACKSON, W.L., CHEN, F.C. and HWANG, B.C. (1987) The Simulation and Performance of a Centrifugal Chiller, *ASHRAE Transactions,* Vol. 93, No. 2, 1987, pp. 1751-1766.

JANSEN VAN VUUREN, S.P. (1983) A Thermal Storage System for Surface Refrigeration Plants, *Journal of the Mine Ventilation Society of South Africa,* Vol. 36, No. 5, May 1983, pp. 45-52.

KLOSTERMANN, K. (1994) Largest Ice Plant in the World, *S A. Refrigeration & Air-Conditioning,* Vol. 10, No. 6, November 1994, pp. 27-32.

KOURELOS, J. (1995) Letter to the Editor, *Journal of the Mine Ventilation Society of South Africa,* Vol. 48, No. 10, October 1995, p. 253.

LUCAS, C.E. (1989) Refrigeration System Stability Linked to Compressor and Process Characteristics, *Chemical Engineering Progress,* November 1989, pp. 37-56.

LUNDBERG, A. (1980) Capacity Control for Partial Load Operation of Screw Compressor Units, *ASHRAE Transactions,* Vol. 86, Part 1, 1980, pp. 485-492.

MEYER, S.L. (1975) Data Analysis for Scientists and Engineers, John Wiley & Sons, Inc., New York, 1975.

MIDDLETON, J.V.G. and MULLER, A. (1986) A Surface Ice Plant for the Provision of Ice for Cooling of Service Water in an OFS Gold Mine, *GOLD 100: Proceedings, International Conference on Gold,* Vol. 1: Gold Mining Technology, Johannesburg, South African Institute of Mining and Metallurgy, 1986, pp. 191-201.

MIDDLETON, N.T. (1984) The Modelling and Control of Refrigeration Plants in Deep South African Gold Mines, unpublished PhD Thesis, University of the Witwatersrand, Johannesburg, South Africa, 1984.

NAPIER, L.G.D. and PATTERSON, A.M. (1992) Technical, Economic and Safety Aspects of the Split Ammonia Refrigeration System, in: *Proceedings, Fifth International Mine Ventilation Congress,* Johannesburg, South Africa, 25-30 October 1992; Hemp, R, ed., The Mine Ventilation Society of South Africa, Johannesburg, 1992, pp. 201-212.

NG, H.T. (1990) Model-based, Multiple Fault Diagnosis of Continuous Physical Devices, *6th Conference on Artificial Intelligence Applications,* Santa Barbara, CA, USA, 5-9 May 1990 (Los Alamitos, CA, USA: IEEE Comput. Soc. Press, 1990), Vol 1, pp 9-15.

PAPE, F.L.F., MITCHELL, J.W. and BECKMAN, W.A. (1991) Optimal Control and Fault Detection in Heating, Ventilating, and Air-Conditioning Systems, *ASHRAE Transactions,* Vol. 97, 1991, Part 1, pp. 729-735.

PATTERSON, A.M. (1984) Maximising the Output of a Closed-Circuit Underground Refrigeration System, in: *Proceedings, Third International Mine Ventilation Congress,* Harrogate, England, 1984; Howes, M.J. and Jones, M.J., eds., Institution of Mining and Metallurgy, London, UK, 1984, pp. 239-242.

PERRY, E.J. (1987a) Performance Testing and Specification of Large Industrial Refrigeration Plant, *Proceedings, Joint Seminar on Performance Testing and Evaluation of Refrigeration Plant*, Institute of Refrigeration and Institution of Mechanical Engineers (UK), 13 May 1987 (Institute of Refrigeration, UK, 1987).

PERRY, E.J. (1987b) Refrigeration System Optimisation, *International Journal of Refrigeration*, Vol. 10, July 1987, pp. 217-223.

PERRY, R.H. and GREEN, D.W. (eds.) (1984) Perry's Chemical Engineer's Handbook, 6th Edition, McGraw-Hill Book Co., New York, 1984.

PHELAN, J., BRANDEMUEHL, M.J. and KRARTI, M. (1997) In-Situ Performance Testing of Chillers for Energy Analysis, *ASHRAE Transactions*, Vol. 103, 1997, Part 1, pp. 290-302.

PULLES, W. (1992) Water Pollution: its Management and Control in the South African Gold Mining Industry, *Journal of the Mine Ventilation Society of South Africa*, Vol. 45, No. 2, February 1992, pp. 18-36.

RAMSDEN, R. and BLUHM, S.J. (1984) Air-Cooling Equipment Used in South African Gold Mines, in: *Proceedings, Third International Mine Ventilation Congress*, Harrogate, England, 1984; Howes, M.J. and Jones, M.J., eds., Institution of Mining and Metallurgy, London, UK, 1984, pp. 243-251.

RAMSDEN, R., BLUHM, S.J., SHEER, T.J. and BURTON, R.C. (1988) Control of the Underground Thermal Environment in South African Gold Mines, *S.A. Refrigeration & Air-Conditioning*, Vol. 4, No. 4, July 1988, pp. 23-32.

RAMSDEN, R. (1990) Mine Cooling Towards the 21st Century, *Journal of the Mine Ventilation Society of South Africa*, Vol. 43, No. 9, September 1990, pp. 162-168.

RAMSDEN, R. and BAKER-DULY, H.C. (1991) Optimum Use of Chilled Service Water in Ultra-Deep Mines, *The South African Mechanical Engineer,* Vol. 41, No. 1, January 1991, pp. 19-22.

RAMSDEN, R. and LLOYD, F. (1992) Investigation into the Use of Slurry Ice at Western Deep Levels, in: *Proceedings, Fifth International Mine Ventilation Congress,* Johannesburg, South Africa, 25-30 October 1992; Hemp, R., ed., The Mine Ventilation Society of South Africa, Johannesburg, 1992, pp. 229-235.

ROGERS, G.F.C. and MAYHEW, Y.R. (1967) Engineering Thermodynamics, Work and Heat Transfer, Second Edition (SI Units), Longman, London, 1967.

ROSE, H.J.M. and BLUHM, S.J. (1994) Ventilation and Refrigeration Design for a New Shaft System at Impala Platinum Limited, *Journal of the Mine Ventilation Society of South Africa,* Vol. 47, No. 6, June 1994, pp. 126-135.

SAUNDERS, E.A.D. (1988) Heat Exchangers: Selection, Design and Construction, Longman Scientific & Technical, London, 1988.

SCRINE, G.R. (1987) Analysis of Results and their Errors, *Proceedings, Joint Seminar on Performance Testing and Evaluation of Refrigeration Plant,* Institute of Refrigeration and Institution of Mechanical Engineers (UK), 13 May 1987 (Institute of Refrigeration, UK, 1987).

SHEER, T.J., CORREIA, R.M., CHAPLAIN, E.J. and HEMP, R. (1984) Research into the Use of Ice for Cooling Deep Mines, in: *Proceedings, Third International Mine Ventilation Congress,* Harrogate, England, 1984; Howes, M.J. and Jones, M.J., eds., Institution of Mining and Metallurgy, London, UK, 1984, pp. 277-282.

SHONE, R.D.C. (1983) The Influence of Compressor Performance on the Part-Duty Operation of a Two-Stage Centrifugal Water Chiller, unpublished M.Sc. dissertation, University of the Witwatersrand, Johannesburg, South Africa, 1983.

SHONE, R.D.C. and SHEER, T.J. (1988) An Overview of Research into the Use of Ice for Cooling Deep Mines, in: *Proceedings, Fourth International Mine Ventilation Congress,* Brisbane, Australia, July 1988.

SHONE, R.D.C. (1989) Research into Slurry Ice for Mine Cooling and the Desalination of Mine Waters, *The South African Mechanical Engineer,* Vol. 39, No. 3, March 1989, pp. 96-106.

STARNER, K.E. (1976) Effect of Fouling Factors on Heat Exchanger Design, *ASHRAE Journal,* Vol. 18, No. 5, May 1976, pp. 39-41.

STEPANOFF, A.J. (1955) Turboblowers, John Wiley and Sons, 1955.

STEWART, J.M. (1982a) Fundamentals of Human Heat Stress, in: *Environmental Engineering in South African Mines,* The Mine Ventilation Society of South Africa, Johannesburg, South Africa, 1982, pp. 495-533.

STEWART, J.M. (1982b) Practical Aspects of Human Heat Stress, in: *Environmental Engineering in South African Mines,* The Mine Ventilation Society of South Africa, Johannesburg, South Africa, 1982, pp. 535-567.

STOSIC, N., MILUTINOVIC, Lj., HANJALIC, K. and KOVACEVIC, A. (1992) Investigation of the Influence of Oil Injection upon the Screw Compressor Working Process, *International Journal of Refrigeration,* Vol. 15, No. 4, 1992, pp. 206-219.

STROH, R.M. (1982) Refrigeration Practice, in: *Environmental Engineering in South African Mines,* The Mine Ventilation Society of South Africa, Johannesburg, South Africa, 1982, pp. 653-683.

STROH, R.M. and KOURELOS, J. (1990) An Evaluation of Refrigeration Systems for Deep Level Gold Mining, in: *Proceedings, ASHRAE-FRIGAIR 90 Conference,* Pretoria, South Africa, 23-25 April 1990; Vol. 2, Mine Cooling Papers, S A. Institute of Refrigeration and Air-Conditioning, Pretoria, South Africa; Paper M.2, 16p.

THORP, N. (1974) Practical Uses of the Pressure-Enthalpy Diagram, *Journal of the Mine Ventilation Society of South Africa,* Vol. 27, No. 3, March 1974, pp. 44-53.

THORP, N. and BLUHM, S.J. (1986) The Use of Small Cooling Plants on a Mine, *Journal of the South African Institute of Mining and Metallurgy,* Vol. 86, No. 2, February 1986, pp. 61-66.

VAN DER WALT, J. and WHILLIER, A. (1978) Considerations in the Design of Integrated Systems for Distributing Refrigeration in Deep Mines, *Journal of the South African Institute of Mining and Metallurgy,* Vol. 79, No. 5, December 1978, pp. 109-124.

VAN DER WALT, J. (1979) Engineering of Refrigeration Installations for Cooling Mines, *The South African Mechanical Engineer,* Vol. 29, No. 10, October 1979, pp. 360-372.

VAN HOUTE, U. and VAN DEN BULCK, E. Modelling Chiller Performance Using Simultaneous Equation-Solving Procedures, *International Journal of Refrigeration,* Vol. 17, No. 3, 1994, pp. 191-198.

WEBB, R.L. (1984) Shell-Side Condensation in Refrigerant Condensers, *ASHRAE Transactions,* Vol. 90, Part 1B, 1984, pp. 5-25.

WEBB, R.L., CHOI, K.D. and APPARAO, T.R. (1989) A Theoretical Model for Prediction of the Heat Load in Flooded Evaporators, *ASHRAE Transactions,* Vol. 95, Part 1, 1989, pp. 326-337.

WEBB, R.L. (1991) Advances in Shell Side Boiling of Refrigerants, *Proceedings of the Institute of Refrigeration,* Vol. 87, 1990-1991, pp. 75-84.

WELTY, J.R., WICKS, C.E. and WILSON, R.E. (1976) Fundamentals of Heat, Momentum and Mass Transfer, Second Edition, John Wiley & Sons, New York, 1976.

WHILLIER, A. (1977) Predicting the Performance of Forced-Draught Cooling Towers, *Journal of the Mine Ventilation Society of South Africa,* Vol. 30, No. 1, January 1977, pp. 2-25.

WHILLIER, A. (1982) Heat Transfer, in: *Environmental Engineering in South African Mines,* The Mine Ventilation Society of South Africa, Johannesburg, South Africa, 1982, pp. 465-494.

WONG, S.P.W. and WANG, S.K. (1989) System Simulation of the Performance of a Centrifugal Chiller Using a Shell-and-Tube-Type Water-Cooled Condenser and R-11 as Refrigerant, *ASHRAE Transactions,* Vol. 95, Part 1, 1989, pp. 445-454.

YORK DIVISION, BORG-WARNER CORPORATION (1971) Field Testing of Liquid Chilling Equipment, Form MS471; The Corporation, York, PA, USA, 1971.

YU, C-C. and LEE, C. (1991) Fault Diagnosis Based on Qualitative/Quantitative Process Knowledge, *AIChE Journal,* Vol. 37, No. 4, April 1991, pp. 617-628.